AD-A189 884 ROLE OF THE CORROSION PRODUCT FILM IN THE CORROSION PROTECTION OF CU-NI A (U) DAVID W TAYLOR NAVAL SHIP RESEARCH AND DEVELOPMENT CENTER ANN H P HACK NOV 87 1/2

UNCLASSIFIED DTNSRDC/SME-87-22 F/G 11/6.1 NL

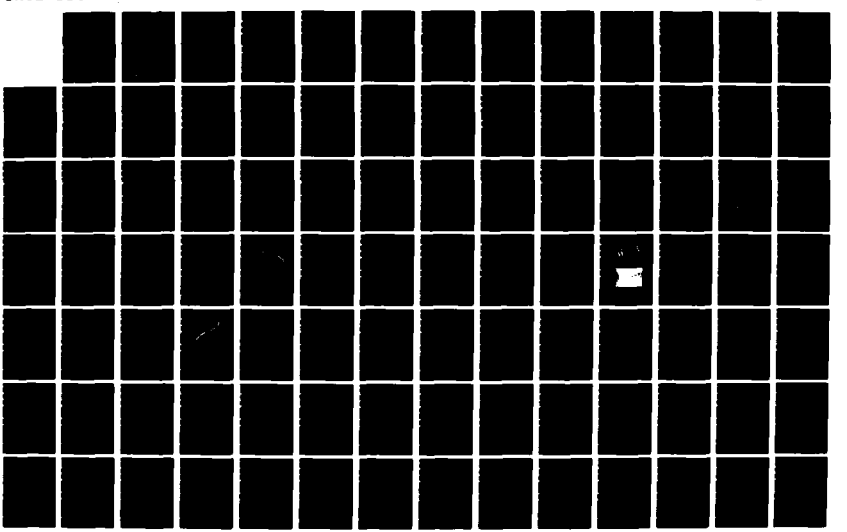

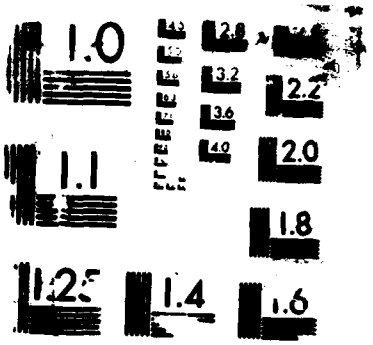

David W. Taylor Naval Ship Research and Development Center
Bethesda, MD 20084-5000

DTNSRDC/SME-87-22 November 1987

Ship Materials Engineering Department
Research and Development Report

ROLE OF THE CORROSION PRODUCT FILM IN THE CORROSION PROTECTION OF CU-NI ALLOYS IN SALTWATER

By
Harvey P. Hack

ROLE OF THE CORROSION PRODUCT FILM IN THE CORROSION PROTECTION OF CU-NI ALLOYS IN SALTWATER
DTNSRDC SME-87-22

UNCLASSIFIED
SECURITY CLASSIFICATION OF THIS PAGE

A189 084

REPORT DOCUMENTATION PAGE

1a. REPORT SECURITY CLASSIFICATION UNCLASSIFIED	1b RESTRICTIVE MARKINGS
2a. SECURITY CLASSIFICATION AUTHORITY UNCLASSIFIED	3. DISTRIBUTION/AVAILABILITY OF REPORT Approved for public release; distribution unlimited.
2b. DECLASSIFICATION/DOWNGRADING SCHEDULE	
4. PERFORMING ORGANIZATION REPORT NUMBER(S) DTNSRDC SME-87-22	5. MONITORING ORGANIZATION REPORT NUMBER(S)
6a. NAME OF PERFORMING ORGANIZATION David Taylor Naval Ship R&D Center 6b. OFFICE SYMBOL (If applicable) Code 2813	7a. NAME OF MONITORING ORGANIZATION
6c. ADDRESS (City, State, and ZIP Code) Annapolis, MD 21402	7b. ADDRESS (City, State, and ZIP Code)
8a. NAME OF FUNDING/SPONSORING ORGANIZATION 8b. OFFICE SYMBOL (If applicable)	9. PROCUREMENT INSTRUMENT IDENTIFICATION NUMBER
8c. ADDRESS (City, State, and ZIP Code)	10. SOURCE OF FUNDING NUMBERS PROGRAM ELEMENT NO. 61152N; PROJECT NO.; TASK NO ZR-000-01-01; WORK UNIT ACCESSION NO. 1-2813-115

11. TITLE (Include Security Classification)
ROLE OF THE CORROSION PRODUCT FILM IN THE CORROSION PROTECTION OF CU-NI ALLOYS IN SALTWATER

12. PERSONAL AUTHOR(S)
Harvey P. Hack

13a. TYPE OF REPORT	13b. TIME COVERED	14. DATE OF REPORT (Year, Month, Day)	15 PAGE COUNT
Research & Development	FROM ____ TO ____	November 1987	158

16. SUPPLEMENTARY NOTATION

17 COSATI CODES		
FIELD	GROUP	SUB-GROUP

18. SUBJECT TERMS (Continue on reverse if necessary and identify by block number)
Corrosion; 70-30 Copper-Nickel; Electrochemical; Copper-Nickel; Saltwater; Impedance; 90-10 Copper-Nickel; Copper

19. ABSTRACT (Continue on reverse if necessary and identify by block number)

Measurements were conducted to determine the impedance of the electrochemical interface on rotating disk specimens of pure copper and commercial 90-10 and 70-30 copper-nickel alloys over a 28 day period while immersed in an aerated aqueous 3.4% (Sodium Chloride) NaCl solution. A sinusoidal voltage was applied to the specimen, and the in-phase and out-of-phase components of the current were measured as a function of frequency using a technique called Electrochemical Impedance Spectroscopy. Specimens were exposed at a rotation speed of 1000 RPM, although brief measurements were conducted from 500 to 2000 RPM at the end of the exposure period. Under circumstances where a cupric hydroxy-chloride corrosion product formed, copper experienced an increase in corrosion resistance with time which could not be correlated with a specific growth law. When the hydroxy-chloride was not present, the corrosion rate of copper was constant over time. Copper-nickel alloys also

(Continued)

20. DISTRIBUTION/AVAILABILITY OF ABSTRACT ☐ UNCLASSIFIED/UNLIMITED ☒ SAME AS RPT. ☐ DTIC USERS	21. ABSTRACT SECURITY CLASSIFICATION UNCLASSIFIED
22a. NAME OF RESPONSIBLE INDIVIDUAL Harvey P. Hack	22b. TELEPHONE (Include Area Code) 301-267-3502 22c. OFFICE SYMBOL Code 2813

DD FORM 1473, 84 MAR 83 APR edition may be used until exhausted. All other editions are obsolete

SECURITY CLASSIFICATION OF THIS PAGE

U.S. Government Printing Office 1988—606-012

Block 19 Continued

experienced increasing corrosion resistance with increased exposure time. On all of the alloys tested, the enhanced corrosion resistance was due to a process associated with the specimen surface, such as diffusion through the corrosion product layer or limited catalysis of the cathodic reaction, rather than by diffusion through a Nernst-like fluid boundary layer. This was evidenced by a lack of rotation speed dependence of the polarization resistance on material exposed for 672 hours. DC bias tests indicated that the corrosion of copper is controlled by the cathodic reaction, probably oxygen reduction, and all data were consistent with the assumption that this was also the case for the copper-nickel alloys.

The corrosion rate of pure Cu was found to be determined by a protective inner corrosion product layer, and under certain circumstances, also by an outer layer. In contrast, the outer, loosely adherent corrosion product layers accounted for the majority of the corrosion resistance of the Cu-Ni alloys, since the corrosion rate increased when the outer layers were removed by stripping with tape, and also when they were Pd sputter coated prior to removal. It follows that the corrosion rate of Cu-Ni is limited by the poor catalytic nature of the corrosion product surface for the oxygen reduction reaction.

ABSTRACT

Measurements were conducted to determine the impedance of the electrochemical interface on rotating disk specimens of pure copper and commercial 90-10 and 70-30 copper-nickel alloys over a 28 day period while immersed in an aerated aqueous 3.4% NaCl solution. A sinusoidal voltage was applied to the specimen, and the in-phase and out-of-phase components of the current were measured as a function of frequency using a technique called Electrochemical Impedance Spectroscopy. Specimens were exposed at a rotation speed of 1000 RPM, although brief measurements were conducted from 500 to 2000 RPM at the end of the exposure period. Under circumstances where a cupric hydroxy-chloride corrosion product formed, copper experienced an increase in corrosion resistance with time which could not be correlated with a specific growth law. When the hydroxy-chloride was not present, the corrosion rate of copper was constant over time. Copper-nickel alloys also experienced increasing corrosion resistance with increased exposure time. On all of the alloys tested, the enhanced corrosion resistance was due to a process associated with the specimen surface, such as diffusion through the corrosion product layer or limited catalysis of the cathodic reaction, rather than by diffusion through a Nernst-like fluid boundary layer. This was evidenced by a lack of rotation speed dependence of the

polarization resistance on material exposed for 672 hours. DC bias tests indicated that the corrosion of copper is controlled by the cathodic reaction, probably oxygen reduction, and all data were consistent with the assumption that this was also the case for the copper-nickel alloys.

The corrosion rate of pure Cu was found to be determined by a protective inner corrosion product layer, and under certain circumstances, also by an outer layer. In contrast, the outer, loosely adherent corrosion product layers accounted for the majority of the corrosion resistance of the Cu-Ni alloys, since the corrosion rate increased when the outer layers were removed by stripping with tape, and also when they were Pd sputter coated prior to removal. It follows that the corrosion rate of Cu-Ni is limited by the poor catalytic nature of the corrosion product surface for the oxygen reduction reaction.

TABLE OF CONTENTS

TABLE OF CONTENTS (continued)

LIST OF TABLES

LIST OF FIGURES

ADMINISTRATIVE INFORMATION

Funding for this project was provided by the David Taylor Naval Ship Research and Development Center, Independent Research Program, sponsored by the Space and Naval Warfare Systems Command, SPAWAR 005, and administered by the Office of the Chief of Naval Research, DTNSRDC Code 012.3 (Dr. Moran) under Program Element 61152N, Task Area RR-000-01-01, Work Unit 1-2813-115.

1. INTRODUCTION

Copper-nickel alloys are used almost exclusively for piping in all ships in the U. S. Navy and for heat exchangers and piping in many commercial ships and power plants cooled by seawater. Since 1974, instances of severe corrosion of 90-10 copper-nickel piping have occurred due to water pollution by hydrogen sulfide, sometimes causing perforation of 0.6 cm wall pipe in as little as 30 days[1,2]. This has led to intensive research which has shown that there are several ways to prevent this corrosion. These are the use of: 1) ferrous sulfate inhibitor[3-5], 2) stimulated iron anodes[6], 3) sodium-dimethyl-dithiocarbamate (SDD) inhibitor, 4) cathodic protection[7], and 5) corrosion product films formed over a long period of time[8]. Addition of ferrous sulfate for systems with large flow rates has been found to involve unacceptable consumption of the inhibitor in ship-based systems. Control difficulties have been experienced with iron anode systems tried on board some ships. SDD use requires the shutdown of the systems involved, a procedure not practical in all installations. Cathodic protection of the inside of piping systems is not practical due to current throwing distance limitations. On a brighter note, the use of a corrosion product film formed over long periods of time in unpolluted seawater can improve corrosion resistance to subsequent polluted seawater exposure. This process cannot be accelerated to time frames

of use in construction due to lack of knowledge of the nature and rate-controlling formation kinetics of corrosion product films of copper-nickel alloys. This has led to a need for more information to help determine which aspect of the corrosion product film causes corrosion resistance of these alloys, and to determine the rate-limiting step in film formation in unpolluted seawater. Knowing the rate-limiting step should lead to a way to improve the speed of development of this protective film, and thus to improve the corrosion performance of copper-nickel piping in service.

Until fairly recently, the corrosion mechanism of copper-nickel alloys was not well understood. The formation of a corrosion product film has been found to greatly reduce the corrosion rate of copper alloys. The role of this film in reducing corrosion is unclear, however. The corrosion product of 90-10 copper-nickel is known to consist of a layered structure consisting of thick, loosely adherent porous layers of cupric hydroxy-chloride over a thin tightly adherent layer of cuprous oxide[9-12]. The iron and nickel from the alloy are not concentrated in the outer part of the porous layer[10]. Until recently, copper-nickel was believed to get its corrosion resistance from the inner cuprous oxide layer as follows: Cuprous oxide has a cubic, copper-deficient lattice, making it a p-type semiconductor[11,12], with low ionic resistance due to highly mobile vacancies and low electronic resistance due to holes

with a low activation energy for movement[13]. Additions of nickel and iron were thought to improve corrosion performance by substitution for copper in the lattice, thus reducing the concentrations of both vacancies and holes[11]. Reduction of the number of mobile charge carriers would increase film resistance[13], providing a more effective barrier to the corrosion process.

More recently, Kato and Pickering[9,14] have developed a more highly-supported mechanism for copper-nickel's corrosion resistance, as follows: These authors looked at the effect of stripping of the outer corrosion product layers on anodic and cathodic polarization behavior. Only cathodic polarization was affected by the presence of the corrosion products, indicating a cathodically controlled corrosion process on alloy covered with corrosion products. In one study, the low rate of the cathodic reaction, assumed to be oxygen reduction, persisted when the outer porous corrosion product layer was stripped off[9]. Thus, the inner cuprous oxide was shown to provide either a diffusion barrier to the cathodic reaction[9], or is, along with the outer layer, a poor catalyst for the oxygen reduction reaction[9,14]. Those conclusions were made under the assumption that the cathodic reaction was controlling corrosion of these alloys, an assumption requiring additional evidence.

Palladium coating of the inner layer greatly increased the (oxygen reduction) reaction kinetics to the diffusion

limited value, an effect attributed by the experimenters to either electrical shorting through the resistive inner cuprous oxide layer or to an increased catalytic activity of the corrosion product surface for oxygen reduction. These results eliminated the possibility that the effect was due to low ionic conductivity in the corrosion product[9,10]. Kato and Pickering[15] later proved that the catalytic effect was the correct one by developing a corrosion product film in sulfide-containing solutions. This film showed high oxygen reduction rates, presumably because the sulfide is a good catalyst, but the reaction rate slowed when the loosely adherent layers were removed. This is a good argument in favor of the catalytic mechanism[14,15].

A catalytic mechanism which is time independent as suggested above leads to linear weight loss kinetics instead of the near parabolic behavior observed by Kato et al.[9,14]. This suggests that the catalytic nature of the surface degrades with time, e.g., as a result of impurity adsorption. Thus, it remains to be shown how the weight loss kinetics are consistent with a catalytic mechanism. In the present study, the dependence of corrosion rate on the cathodic reaction is further explored, and the kinetics of the development of the corrosion product film is examined over the duration of the exposure by the use of electrochemical impedance measurements. The effect of nickel and iron on the catalysis is not understood sufficiently to explain differences in behavior between pure

copper, 90-10 copper-nickel, and 70-30 copper-nickel.

The present research was designed as a first step in filling gaps in the knowledge about the action of the corrosion product layers on these alloys. The impedance of the electrochemical interface was monitored as a function of exposure duration as a non-destructive method of following corrosion rate behavior. This technique, known as electrochemical impedance spectroscopy, is described in Appendix C. Changes in oxygen reduction catalysis (by palladium coating), rotation speed and DC bias were used to determine the rate-controlling step in the corrosion process. Finally, three alloys were used, containing from 0 to 30 percent nickel to find out what the effect of nickel is on the rate-controlling step, and from this, why addition of nickel to copper imparts increased corrosion resistance.

2. REVIEW OF RELEVANT LITERATURE

2.1 General

Copper and nickel form a continuous solid solution in all composition ranges. Typically, the commercial alloys are alloyed with iron, at 1.5% for 90-10 copper-nickel and 0.5% for 70-30 copper-nickel.[16] Although the higher nickel alloys are supposed to have greater corrosion resistance, particularly under flowing conditions, under low flow and well-oxygenated conditions the 90-10 alloy has sometimes been reported to have equal or greater corrosion resistance than the 70-30 alloy.[17,18,19,20] Iron is added primarily for erosion-corrosion resistance in seawater, and has its maximum benefit when in solid solution.[21] Slow cooling or aging of the 90-10 alloy will cause some of the iron to precipitate out of solution, primarily at grain boundaries, as either a continuous or discontinuous precipitate, thus adversely affecting the corrosion properties of the alloy.[21]

2.2 Corrosion Mechanism in Electrolytes Without Chloride

Osterwald and Uhlig[22], Koizumi and Uhlig[23], and Mansfeld and Uhlig[24] have stated that passivity in the copper-nickel system is dependent on the number of "d" shell electron vacancies. At 30-40% nickel the amount of nickel is sufficient to create "d" shell vacancies, and the alloy

exhibits passive behavior in aqueous hydrochloric acid. Iron enhances passivity by accepting electrons, thus decreasing the nickel content necessary for these vacancies to be formed.

Mansfeld and Uhlig[24] measured an anodic Tafel slope of 30 mV/decade for several copper-nickel alloys in sulfuric acid. Nobe and Bauerle[25] measured slopes of 40 and 45 mV/decade for 90-10 and 70-30 respectively. Nobe et al[26] measured the slope for copper to be 40 mV/decade. Shen and Nobe have recently reported the results of their own experiments in sulfuric acid and summarized those of others.[27] They conclude that the anodic Tafel slope for copper and copper-nickels is 40 mV/decade. In this environment copper dissolution proceeds by oxidation to copper(II) ions, and the rate of the anodic reaction is activation controlled. Copper dissolution is a two-step process, where the first step, oxidation to copper(I) is fast and the second step, oxidation of copper(I) to copper(II), is slow and rate-limiting.

Ghandehari et al[28] investigated cathodic polarization of copper in sulfuric acid. They found a cathodic "hump" in the polarization curve generated in aerated solutions which was not present in deaerated solutions. This hump was attributed to an adsorbed intermediate in the oxygen reduction reaction, such as HO_2, which decatalyzed the cathodic reaction.

Ashworth and Fairhurst[29] investigated the mechanism of

copper corrosion in aqueous sodium hydroxide. Their conclusion was that copper was removed as a cuprous $Cu(OH)_2^-$ complex, which eventually precipitated as cuprous oxide on the surface. A nucleation and growth mechanism was proposed for oxide formation, and the overall rate was stated to be controlled by slow charge transfer. Ambrose et al[30] concluded that diffusion of a cupric hydroxyl complex away from the surface was rate controlling. They found a hydroxyl reaction order of 1.4 and an anodic Tafel slope of 60 mV/decade. They stated that the addition of the first two hydroxyls was the slow step, while a subsequent addition of two more was fast.

A number of studies have been done of copper in neutral distilled water. Ives and Rawson[31,32] studied the effects of dissolved oxygen and carbon dioxide. Although a cuprous oxide film was formed of up to 25000 Angstroms thickness, they concluded that the film did not reduce the rate of the anodic reaction, implying cathodic control by the film. Earlier, Kruger[33,34] had observed the development of cuprous or cupric oxide films on copper, depending on the dissolved oxygen content. The cuprous oxide grew with parabolic kinetics, implying a film diffusion controlled corrosion process.

2.3 Corrosion Mechanism in Acid Chlorides

A large number of investigators have looked at corrosion of copper and copper-nickel alloys in aqueous hydrochloric acid or hydrochloric-sulfuric acid mixtures. In this case, a corrosion product layer does not form on the surface of the metal. Anodic Tafel slopes have been reported of 62[35], 60[26,36-38], 65 and 158[39], 68-91[40], and 58[41,42] mV/decade for copper, 70[25,37], and 130[39] mV/decade for 90-10 copper-nickel, and 70[25] and 138[39] mV/decade for 70-30 copper-nickel. Pure nickel under similar circumstances had Tafel slopes of 105 and 165 mV/decade.[39] Reaction orders for chloride have been reported of 0.9[35], 2[26,41], and 2 or 3 (for chloride concentrations of less than or greater than 1 M respectively)[37,42] for copper, 1.3,[25] 1.3 (for less than 1 M) or 1.6 (for greater than 1 M chloride)[37], and 1.8[40] for 90-10 copper-nickel, and 1.2[25] for 70-30 copper-nickel. Reaction products have usually been observed to be cuprous chloride complex and nickel(II) ions.[25,26,35,38,40,41,43] The cuprous chloride complex may have from 1 to 3 chlorine atoms, depending on the chloride concentration in solution, with 2 being common below 1 M, and 3 being common above 1M.

Most investigators came to the conclusion that the rate-controlling step in anodic dissolution is not electron exchange, but diffusion. Usually the rate-limiting diffusing species was considered to be the chloride ion

complex, diffusing away from the surface[26,35,41], although chloride ions diffusing towards the surface were also mentioned[37]. This is supported by a lack of crystallographic etching evident on micrographs in the paper by Bockris et al.[39] Smyrl and Stephenson[38,44] have argued convincingly of a mechanism involving mixed kinetic and mass-transfer control, with the kinetic contribution being minor, although not insignificant. They developed a model of the corrosion process which accurately predicted the diffusivity of the copper chloride complex. Lee and Nobe[37] divided the anodic polarization curve for 90-10 copper-nickel into regions. At low overpotentials (less than 50 mV) selective dissolution of nickel occurred. At greater overpotentials (more than 50 mV) cupric ions were found. Ideal diffusion-controlled behavior was found only in a plateau region of the curve. Tafel slopes for the copper and nickel components of the alloy were 60 and 100 mV/decade respectively, as compared to the intermediate value of 70 mV/decade for the alloy. Walton and Brook[40] also noted active and passive regions in the polarization behavior for 70-30 copper-nickel, where in the active region cuprous ions were formed upon dissolution, in the passive region the copper-chloride complex was generated, and in the transpassive region cupric ions were generated.

2.4 Corrosion Mechanism in Neutral Chlorides

The primary difference in behavior between corrosion of the copper-nickel alloys in neutral chlorides versus the acidic chlorides is due to the development of a corrosion product film in the neutral solutions. The descriptions below lead to the conclusion that if exposure times are short so that a corrosion product film has not yet formed, the corrosion mechanism for this alloy series is similar to that in acid chlorides, whereas the behavior departs from this when corrosion products are allowed to accumulate.

2.4.1 Thermodynamics and Stability

Several authors have presented Pourbaix diagrams for copper in water with chlorides.[20,45,46] All show that at the observed corrosion potential of copper or copper-nickel the stable species is cuprous oxide. Regardless, Ives and Rawson[47] claim that cuprous oxide is not stable and will dissolve in water. Efird used electrochemical hysteresis to obtain experimentally the Pourbaix diagrams for 90-10 and 70-30 copper-nickel in seawater.[20] Of particular interest is that the line between corrosion and immunity for both alloys corresponds well with the equilibrium reaction between copper and $CuCl_2^-$. This gives support to the supposition that the copper chloride complex ion is involved in corrosion of these alloys.

2.4.2 Corrosion Product Analyses

In most cases, when copper-nickels react with neutral solutions containing chlorides, a multilayered corrosion product is formed. The inner layer is usually thought to be a tightly adherent cuprous oxide[9,10,14,15,21,48-55], while the outermost layer is a loosely adherent hydroxy-chloride called paratacamite[9,10,14,15,17,21,48,54-56]. This is supported by qualitative observations of corrosion product film colors by other investigators.[57,58] Malachite has also been claimed as the outer layer[51], and cuprous chloride as the inner layer[56]. In some cases, the outer layer has not been observed, and this has sometimes been attributed to the use of refreshed versus recirculated water. The inner cuprous oxide is a p-type semiconductor in its pure form[13,53,59], and the addition of chloride ions into the film would create additional cation vacancies[48,51]. North and Pryor[53] have proposed a mechanism for the beneficial effect of nickel by its incorporation into the solid state cuprous oxide, thus using up vacancies and holes and lowering both ionic and electronic conductance through the film. Bacarella and Griess[60] have calculated that this cuprous oxide film can be precipitated by combination of the copper chloride complex with water. Nickel and iron enrichment have been reported in the films.[17,50,58] Blundy and Pryor found the nickel mostly in the inner cuprous

oxide,[48] as did McGuire et al[49]. Castle and Parvizi found nickel and iron enrichment in a middle layer, containing lots of oxides and chlorides.[56] Extensive corrosion product analysis was also done by Kato and Pickering,[9,10,14,15] who found nickel and iron enrichment in the middle layer. These authors gave an excellent summary of the development over time of the corrosion product film on 90-10 copper-nickel.[10] They also developed a technique for removing all outer layers of the corrosion product film while leaving only the cuprous oxide inner layer.

2.4.3 Mechanism Studies

Castle and Parvizi[56] presented a good summary of the literature on the corrosion mechanism of 90-10 copper-nickel. Tafel slopes for anodic dissolution of copper have been measured as 60 mV/decade for copper in NaCl which is deaerated[60,61] or aerated[55,61] in temperatures up to boiling[61]. Dhar et al[55] measured an anodic Tafel slope of 90 mV/decade and a cathodic slope of 200 mV/decade for 70-30 copper-nickel in seawater. The extrapolation technique used by Dhar does not give accurate results however, since extrapolation to the freely corroding potential was made from portions of the curves far enough from this potential for a change in mechanism to occur, as evidenced by the appearance of peaks in the curves. Bacarella and Griess[60] measured a chloride reaction order of

2 for copper in a flowing, deaerated NaCl solution. The reaction product has been stated to be in the cuprous form by Ali and Ambrose for Monel (70-30 nickel-copper)[62], and Taylor[63], and Bomberger et al[64] have reported this for pure copper in NaCl solutions. The oxygen reduction reaction is reportedly sluggish on copper and copper-nickels in both saltwater and seawater, and the overall corrosion reaction is reportedly under cathodic control.[17,50,64-66] Bjorndahl and Nobe[65] reported that oxygen reduction on copper is under activation control.

2.4.4 Effects of Corrosion Products on Partial Reactions

Although the corrosion products on copper-nickels have a profound effect on their corrosion in neutral chloride solutions, only a few investigators have studied this in detail. Melton et al[67] reported that a copper-nickel cathode with a corrosion product film supports lower galvanic currents when coupled to steel in seawater. Castle and Parvizi[56] studied the effect of the corrosion product film over time on the behavior of 90-10 copper-nickel in NaCl and seawater. They noted increased polarization of both the anodic and cathodic reactions with time, along with a decrease in the anodic Tafel slope and a decrease in the ability of the surface to sustain oxygen reduction. Cathodic inhibition was not affected by stripping the outer corrosion product layers, but this stripping did increase

the anodic Tafel slope to values equivalent to freshly exposed material. Anodic polarization developed an inner corrosion product layer that inhibited the corrosion reaction. From this the authors concluded that the inner corrosion product layer provides the majority of the barrier to the corrosion of this alloy. Admiral et al[59] have shown that the presence of a protective layer on the 90-10 alloy in seawater results in little rotation speed dependence on a rotating cylinder electrode, but a poorly protective film gives a current dependence proportional to the square root of rotation speed.

The most comprehensive study on the effect of corrosion products on 90-10 copper-nickel in saltwater was conducted by Kato and Pickering and presented in a series of four papers.[9,10,14,15] In the first reference,[9] stationary specimens were exposed for up to 191 days. They found parabolic growth of the corrosion product film, and parabolic weight loss kinetics, with a significant portion of the lost weight not being incorporated into the film. The corrosion product film was found to reduce the anodic reaction somewhat, as determined by an increasing Tafel slope (70 to 120 mV/decade) and a decreasing current plateau with increasing exposure time. This effect was due almost entirely to the outer, porous layers, since it almost vanished when these layers were stripped off. The cathodic reaction (oxygen reduction) was decreased by at least an order of magnitude by the presence of the corrosion product

layers, with the effect being unchanged if the outer layers were removed. Thus, the reduction reaction was claimed to occur at the interface between the inner and outer layers, and the rate-controlling step was claimed to be slow electronic conductance through the inner cuprous oxide layer, which grew in thickness by a parabolic growth law. Palladium or platinum coating of the surface of the inner layer after removal of the outer layer increased the oxygen reduction rate to that of unfilmed surface, but this effect was attributed to electrical shorting of the noble metal to the alloy through cracks in the thin inner layer. This information, along with extensive corrosion product analysis, was used in the second paper[10] to make conclusions regarding the nature of the growth of the corrosion product.

A rotating disk electrode was used in the other two studies by Kato and Pickering. In the first of these papers,[14] pure diffusion control was found for the anodic reaction on a freshly exposed surface, while higher rotation speeds led to less current for the cathodic reaction. Development of corrosion product films reduced both anodic and cathodic reaction rates, and made these rates rotation speed independent. Stripping of the outer corrosion product layers caused the anodic reaction rate to return to that on a fresh surface, the cathodic rate to return to a rate slightly below that on a fresh surface, and restored rotation speed dependence for the anodic reaction. Palladium coating of the inner layer further increased the

cathodic reaction rate, to one well above that on a fresh surface. The authors concluded that the cathodic reaction, and therefore the corrosion process, was controlled by the poor catalytic nature of the corrosion product film for the oxygen reduction reaction. The data presented was more consistent with cathodic control by the outer layers, although the authors do not state in the paper which layer controls the reaction. They do state, however, that transport through the inner layer can not be rate controlling for this system.

The question of control of the oxygen reduction reaction by poor catalysis versus by low conductivity was put to rest by the final paper in the series,[15] in which hydrogen sulfide additions were made to the saltwater. The resulting corrosion product films were thicker and supported a 100-fold increase in the cathodic reaction rate. When the outer layers were stripped off, the reaction rate dropped to that of a fresh surface, an observation which could only be explained by catalysis control of the oxygen reduction reaction.

2.5 Impedance Behavior

Cahan and Chen[68] have stated that the use of DC techniques alone is inadequate to study corrosion processes, due to the large variety of electrical equivalent circuits that could represent the electrochemical interface. The

development of electrochemical impedance measurement techniques and equipment has led to a broad use of impedance techniques to study corrosion reactions.[69-76] This technique has been applied successfully to coated materials as well.[77-81] Since corrosion product layers are a form of coating, it is logical to use impedance techniques to study corrosion product films, and this has been done both by transient analyses[82] and by traditional sine wave techniques.[68,69,74]

Some limited impedance studies have been performed on copper-nickel alloys in seawater or NaCl solutions, as discussed below, but there is a paucity of data for pure copper in NaCl. MacDonald et al[17] studied the behavior of 90-10 and 70-30 copper-nickel in flowing seawater over a period of up to 330 hours. Both alloys were observed to have two relaxation processes, which after 78 hours were resolvable for 90-10 but not for the 70-30 alloy. After 78 hours, polarization resistances of 33 and 530 kohm-cm^2 were observed for these two alloys respectively. Syrett and MacDonald[19] also found good correspondence for these two alloys between impedance measurements and polarization resistance or weight loss. Macdonald et al[83] and Eiselstein, et al[84] also performed impedance measurements on 90-10 copper-nickel as a function of time in sulfide-polluted seawater. Sulfide was found to have a profound effect on both the corrosion rate, and the corrosion product films of this alloy.

Castle and Parvizi[56] used DC techniques to monitor polarization resistance and found an initial polarization resistance on 90-10 copper-nickel of 1.5-2 kohm-cm^2 which increased with exposure time. Also using DC techniques, IJsseling et al[57] measured a polarization resistance on 90-10 of 2 kohm-cm^2 which increased after 1400 hours exposure time to 20 kohm-cm^2, and was higher at higher temperatures. In a similar study, Drolenga et al[58] found polarization resistances for 90-10 copper-nickel which increased up to as much as 100 kohm-cm^2.

3. EXPERIMENTAL

3.1 Materials

The metals studied were pure copper, commercial 90-10 copper-nickel, and commercial 70-30 copper-nickel. Compositions and processing of these materials are listed in Table 1. Specimens of these materials were machined to final size and the edges coated with Glyptol to prevent water access. Then they were press fit into the rotating disk electrode holder described below for the actual testing.

The test solution was made from 3.4% reagent grade sodium chloride in double-distilled water. The pH of the solution after mixing was not adjusted and, for all batches of solution tested, remained within 1 pH unit of 7.0.

3.2 Apparatus and Specimen Preparation

A rotating disk electrode apparatus was used because of the mathematically well-established and reproducible nature of the flow which this apparatus provides across the specimen surface[85,86]. A base rotation speed of 1000 RPM was used, although limited runs were conducted at other rotation speeds from 200 to 2500 RPM as detailed below. The rotating disk apparatus used is illustrated in Figure 1. In this apparatus the specimen was mounted in a Plexiglas mount

TABLE 1. COMPOSITION OF MATERIALS STUDIED

	COPPER	90-10 CU-NI	70-30 CU-NI
UNS* NUMBER	C11000	C70600	C71500
PURCHASE SPEC	Electrol. tough pitch	ASME-SB-402	MIL-C-15726E
FORM	1/16" sheet	1/4" plate	1/4" plate
PROCESSING	Not Deoxydized	Annealed + Rolled	Annealed + Rolled
SOURCE	LaQue Center Stock	Hussey Metals	Revere Copper
ADDRESS	Wrightsville Beach, NC	Leetsdale, PA	New Bedford, MA
PROPERTIES			
Tensile, KSI		40	56.4-57.6
.5% Yield, KSI		15.4-16.3	25.9-30.0
Elong in 2", %		48.0-48.5	45-46
COMPOSITION, wt%			
Cu	99.9+	88.04	68.52
Ni		10.2	30.12
Fe		1.45	0.49
Mn		0.10	0.74
Zn		0.13	0.03
Pb		0.02-	0.01
P		0.02-	0.001
S		0.02-	0.004

* Unified Numbering System, ASTM DS-56A and SAE HS1086a

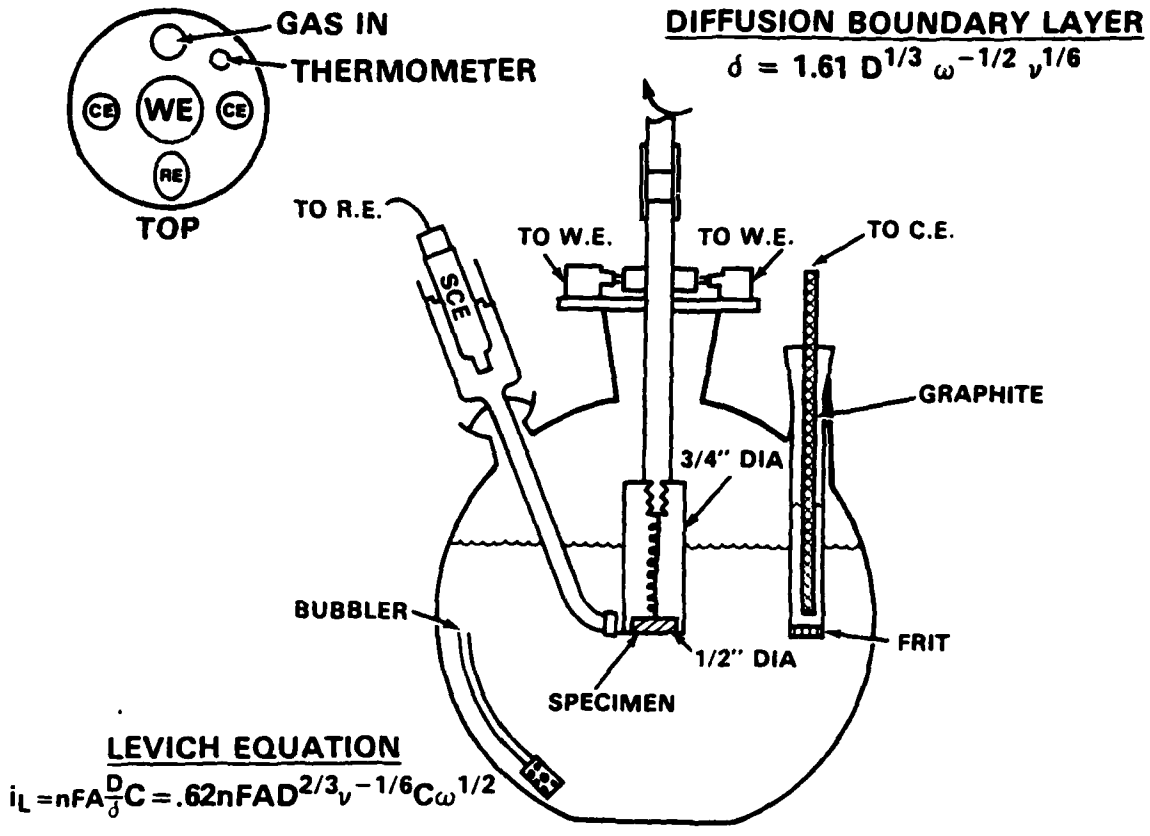

Figure 1.
Rotating Disk Apparatus

and spun face down. A Cole-Parmer lab stirrer model 4376-00 was used to spin the specimen holder. This motor was measured to have a speed error of less than 1% over the entire range of rotation speeds used in this study. Rotation speed was checked at first with a strobe, but later a photo tachometer was used (Model 36, Pioneer Electric and Research Corporation, Forest Park, IL). Specimen area was 1.277 cm^2 (0.5 inch diameter). Connection between the specimen and the rotator shaft was accomplished with a spring-loaded contact assembly using carbon-silver brushes. Potentials were measured using a saturated calomel half-cell electrode with a Luggin capillary equipped with a Vycor fritted tip. The tip was located just above the plane of specimen rotation and 1-3 mm from the edge of the specimen holder. Counter electrodes were densified graphite and were located inside containers separated from the cell electrolyte by porous glass frits. Two counter electrodes were used for current symmetry.

Rotating disk specimens were polished through 600 grit, then exposed for 28 days (672 hours) while rotating in aerated 3.4% sodium chloride solution. Acid cleaning in a 10 volume percent H_2SO_4 solution and degreasing of specimens were initially performed, but were found to have no significant effect on the results and were therefore discontinued.

The corrosion rate of the specimen and the corrosion product film properties were studied using several

electrochemical techniques. One of these techniques, called Electrochemical Impedance Spectroscopy, consists of applying a small sinusoidal voltage signal to the specimen as it is rotating, and measuring the amplitude and phase shift of the resultant current[69]. This is done at a series of frequencies and the results are used to calculate a complex impedance which describes the electrochemical interface, and from which polarization and film resistance can be calculated[75]. A brief discussion of the theory of this technique is contained in Appendix A. The applied signal had an amplitude of 10 mV, which is small enough to have little effect on the corrosion of the specimen as it was being studied. This allowed the time-dependent formation of the corrosion product film to be studied as it occurred. Frequencies used ranged from 10^5 to 10^{-3} Hz. An alternate technique was used at the lower frequencies. In this technique several sine waves of different frequencies were applied simultaneously and a Fast Fourier Transform (FFT) was employed to separate the results. Both the FFT and the stepped frequency techniques gave similar results where the frequencies overlapped.

Two different groups of equipment were used to obtain the impedance data. The first was an equipment package marketed by E. G. and G. Princeton Applied Research (PAR). The PAR package was controlled and the data analyzed by an Apple IIe microcomputer with an Epson FX-80+ printer, using software supplied by PAR and written in PASCAL. With this

system, the high frequency data down to 5 Hz is taken using a PAR model 1508 two-phase lock-in amplifier in a swept-frequency sine-wave mode. Lower frequency data is taken using the FFT technique by applying a composite waveform through the PAR model 273 programmable potentiostat. The low-frequency waveform was applied for three cycles to get the data reported below. The setup and interconnection of the components of the PAR impedance measurement system are illustrated in Figure 2.

The second group of equipment used for impedance measurements was constructed using a Schlumberger Solartron model 1250 frequency-response analyzer and a Stonehart Associates, Inc. model BC1200 potentiostat. Only the swept-sine technique was employed using up to 10 cycles at each frequency down to 200 mHz and 1 cycle below 200 mHz. The number of cycles at high frequency was set as the number needed for 1% accuracy in the data using a Student's t test, or 10, whichever was lower. Control of this equipment and data analysis was performed by a Tektronix 4052A microcomputer and a 4662 10 color plotter, 4907 disc drive, and a 4631 hard-copy unit. The software to control the Solartron, analyze and store the data, and make the data plots had to be written in Basic just for this study. The setup and interconnection of the components of the Solartron impedance measurement system are illustrated in Figure 3.

The total time required to get data for all frequencies was about 2 hours. All data from 100,000 to .01 Hz was

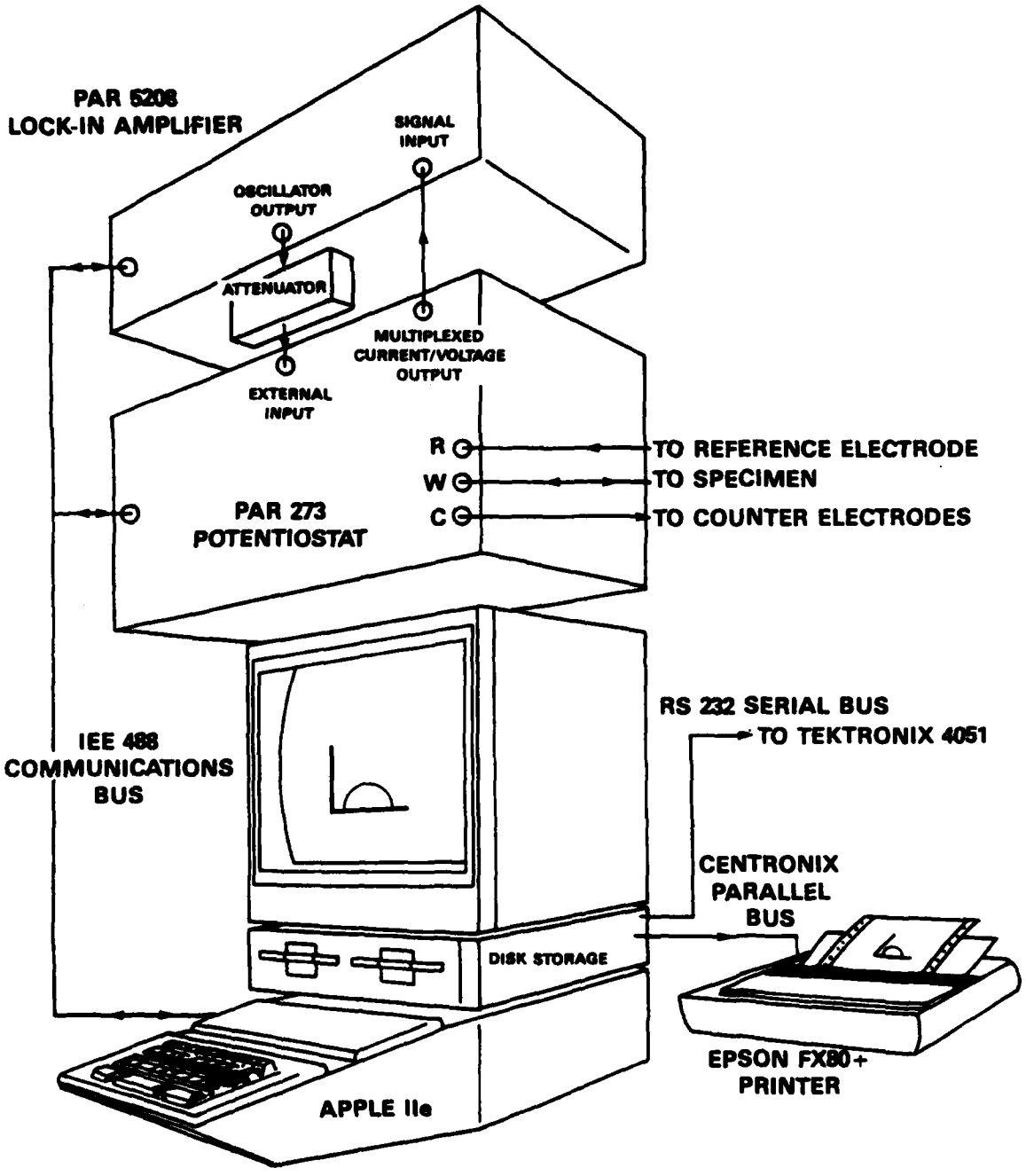

Figure 2.
PAR Impedance Measurement System

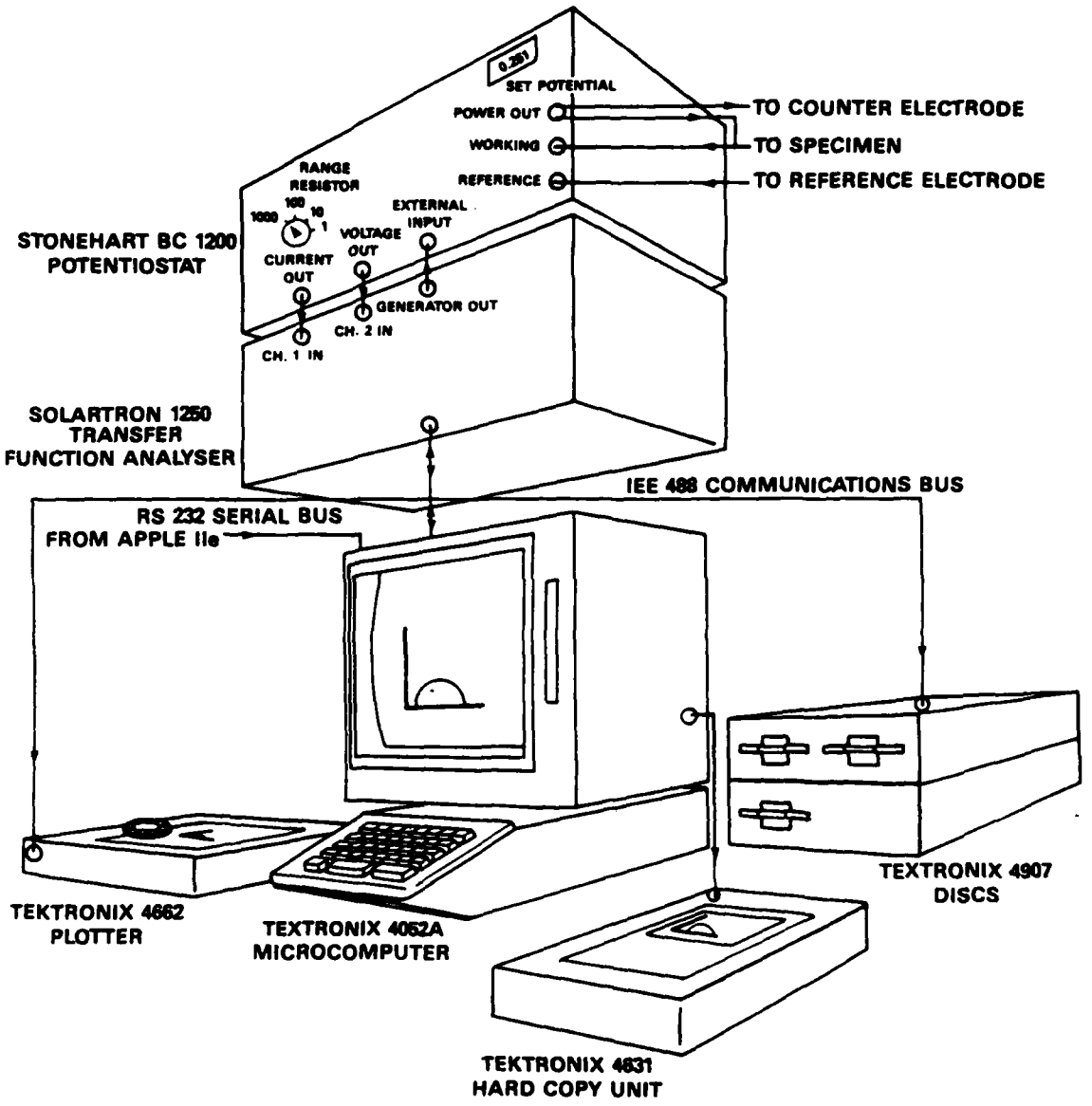

Figure 3.
Solartron Impedance Measurement System

obtained in the first 15 minutes of this interval, however. Thus, for short (1 to 7 hour) exposures the low frequency data may be significantly influenced by exposure time effects. These short exposures tended to have all of the significant data occur above .01 Hz, so this effect in practice was minimal. Exposure time effects would be expected to be insignificant over the 2 hour measurement period for exposures of 24 hours or greater, since the rate of change in the corrosion system decreased with exposure time.

Potentiodynamic polarization curve generation was also used to characterize the materials' corrosion behavior. In this technique the potential of the specimen is varied slowly and linearly over time while the resultant current is being measured. The magnitude of the resultant current gives a measure of the polarization resistance. Cathodic polarization curves were generated in the aerated solution while anodic polarization curves were generated after first deaerating the test cell for one hour with nitrogen or argon which had been dried with Drierite, run over hot copper filings at 300^{o}C to remove residual oxygen, then water saturated by bubbling through distilled water to cool the gas as well as to minimize evaporation from the test cell. During the actual data acquisition process the bubbling device in the cell was not used. Instead the gas was run at a slight positive pressure over the surface of the test solution to prevent re-aeration. This precaution was

necessary to prevent any effects of bubble motion on the fluid dynamics of the rotating disk specimen. Potentiodynamic scans were always conducted from the most electronegative potential to the most electropositive potential at a scan rate of 0.01 $mV\text{-}s^{-1}$. Cathodic curves were generated after holding at the starting potential for 10 minutes to allow for stabilization of the current. This hold time was determined by looking at current stability and curve reproducibility for a number of different hold times. Ten minutes was deemed to be the shortest practical time to get stable, reproducible potentiodynamic curves.

Two different apparatus were used for the potentiodynamic polarization runs. The first was a PAR model 350A corrosion measurement system, which proved to be unreliable. Later runs used a PAR 273 potentiostat with an Apple IIe microcomputer controller and corrosion measurement software supplied by PAR.

Before beginning this study, it was first necessary to verify that the hydrodynamics of the rotating disk apparatus were proper for this type of configuration. A properly functioning rotating disk apparatus should operate according to equations first developed by Levich[85,86] which predict that the disk current should be proportional to the square root of the rotation speed if the reaction limiting the current is controlled by diffusion through the solution:

Levich Equation: $i_L = .62\ n\ F\ A\ D^{2/3}\ v^{-1/6}\ C\ w^{1/2}$ (I)

where: i_L = diffusion limited current density (A/cm^2)

n = number of equivalents per mole (4 for O_2 reduction)

F = Faraday's constant (96487 coulombs/equivalent)

A = area exposed (1.277 cm^2)

D = diffusivity (1.9×10^{-5} cm^2/s for O_2 in water)

v = kinematic viscosity (0.008 cm^2/s for water at 30^oC)

C = concentration in the bulk solution (2.5×10^{-7} mo/cm^3 for O_2 in water at 30^oC)

w = rotation speed in radians per second (pi/30 RPM)

Diffusion limits the cathodic reaction of oxygen reduction in the portion of the polarization curve in which current is essentially potential-independent. Polarization curves were obtained for the purposes of checking the rotating disk equipment at rotation speeds of from 200 to 2500 RPM, and are shown in Figure 4. All curves show a vertical region where diffusion would be expected to control the reaction rate. These curves were then scaled by dividing the observed current densities by the square root of the rotation speed, thus removing the theoretical rotation speed dependence. The result, shown in Figure 5, illustrates that the diffusion-controlled portions of all of the curves

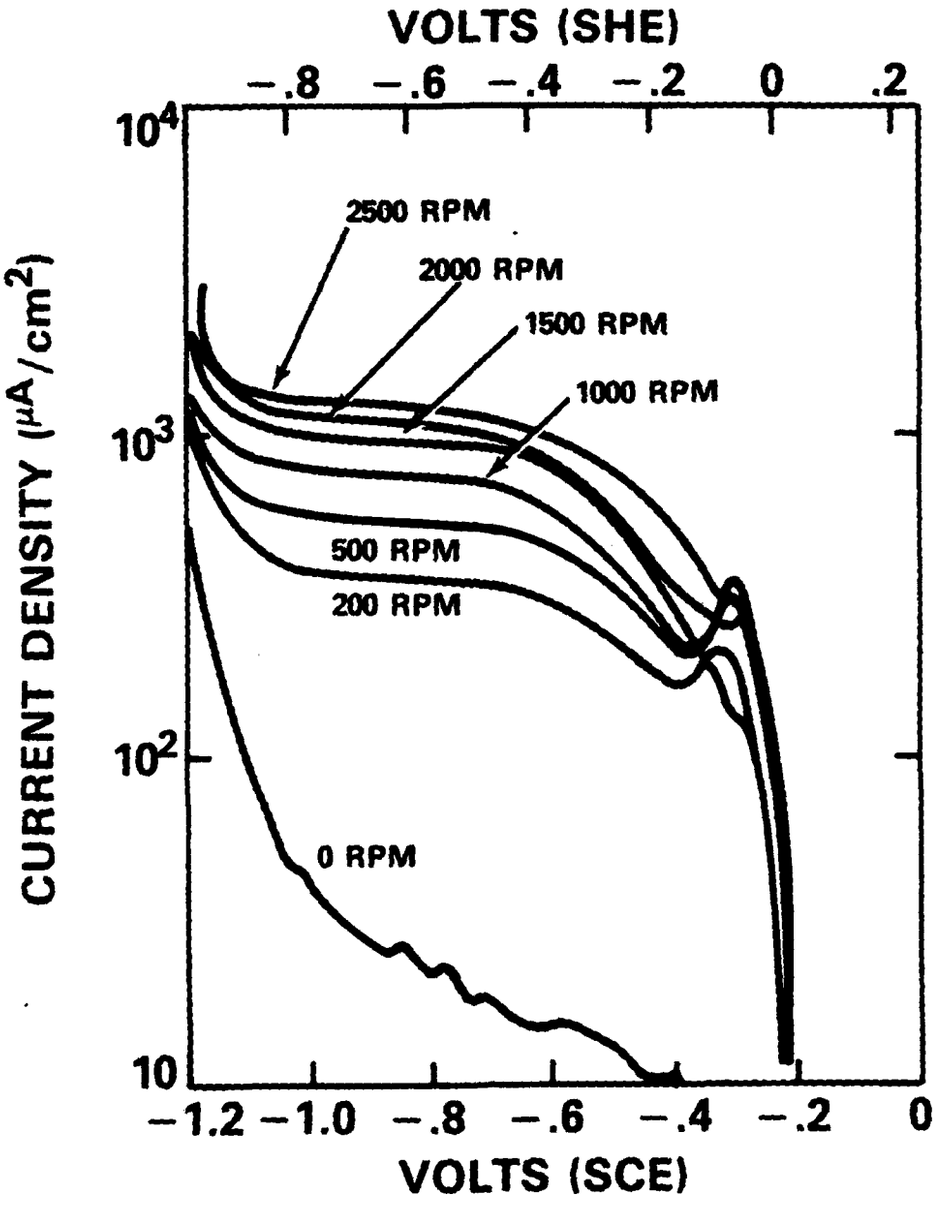

Figure 4.
Cathodic Polarization of 90-10 Copper-Nickel

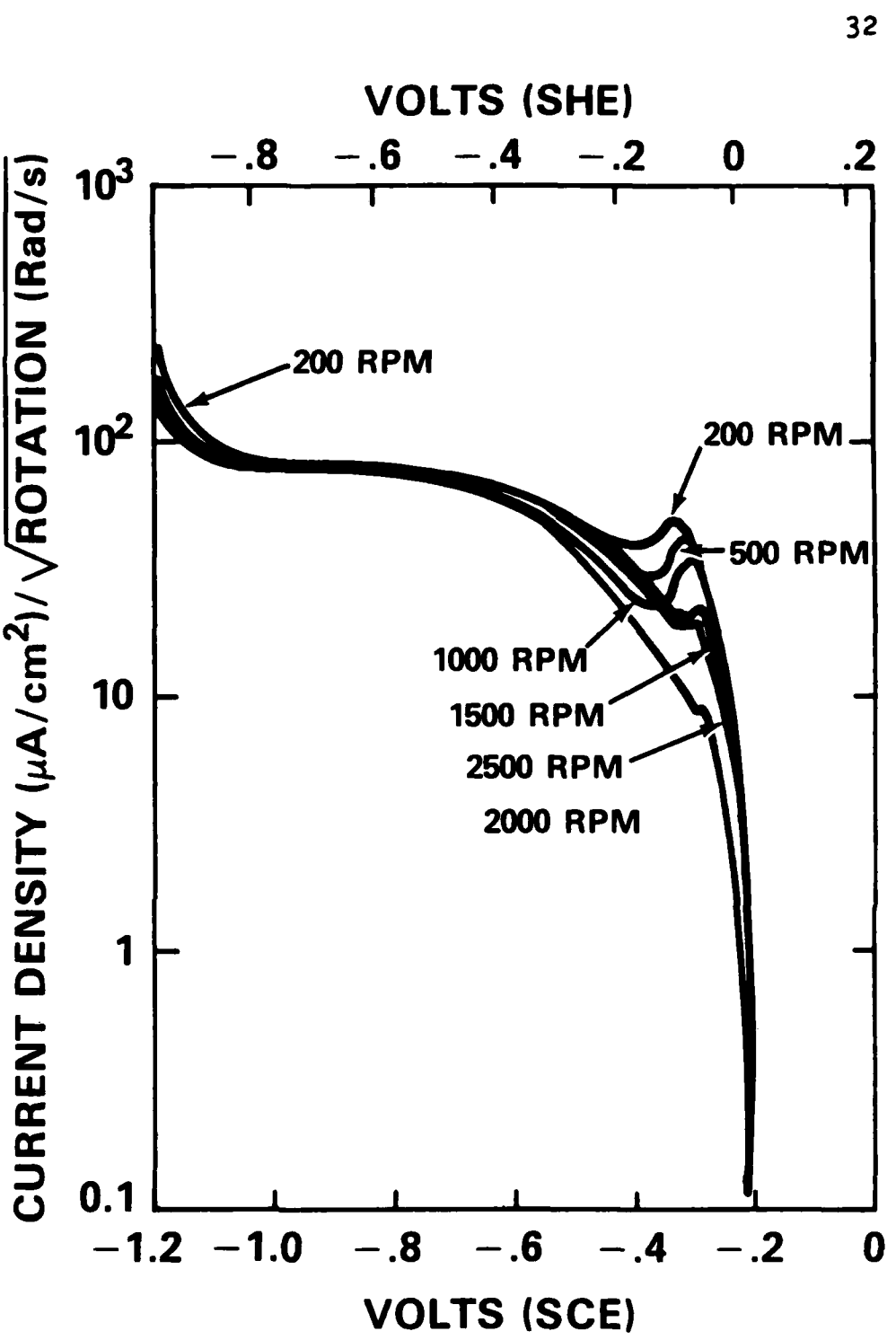

Figure 5.
Rotation Speed Dependence of Polarization of 90-10 Cu-Ni

except one overlap, to within the thickness of the plotter pen. In addition, the value of this overlap point is close to the value of 69 uA/cm^2 calculated from the Levich Equation using the values for the parameters listed above in Equation I. This proves that current in this region is a function of the square root of rotation speed, as predicted if the apparatus were following the Levich Equation. This was considered sufficient verification for this study that the apparatus was behaving as the Levich Equation predicts. The one curve which did not exactly overlap the others was still very close, and was made at the lowest rotation speed, where speed measurement was inaccurate, and where natural convection in the apparatus could have contributed to a larger-than-anticipated current.

It was also necessary to check the performance of the Electrochemical Impedance apparatus before beginning testing. This was done by constructing a variety of dummy cells consisting of networks of known-valued resistors and capacitors. The ideal behavior of these networks was first calculated, then measured using the impedance instrumentation. In all cases, the instrumentation measured the correct value of resistances to within 1% and of capacitances to within about 10%. Since calculated capacitances were not to be used in this study, this was considered sufficient accuracy.

3.3 Experimental Procedure

Initially the polarization behavior of all three alloys was obtained by a series of potentiodynamic tests. The conditions of each test will be discussed in the Results section below. To elucidate the role of the corrosion product film on corrosion behavior, the specimens were next tested using electrochemical impedance spectroscopy after a brief, one hour, exposure where the corrosion resisting character of the corrosion product film presumably was still undeveloped, and again after various exposure periods up to 28 days, when the film was presumably well established. Typically, periods of 1, 3, 7, 24, 31, 48, 72, 144, 168, 192, 216, 242, 314, 337, 362, 386, 411, 433, 457, 482, 504, 532, 578, 604, 640, and 672 hours were used for the impedance runs, although these periods varied somewhat between tests. After growth of the corrosion product layers for 28 days, impedance measurements were taken at rotation speeds of 500 and 2000 RPM. Measurements were then taken at 1000 RPM while the specimen was held potentiostatically, first at 50 mV cathodic to its corrosion potential, and then at 30 mV anodic to this same corrosion potential. Then the loosely adherent layers were stripped off using adhesive poly-tape. This procedure has been shown to remove the outer porous layers of the corrosion products while leaving intact the inner, tightly adherent layer[9,10,14,15]. By comparing the data with no film, a full film, and a stripped

film (inner layer only), the effect of the various film layers could be be studied independently.

A unique method for determining whether the film was limiting the corrosion reaction 1)by an electrically-insulating effect, or 2)by affecting the catalysis of the cathodic reaction, is sputter-coating of palladium on the corrosion product surface. Since palladium is a good catalyst for the cathodic reaction (oxygen reduction), and its use on top of the film would not affect film resistance, this technique provides a good method for separating out the relative effects of these two possible rate-limiting steps. After 28 days of exposure the specimens were tested, lightly rinsed with distilled water, dried in a dessicator overnight, then re-wet and retested to first determine the effect of drying. Although drying the specimens did, in some cases, slightly affect the shape of the impedance curves, this change was small enough to have no bearing on the results reported below. The specimens were next dried again, placed in a device to mask off the specimen holder, then sputter-coated with palladium until the surface appeared silvery in color using a Hummer II sputter-coater manufactured by Technics, Inc.. This usually took 3 to 5 minutes at 20 mA current. The specimen was sputter coated at a 45 degree angle, then reversed and sputter coated at the same angle from the opposite direction. This procedure minimized the possibility of plating through cracks in the film, which could result in

electrical shorting through the film to the metal surface. After testing and stripping off the outer corrosion product layer and the palladium layer, the remaining specimen surface was analyzed for palladium. If palladium had plated through a crack in the corrosion products until it contacted the surface to create an electrical short-circuit through the film, then some palladium should remain on the surface when the outer corrosion product is removed. Analyses were conducted on the copper and the 90-10 copper-nickel sample using energy dispersive x-ray analysis in a scanning electron microscope. For the alloy, the dot-mapping mode was used to try to detect local areas of palladium concentration. Analysis was also conducted on 70-30 copper-nickel using a new technique called energy dispersive x-ray diffraction which uses a broad spectrum X-ray source and an energy dispersive detector at a single angle.[87] Figure 6 shows that less than about 1% palladium was present on the copper surface. Figure 7b shows that no areas of concentration of palladium were present on the 90-10 alloy, while Figure 7a is an image of the surface covered by the scan of 7b. Figure 8 shows that no palladium diffraction lines were observed on 70-30 copper-nickel, indicating a concentration of less than about 5%. These results support the supposition that the sputter-coated palladium film did not develop an electrical short-circuit through the corrosion product layers to the metal surface on any material tested.

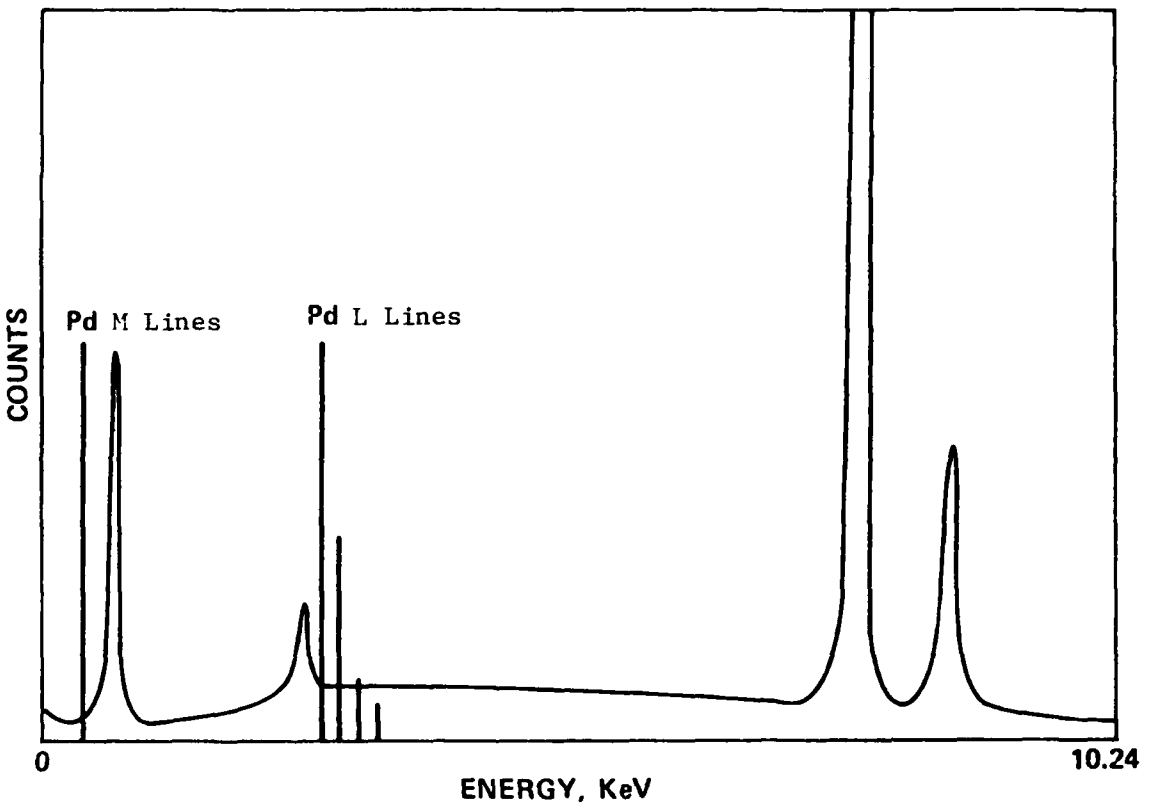

Figure 6.
Energy Dispersive X-Ray Analysis on Stripped Copper

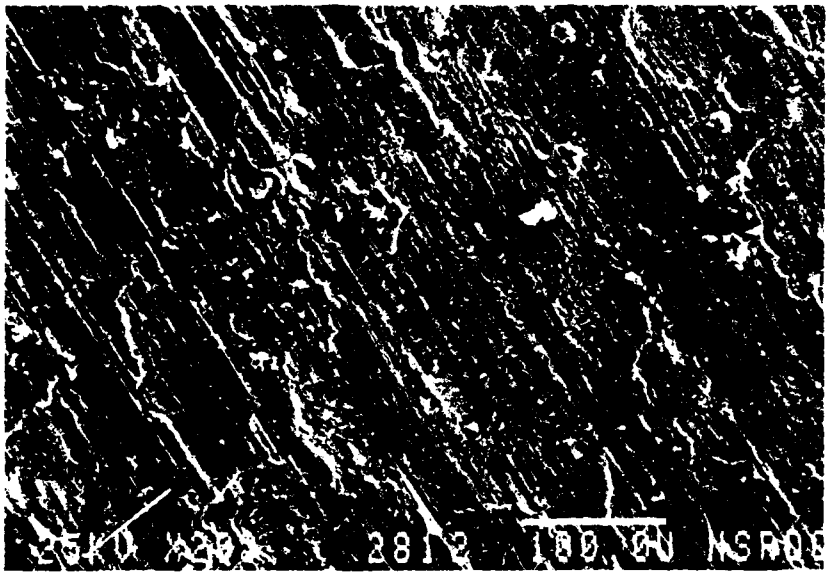

a) Absorbed Electron Image

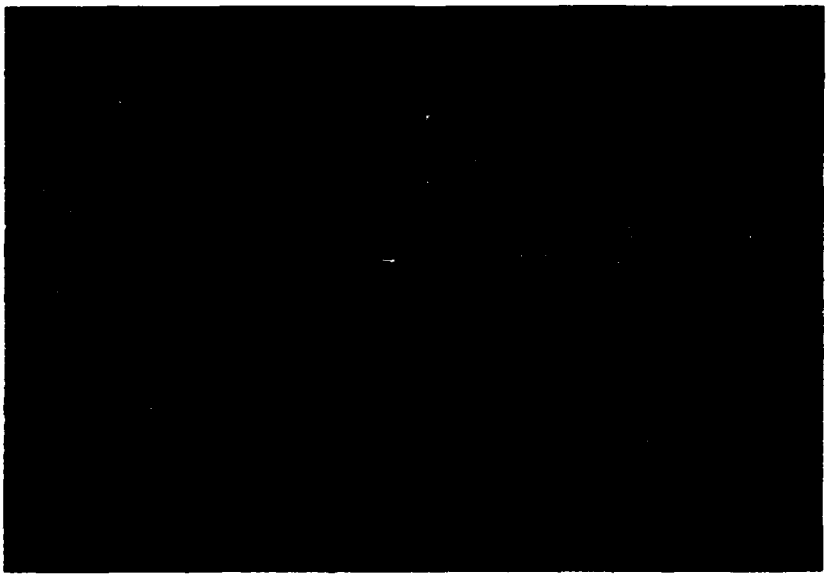

b) X-Ray Map for Palladium

Figure 7.
Energy Dispersive X-Ray Analysis on Stripped 90-10 Cu-Ni

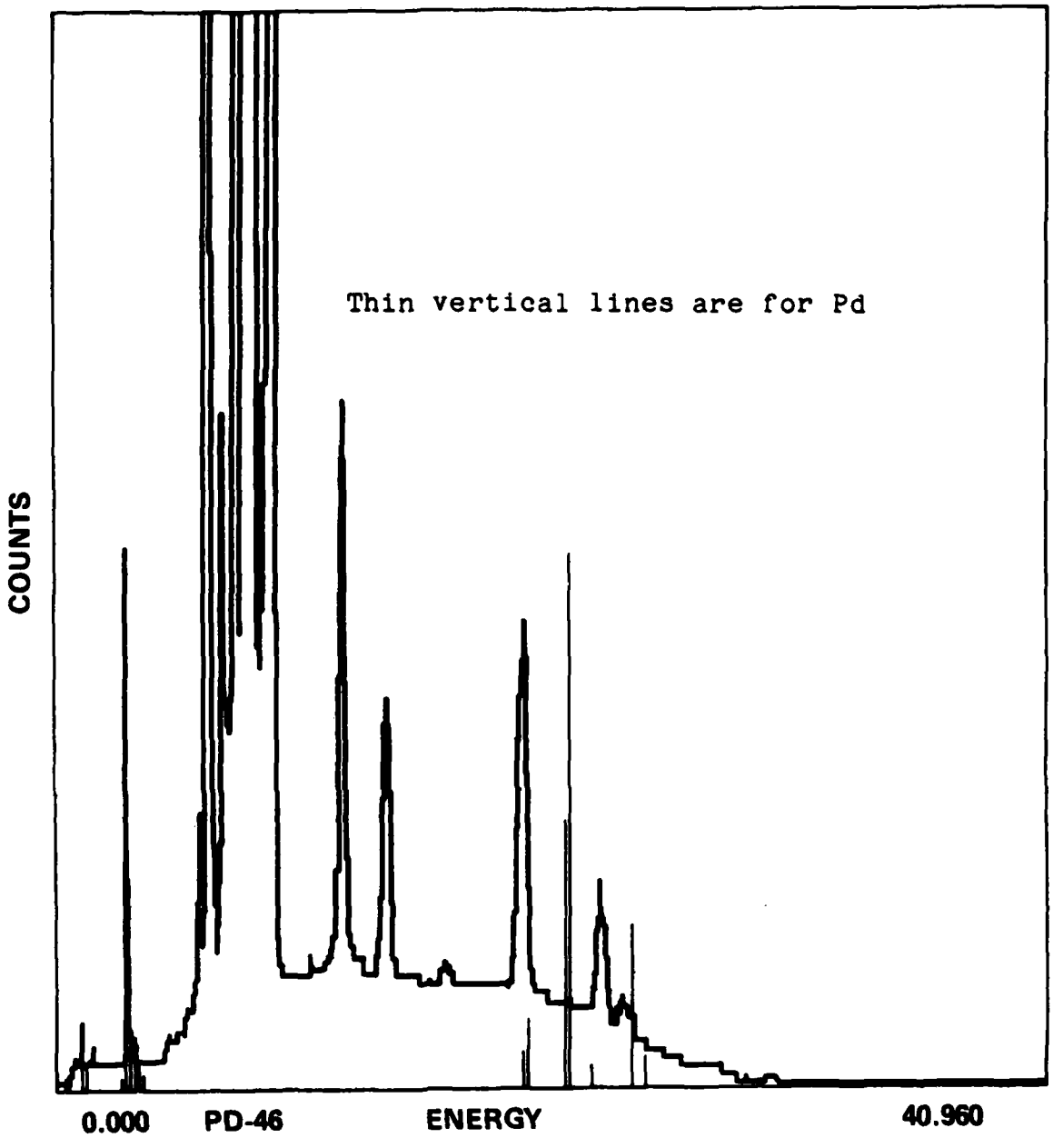

Figure 8.
Energy Dispersive X-Ray Diffraction on Stripped 70-30 Cu-Ni

4. RESULTS AND DISCUSSION

A total of 8 separate 28 day exposures were conducted on copper, 5 on 90-10 copper-nickel, and 3 on 70-30 copper-nickel. Due to the length of these exposures, experimental difficulties were occasionally experienced, making it difficult to get all necessary data from a single exposure. All data from all exposures are not presented herein. Almost all data presented for any material are from the same exposure, which was considered typical for that material. The data presented below is reproducible when experimental difficulties are not encountered, and typical of the behavior in all of the exposures for that material.

Mathematical modelling of a rotating disk of copper in HCl was conducted as a first step in understanding copper corrosion behavior before corrosion products form in saltwater. This analysis is in Appendix A. Since the model breaks down when the diffusivity of chloride ions is greater than twice that of a chloride ion complex, the analysis was not extended to include Na and OH^- ions found in saltwater. Another attempt to look at the rate controlling step in the dissolution of the copper-nickels was made using anodic etching, shown in Appendix B. Although yielding some interesting results, this technique could not adequately distinguish between the rate-limiting steps of interest, and was not developed further.

4.1 Copper

Figure 9 presents the results of a slow (0.03 mV/s) potentiodynamic scan for a freshly exposed (10 minutes) copper specimen in de-aerated saltwater. The copper has an anodic Tafel slope of 58 mV per decade, consistent with a diffusion-controlled reaction. This slope is similar to the 58-62 mV per decade found in acid chlorides[26,35-39,41,42] and neutral chlorides.[55,60,61] The effect of rotation speed of the disk on polarization behavior is difficult to determine, since scaling the currents by the square root of the rotation speed leads to roughly the same separation of the curves. The curves are therefore not inconsistent with rotation speed dependence as predicted by diffusion control.

Figure 10 shows the impedance results for copper. This figure, known as a Nyquist plot[69,75], shows the relationship between real and imaginary components of impedance as the frequency is changed. The curve as plotted is a series of straight lines connecting all of the data points. Data scatter tends to increase at lower frequencies, leading to complicated curve shapes on the right side of the semicircles. The lowest value of the intercept on the real axis indicates an compensated cell resistance that is consistently around 5-6 ohms, which is negligible. The highest value of the intercept on the real axis is, in this case of low solution resistance, the polarization resistance of the alloy. Corrosion rate is related to the reciprocal

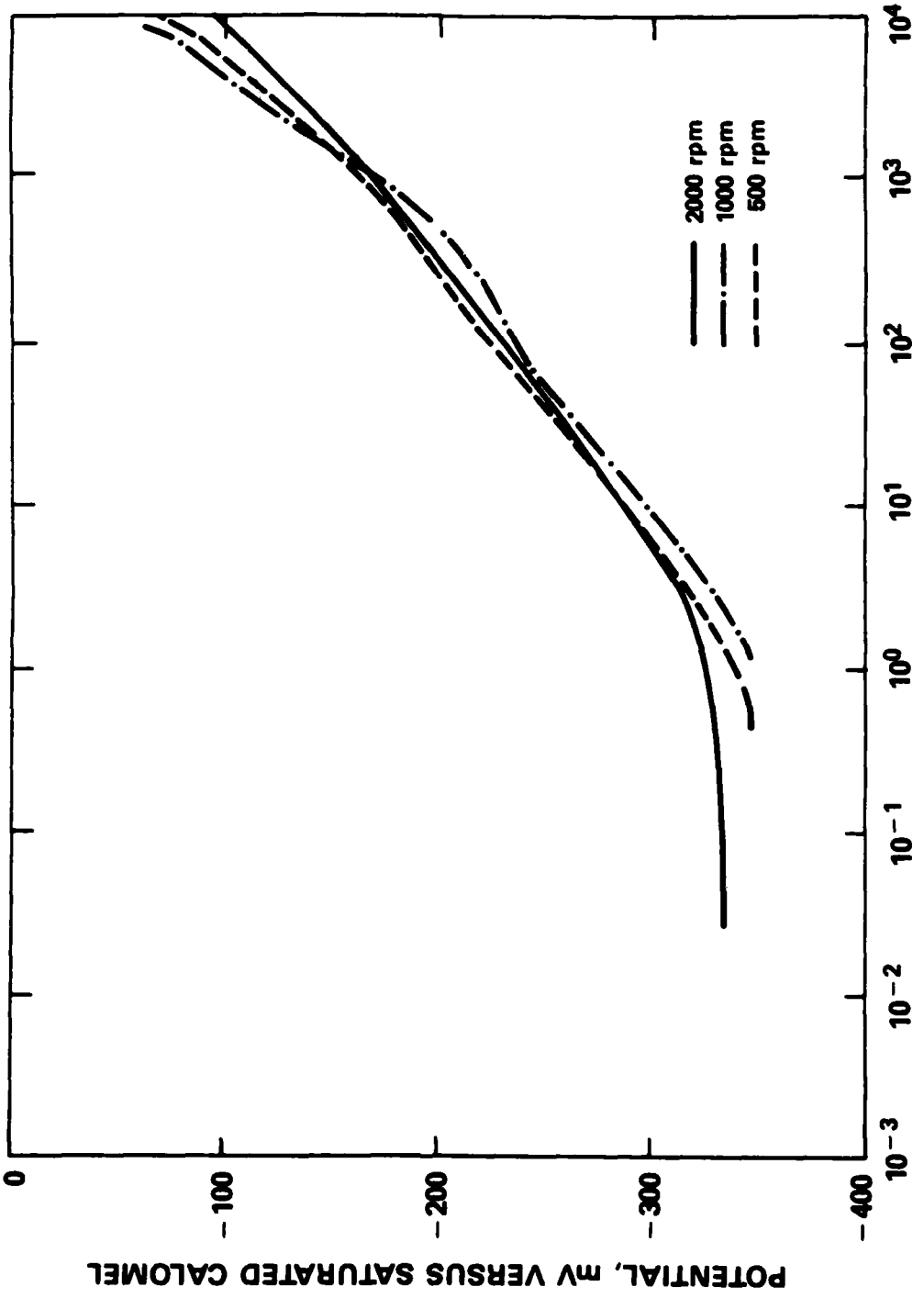

Figure 9.
Potentiodynamic Scan for Copper in Deaerated Saltwater

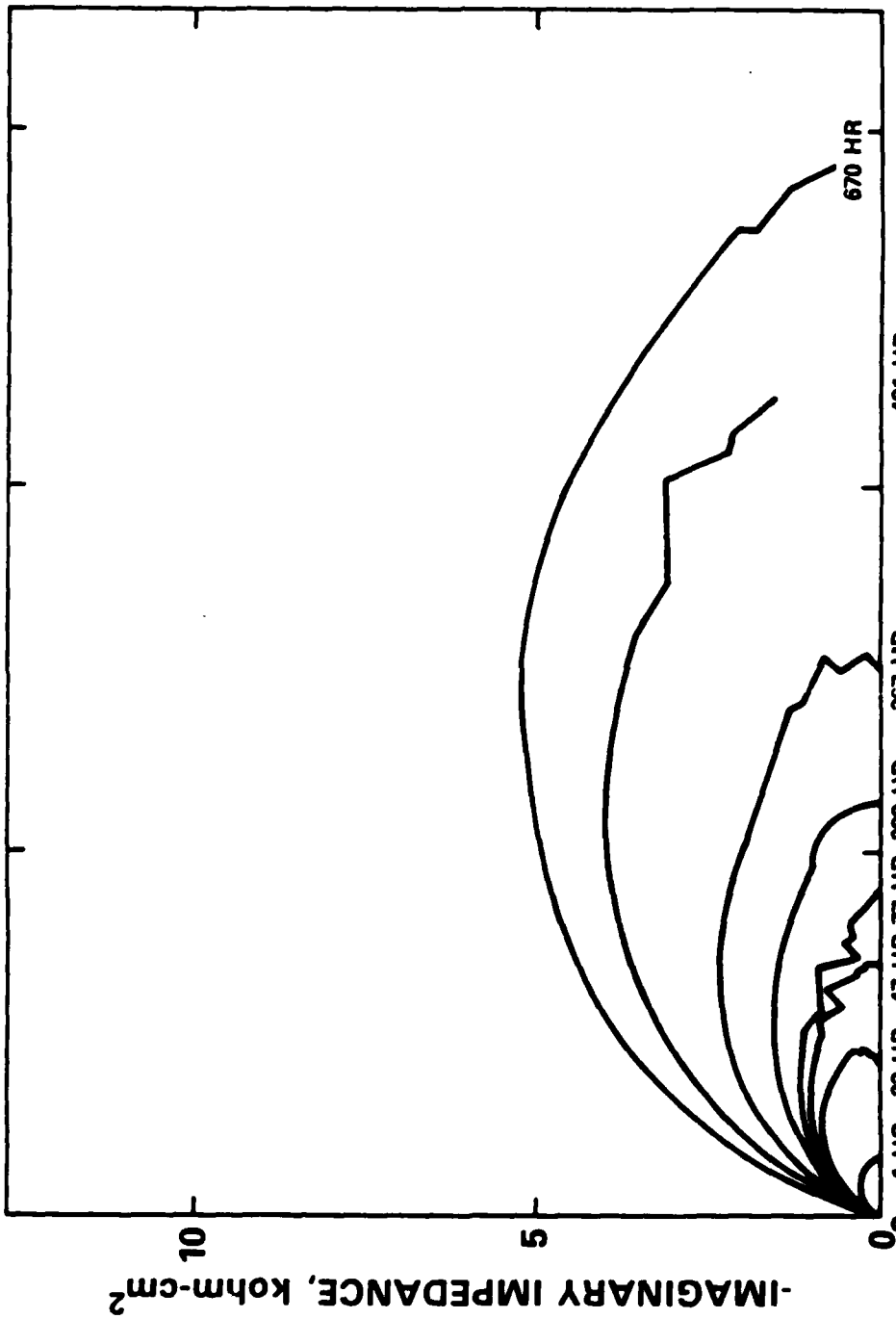

Figure 10.
Effect of Time on Nyquist Curves for Copper - First Exposure

of polarization resistance through the Stearn-Geary Equation. Figure 11 is a Bode phase plot that shows the phase shift between the applied voltage and the current response as a function of frequency. Each peak results from a capacitive process with a unique time constant.

Figure 10 shows the effect of exposure time on the impedance behavior of copper at 1000 RPM. Each curve has only one semicircle, thus only one time constant is present. The polarization resistance increased systematically with exposure time from less than 1 kohm-cm^2 after one hour up to about 15 kohm-cm^2 after 670 hours. Figure 11 is a Bode Phase plot showing the phase shift as a function of frequency for a number of exposure durations. A single phase shift peak is seen, indicating the presence of only one time constant. This peak is centered at 500 Hz after one hour, and systematically shifts to lower frequencies as exposure time increases, reaching 5 Hz after 670 hours of exposure. This shift to lower frequencies is an indication of the increased polarization resistance, and can occur without a shift in interfacial capacitance.

Figure 12 is a plot of the polarization resistance versus exposure time in a log-log format. Linear kinetics, as expected from time-independent catalytic control of the corrosion reaction, is indicated by a slope of 1 on this plot. Parabolic kinetics, as expected from film-diffusion controlled reactions, is indicated by a slope of 0.5 on this plot. A slope of 0.5 provides a reasonable fit to the data,

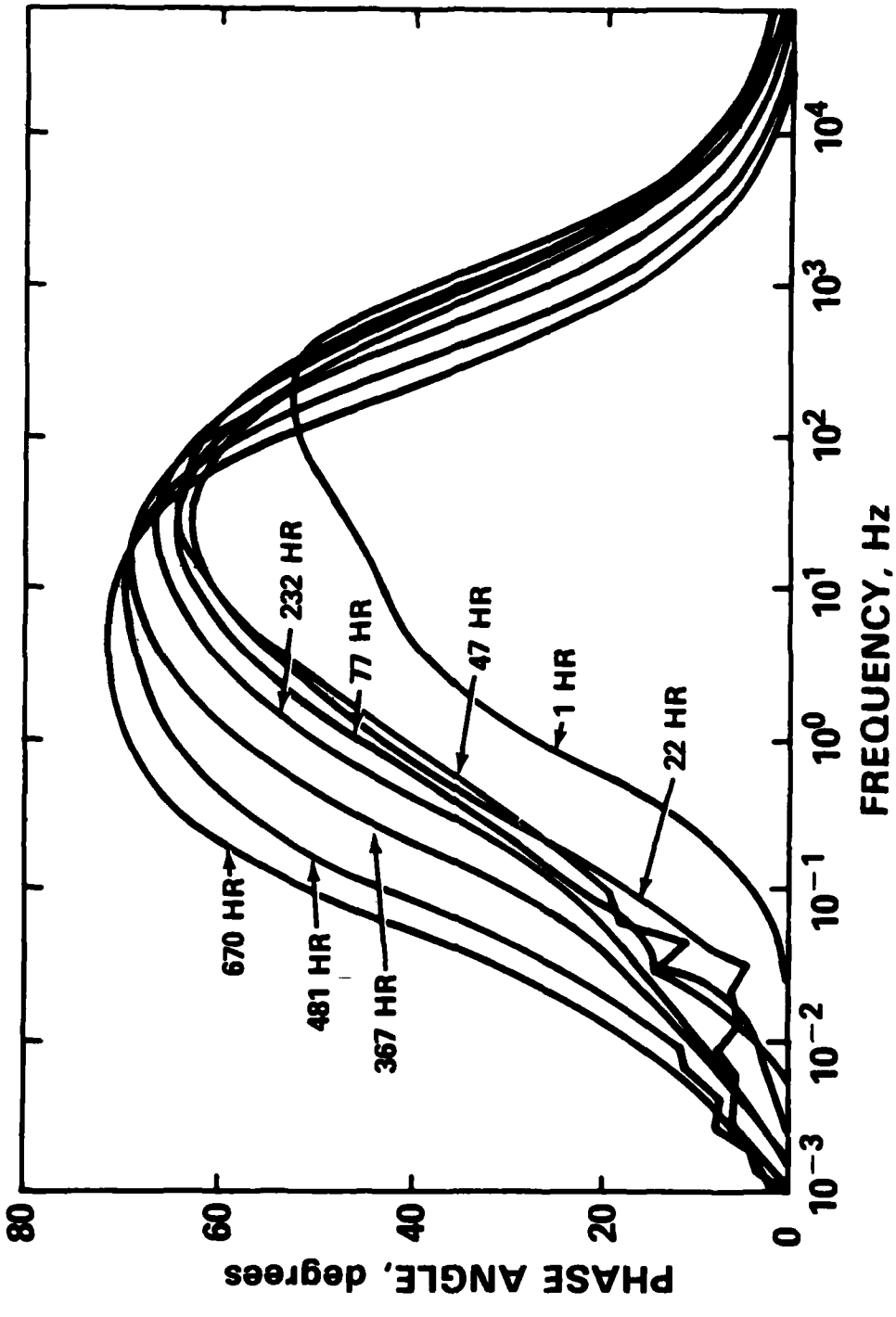

Figure 11.
Effect of Time on Bode Curves for Copper - First Exposure

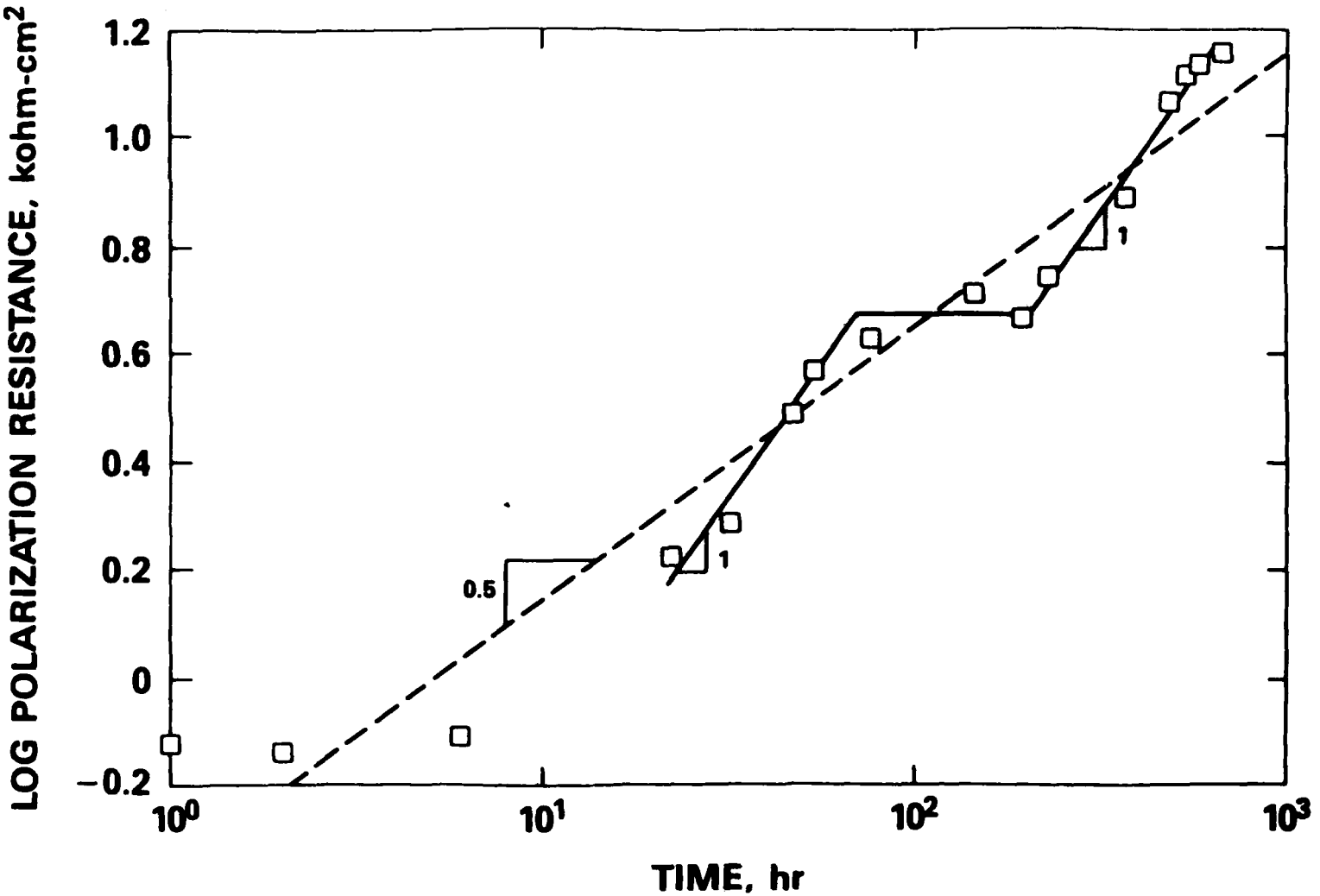

Figure 12.
Polarization Resistance of Copper in Saltwater - First Exposure

however, a slope of 1 could fit these data even better if it is assumed that several times during the test a portion of the corrosion product film was stripped off due to the flow. This is reasonable considering the lack of tenacity of the cupric hydroxy-chloride layer that formed on this material. A regression fit to the points gives a slope between 0.5 and 1. Thus, a conclusion cannot be reached about the type of reaction kinetics based solely on impedance increases.

The copper specimen in this exposure developed a green cupric hydroxy-chloride corrosion product layer over a reddish-brown cuprous oxide. In other, supposedly identical, exposures of the same copper specimen, the hydroxy-chloride deposited not on the specimen surface, but on the specimen holder and glassware. The reason for this behavior difference may be due to poor adherence of the outer film, which may be prevented from developing by minor differences in temperature or flow caused by small changes in specimen flatness, surface finish, or wobble during rotation. When the hydroxy-chloride did not deposit on the specimen, different electrochemical behavior was observed.

Figures 13 and 14 present impedance data for exposure of copper under supposedly identical conditions, but where the hydroxy-chloride did not deposit on the specimen surface. The polarization resistance, as determined from Figure 13, did not change significantly during the exposure, remaining near 1 kohm-cm^2. The phase behavior also did not change significantly with increasing exposure duration.

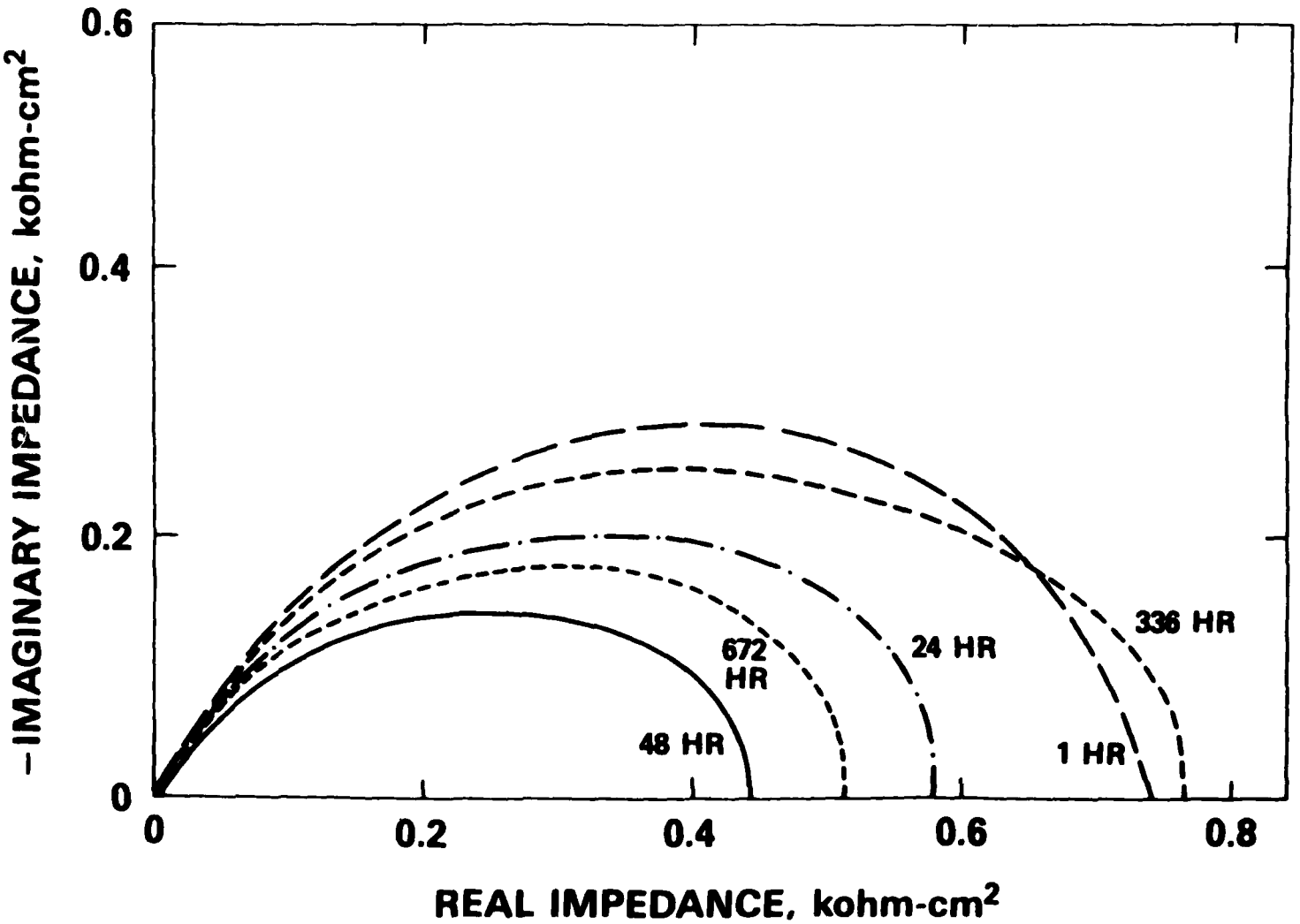

Figure 13.
Effect of Time on Nyquist Curves for Copper - Second Exposure

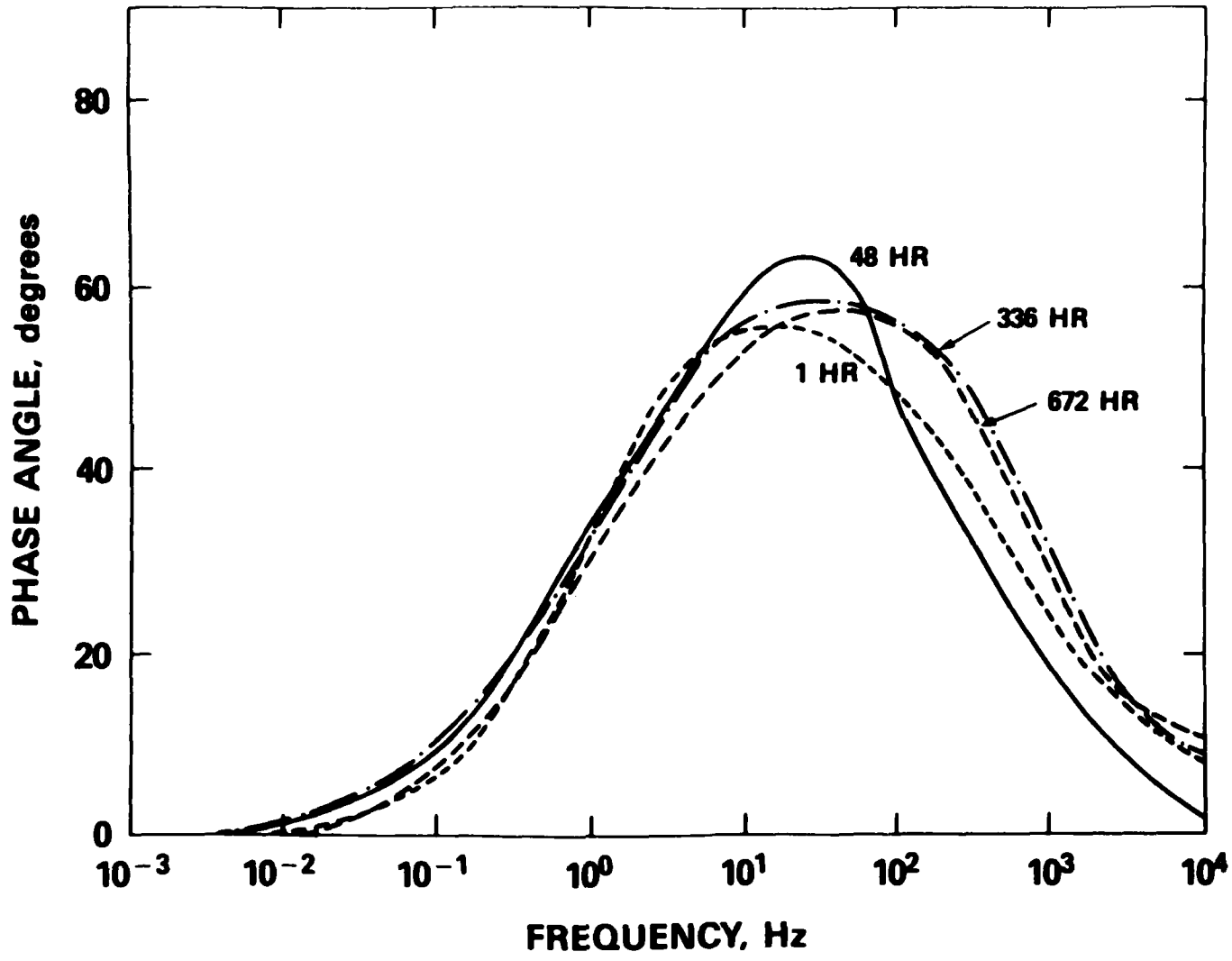

Figure 14.
Effect of Time on Bode Curves for Copper - Second Exposure

Figure 15 presents a plot of polarization resistance versus duration for this exposure. There is considerable data scatter for this technique, which should be able to measure resistance to better than 1%. This scatter must therefore be due to instability of the corrosion system. All data are well within the range for corroding material and never reach values indicative of protection. This implies that there was no significant effect of exposure duration on polarization resistance. Thus, the process that allows formation of the hydroxy-chloride layer must be causing the increased polarization resistance in the first exposure.

Figures 16 and 17 present the results of varying rotation speed or applying a DC Bias on the impedance behavior in the copper exposure with a well developed hydroxy-chloride corrosion product film. Changing rotation speed to 500 or 2000 RPM showed no effect in either plot. This indicates that the corrosion reactions are not controlled by diffusion through a fluid boundary layer, but by a surface process such as diffusion through a corrosion product, surface adsorption or desorption, or electron exchange. A 50 mV cathodic bias from the corrosion potential superimposed on the sinusoidal applied signal should suppress any anodic reactions, but had no effect on the resulting impedance spectra. Half of this amount of bias, 30mV, in the anodic direction should mildly suppress the cathodic reaction. This resulted in a considerable change in both plots of the impedance data. Thus, the

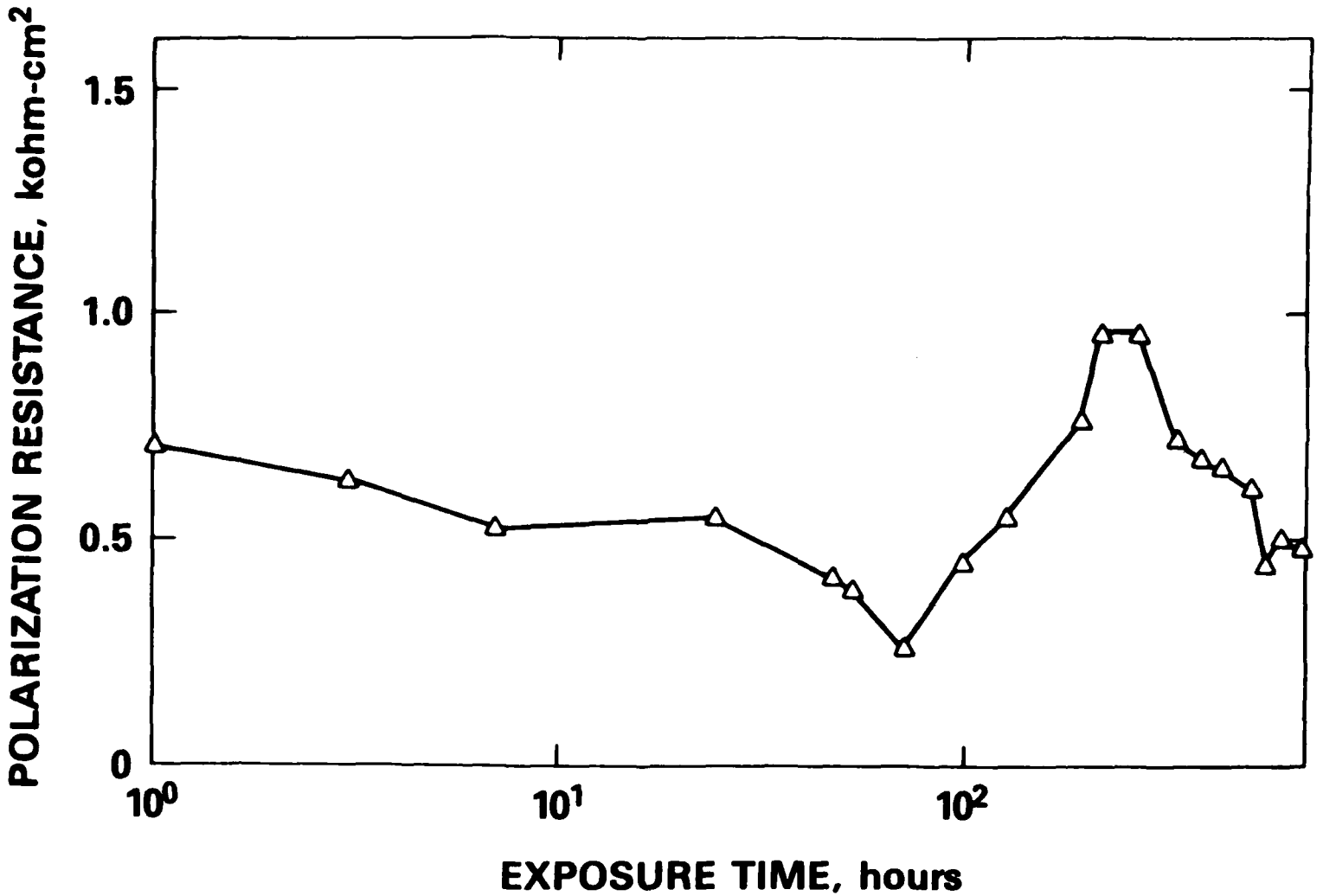

Figure 15.
Polarization Resistance of Copper in Saltwater - Second Exposure

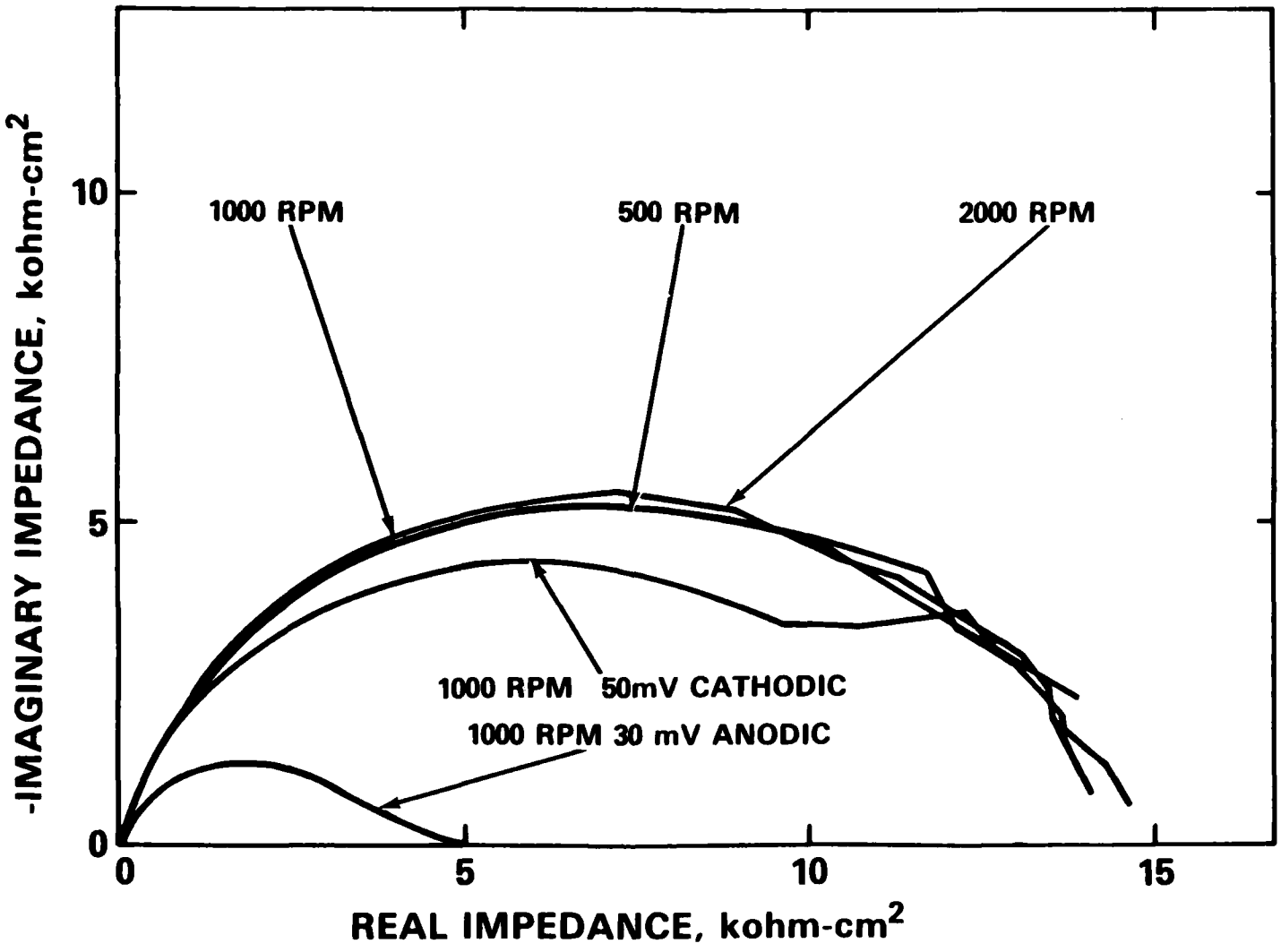

Figure 16.
Effect of Rotation and Bias on Nyquist Curves for Copper - First Exposure

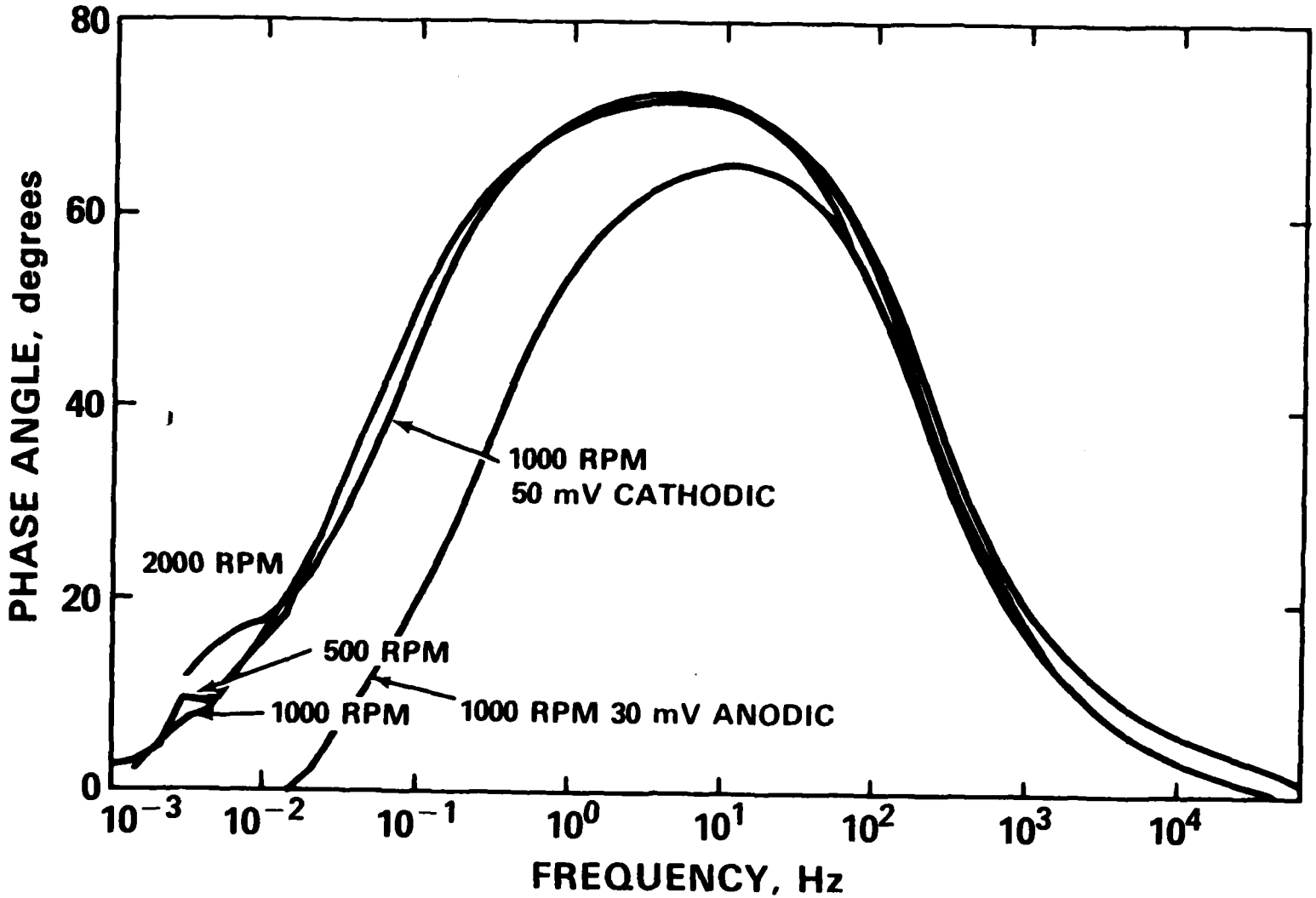

Figure 17.
Effect of Rotation and Bias on Bode Curves for Copper - First Exposure

cathodic reaction controls corrosion on pure copper in saltwater.

Figures 18 and 19 present the results of similar tests for the copper exposure where a cupric hydroxy-chloride layer did not develop on the specimen surface. Here the behavior is somewhat different. Increasing rotation speed decreased the polarization resistance by a factor large enough to suggest some reaction control by boundary layer diffusion, but less than that predicted by the Levich equation[85]. Thus, the reaction on this material must be under mixed control, with diffusion through a Nernst-like fluid boundary layer being one of the slow steps. Cathodic bias to suppress the anodic reaction, although altering the shape of the Nyquist semicircle somewhat, caused little change in the polarization resistance of copper in this exposure. Anodic bias to depress the cathodic reaction had a large effect on the polarization resistance, indicating that corrosion is controlled by the cathodic reaction. The height of the peak in the Bode plot varies directly as the magnitude of the cathodic reaction, indicating that the cathodic reaction is causing this peak.

Figures 20 and 21 present the results of palladium coating and stripping of the corrosion product layers in the first type of copper exposure. Palladium coating over the corrosion product slightly increases the polarization resistance, probably because of the barrier effect of the coating to oxygen diffusion. Thus, the catalytic nature of

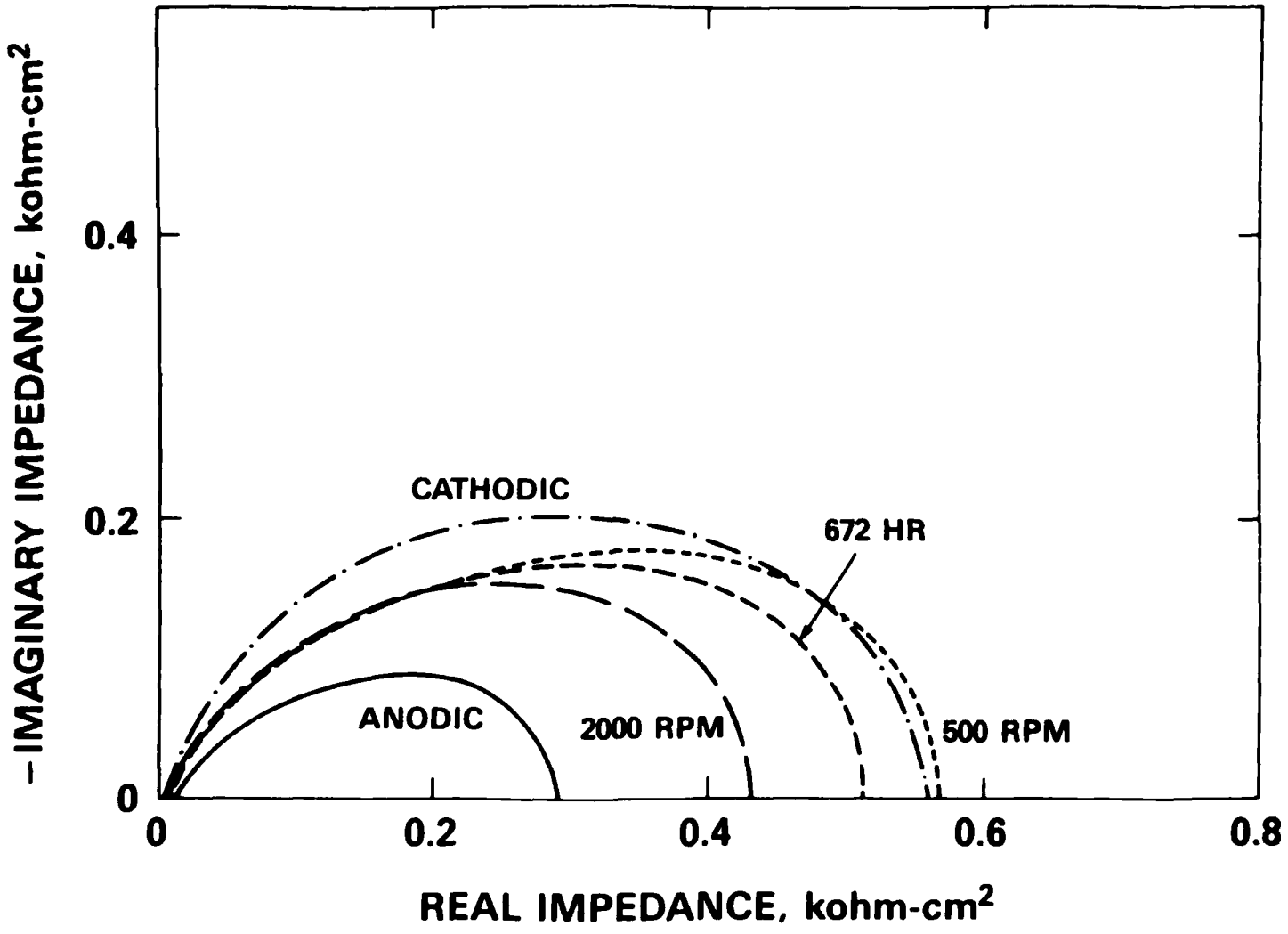

Figure 18.
Effect of Rotation and Bias on Nyquist Curves for Copper - Second Exposure

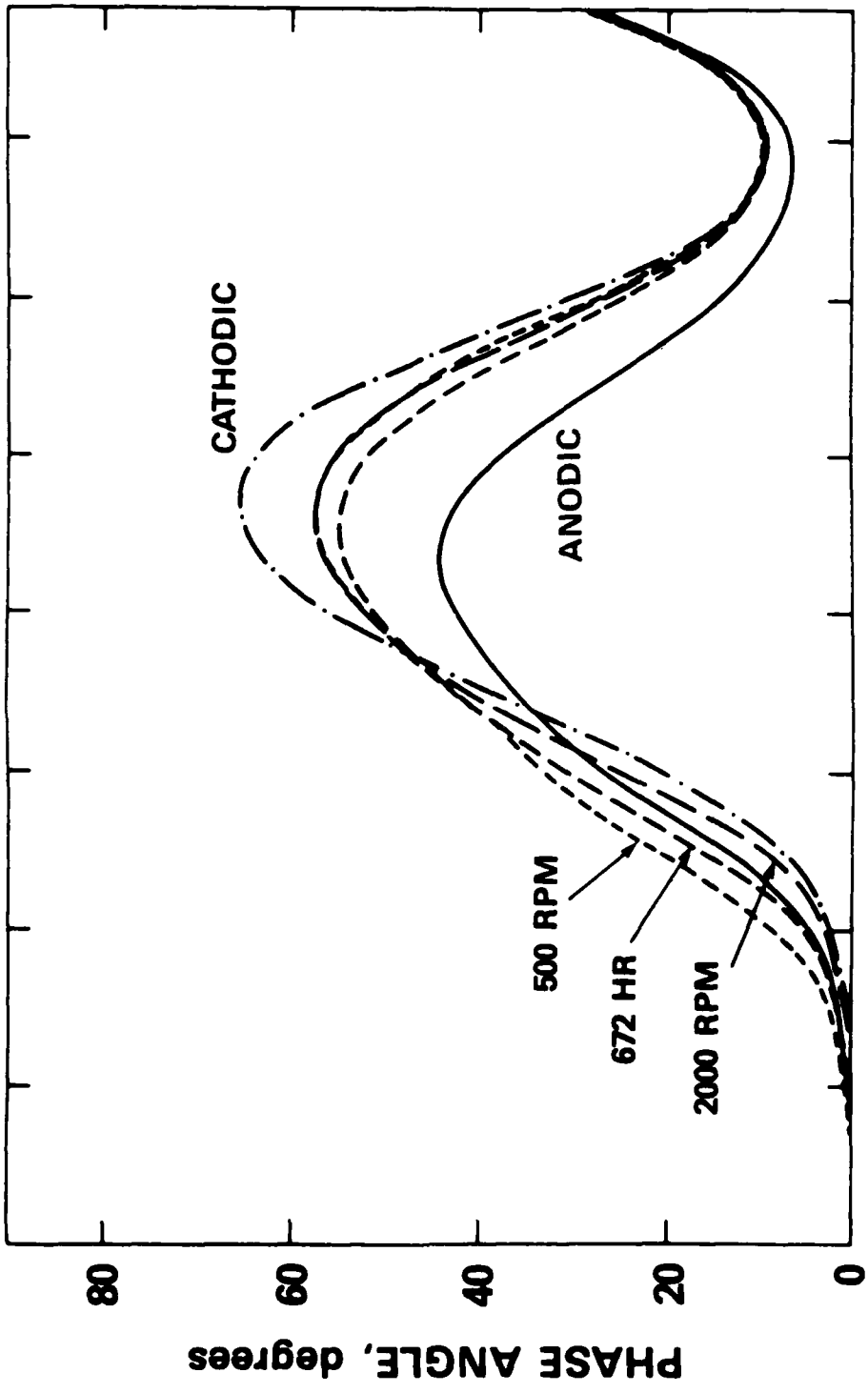

Figure 19.
Effect of Rotation and Bias on Bode Curves for Copper - Second Exposure

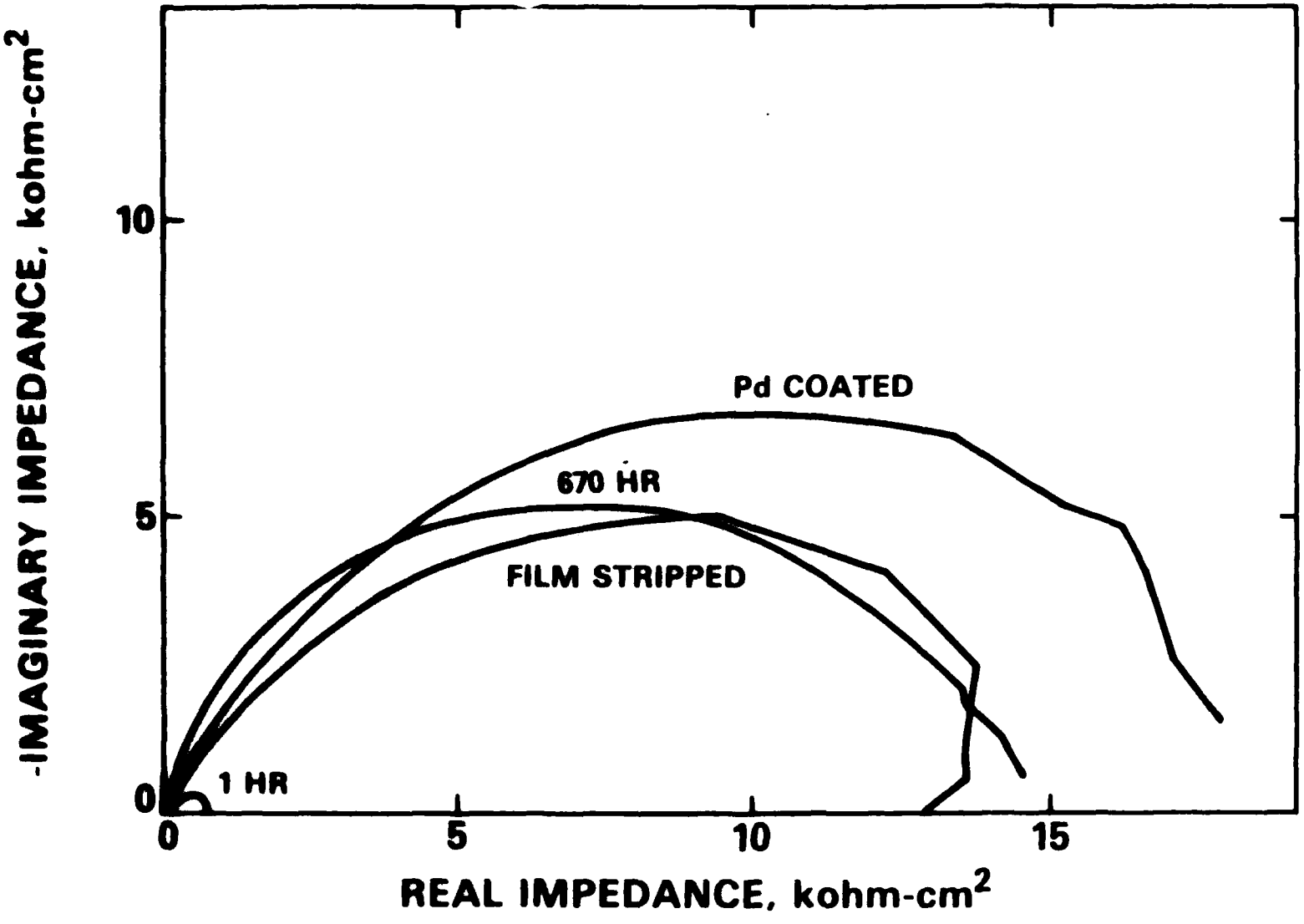

Figure 20.
Effect of Palladium Coating and Stripping on Nyquist Curves for Copper - First Exposure

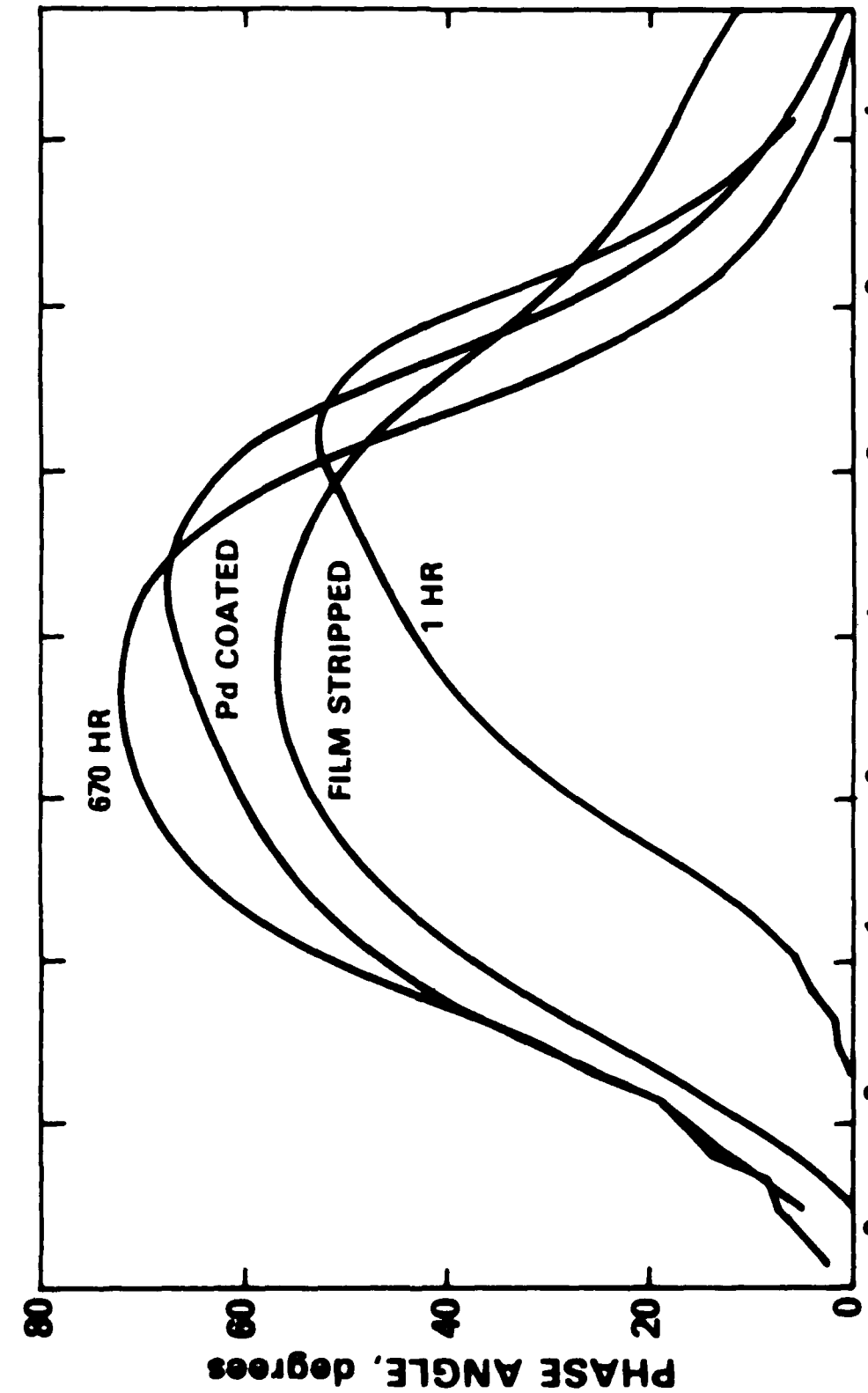

Figure 21.
Effect of Palladium Coating and Stripping on Bode Curves for Copper - First Exposure

this layer for the oxygen reduction reaction must be unimportant in the control of the overall reaction rate of copper. It follows that the corrosion reaction on copper must be controlled by diffusion through, or catalysis on the surface of, the inner corrosion product layer. Removal of the outer layer has little effect on the polarization resistance. Figure 21 illustrates that palladium coating and stripping of the outer corrosion product also had little effect on the value of the time constant.

Figure 22 is a composite of a number of polarization curves generated during the first type of exposure of copper. The intersection of the anodic curve with the cathodic curve for the material under the same conditions roughly defines a current density which can be related through Faraday's Law to the corrosion rate of the material under those conditions. The current density for copper exposed for 1 hour (curve labeled FRESH) was about 30 $uA\text{-}cm^{-2}$, and has a limiting value of cathodic current density of about 100 $uA\text{-}cm^{-2}$. The limiting value for cathodic current density based on oxygen diffusion calculated from the Levich Equation[85] is about 310 $uA\text{-}cm^{-2}$ at 1000 RPM on a disk electrode. All other curves intersect at a value of 2-5 $uA\text{-}cm^{-2}$ except for those for a palladium coated surface, where intersection was not obtained. As with the impedance data, this shows that palladium coating or stripping of the outer corrosion product film had little effect on the corrosion rate of copper exposed for 672

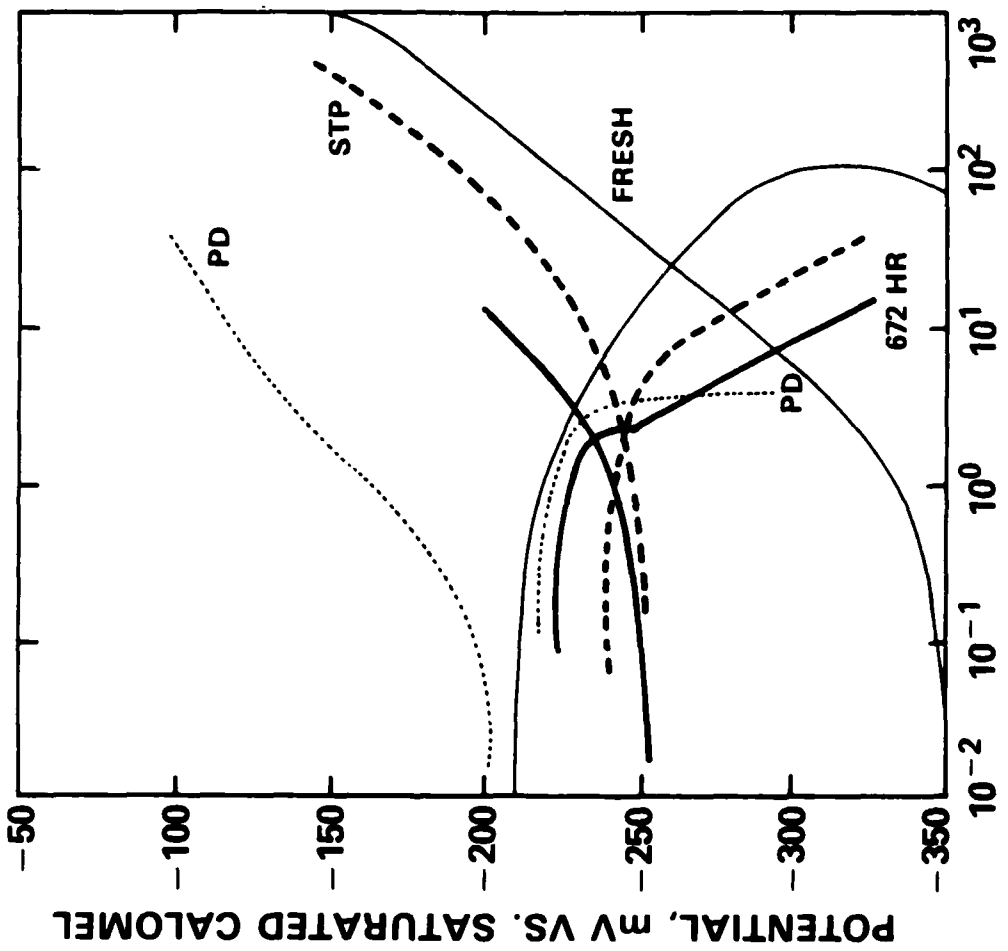

Figure 22.
Polarization Behavior of Copper - First Exposure

hours. Notice that 2-5 uA-cm^{-2} is equivalent to a corrosion rate of 2-5 mils per year. This is very close to the reported corrosion rate range for copper of 1-4 mils per year[88].

Figures 23 and 24 illustrate that, although initially appearing identical to the first type of exposure, when the specimen did not develop the hydroxy-chloride layer then it also did not show any significant change in impedance behavior with increasing exposure time. Attempting to strip the brown outer layer did not remove much material, and also did not cause a significant change in impedance behavior. Thus, the process that forms the hydroxy-chloride layer appears to also form a barrier to the corrosion reaction of copper on the inner layer. This is supported by the polarization data in Figure 25, where the corrosion current was between 10-30 uA-cm^{-2} regardless of exposure time, stripping of the outer film, or palladium coating.

4.2 90-10 Copper-Nickel

Figure 26 shows the results of slow potentiodynamic scans on freshly exposed 90-10 copper-nickel as a function of disk rotation speed. The Tafel slope at low overpotentials is rotation-speed independent at a value of 53 mV per decade, somewhat lower than the value found by Kato and Pickering of 60-62 mV per decade.[14] At higher overpotentials, an area of passivity is present at the

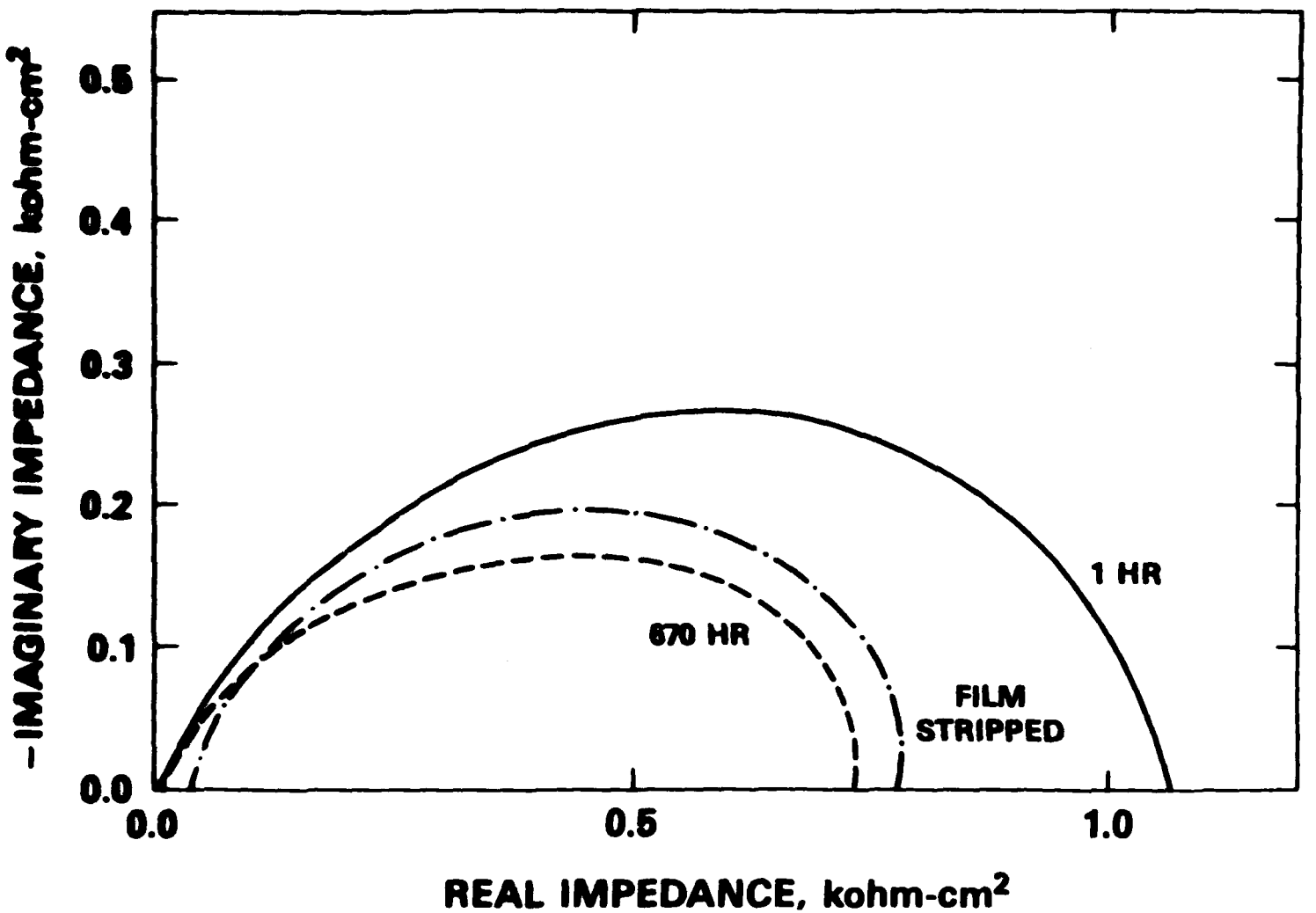

Figure 23.
Effect of Palladium Coating and Stripping on Nyquist Curves for Copper - Second Exposure

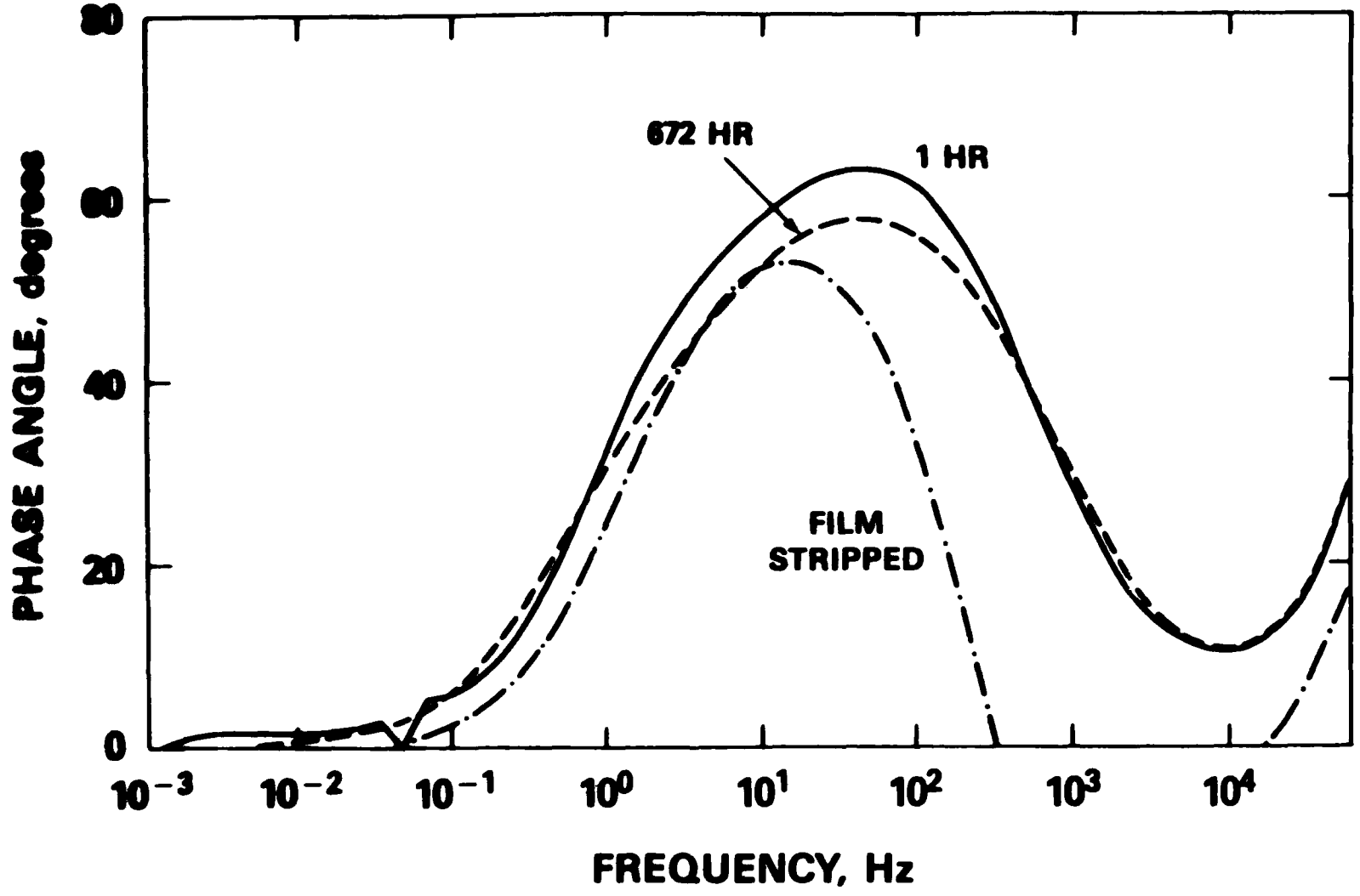

Figure 24.
Effect of Palladium Coating and Stripping on Bode Curves for Copper - Second Exposure

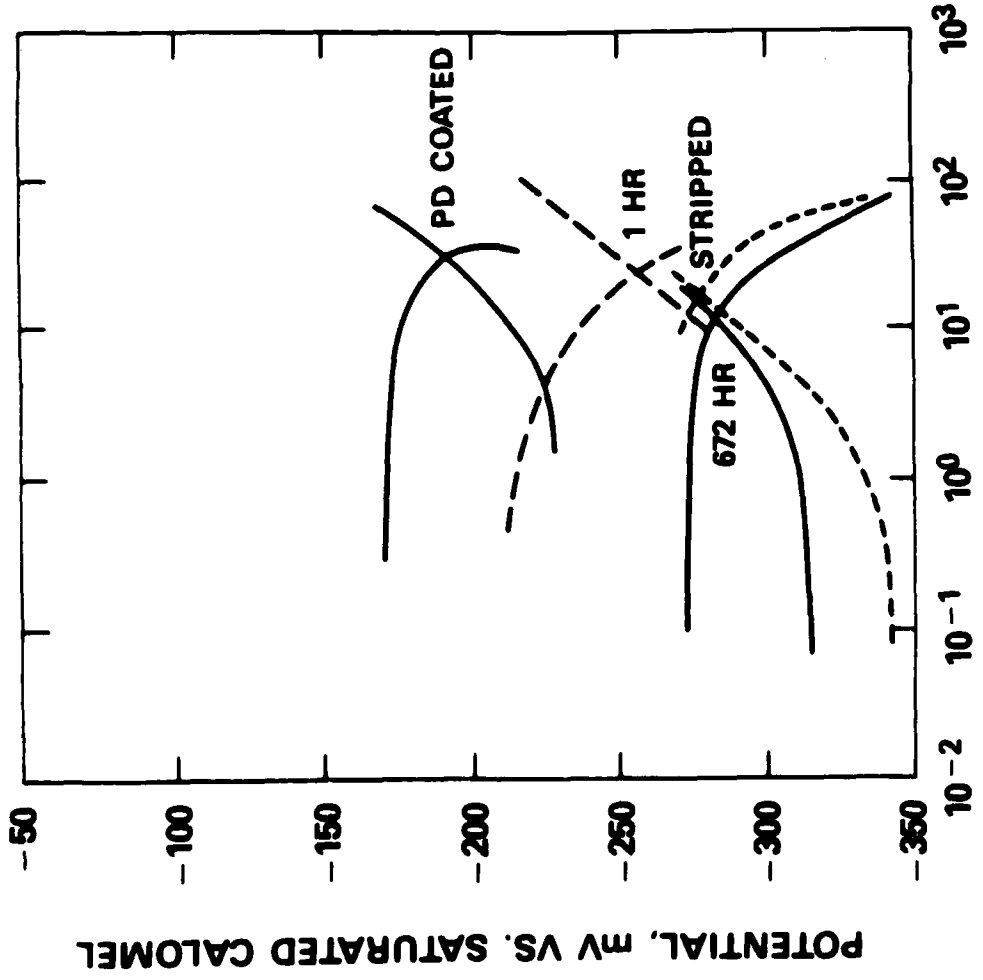

Figure 25.
Polarization Behavior of Copper - Second Exposure

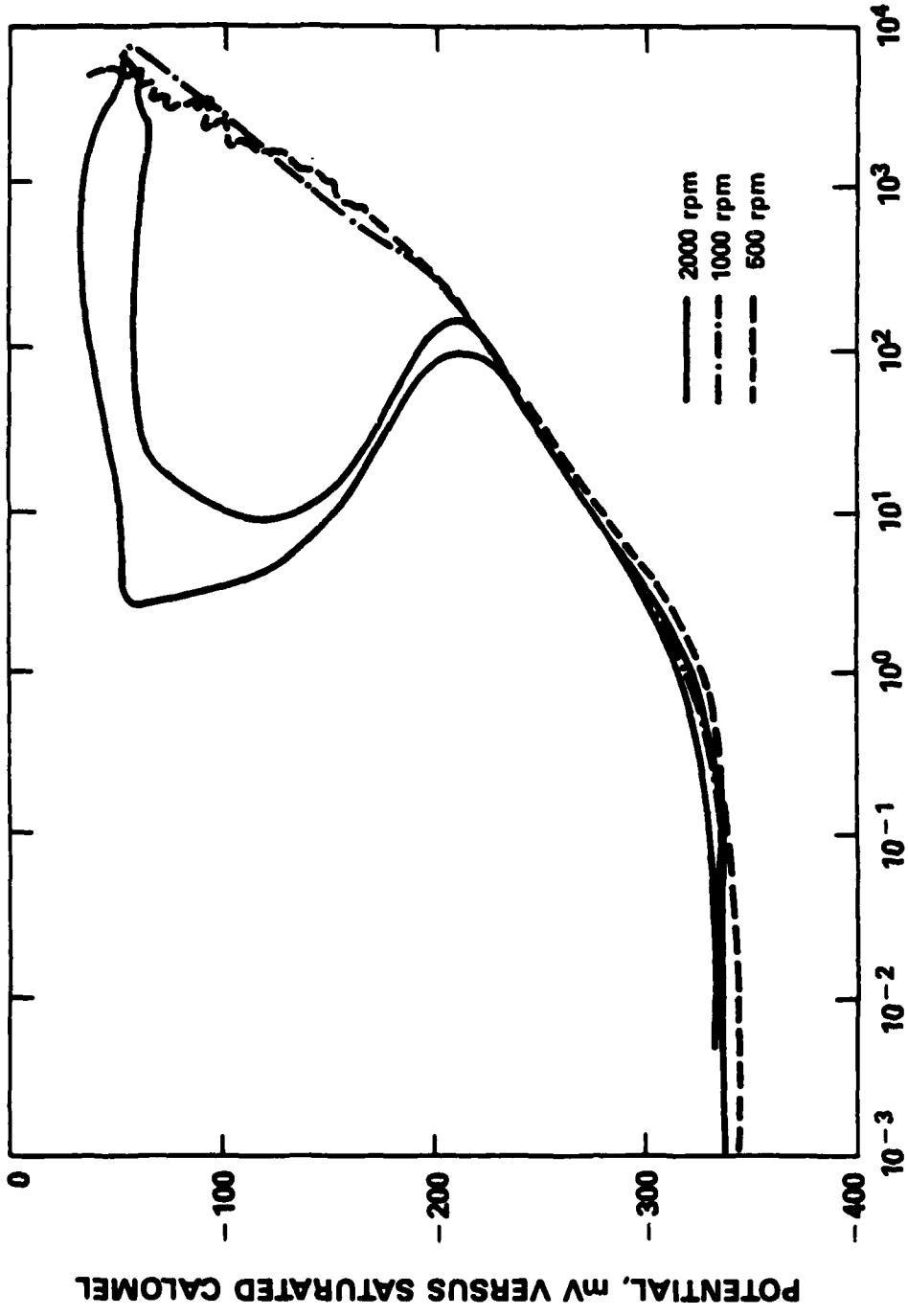

Figure 26.
Potentiodynamic Scan for 90-10 Copper-Nickel in Deaerated Saltwater

highest rotation speed, but only a change in slope is in evidence at lower rotations. This change in slope has been noted by others.[47] The effect was reproducible, although the behavior at the intermediate rotation speed occasionally displayed limited passivity. The potential range of the area of passivity includes the freely-corroding potential of the alloy in aerated solutions and is of particular interest. Faster rotation speeds may increase the rate of formation of the passive film through increased transport of reactants. Long term exposures of 90-10 copper-nickel show an increasing amount of passivity in this potential range with increasing exposure time[89], indicating that the passive nature of the corrosion product at these potentials takes some time to develop.

90-10 copper-nickel has a much more complex impedance behavior than pure copper. This can be seen, along with the effect of exposure duration, in Figures 27 and 28. After one hour a reasonable semicircle was obtained with a polarization resistance of approximately 0.7 kohm-cm^2, consistent with the polarization resistance measurements by others.[56] By 24 hours of exposure low enough frequencies could not be reached in the test to record the point where the semicircle intersects the real axis. Thus, the intersection point can only be exactly obtained by appropriate mathematical modelling of the data. This effect became more pronounced with increasing exposure duration, while the estimated polarization resistance increased to

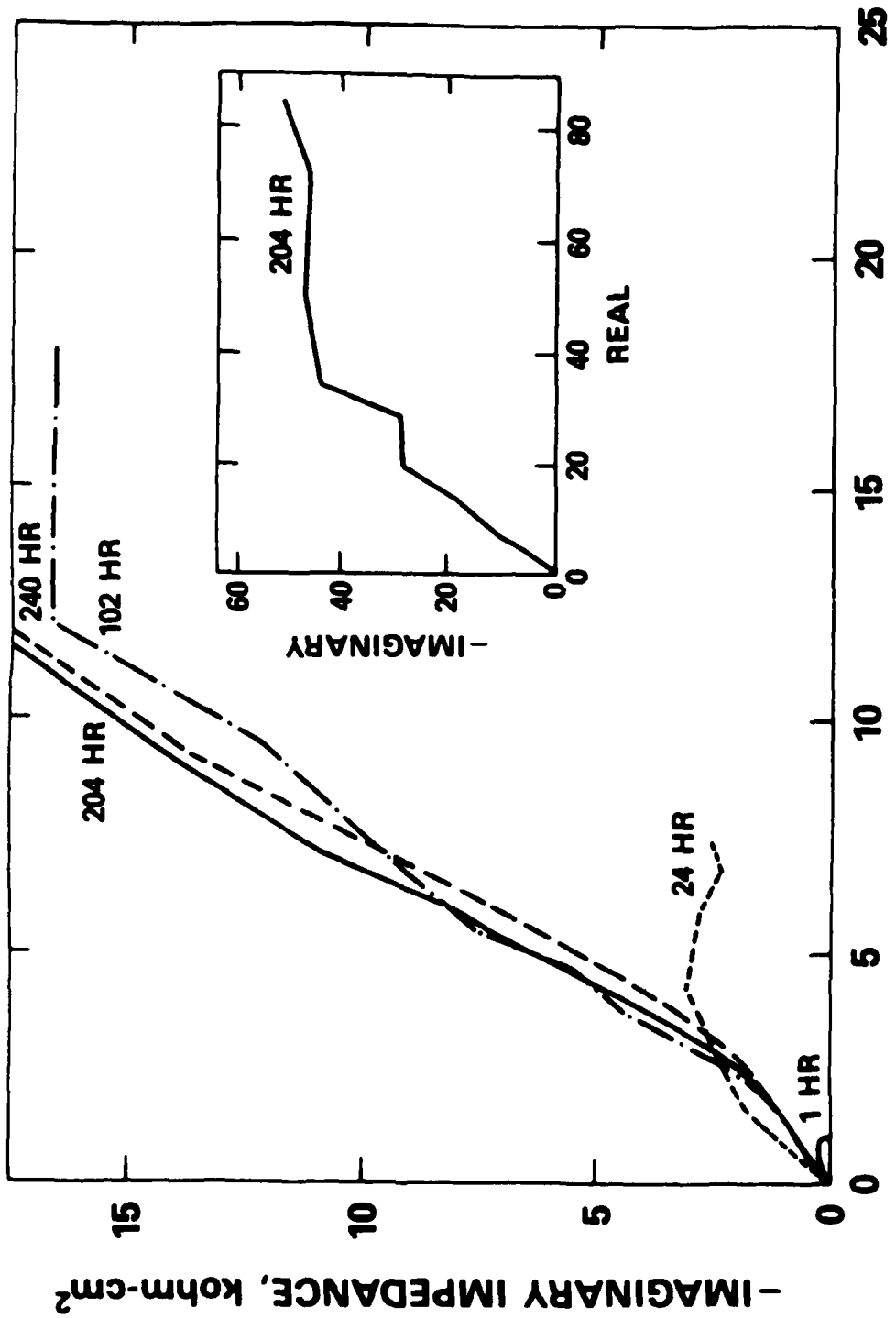

Figure 27.
Effect of Time on Nyquist Curves for 90-10 Copper-Nickel

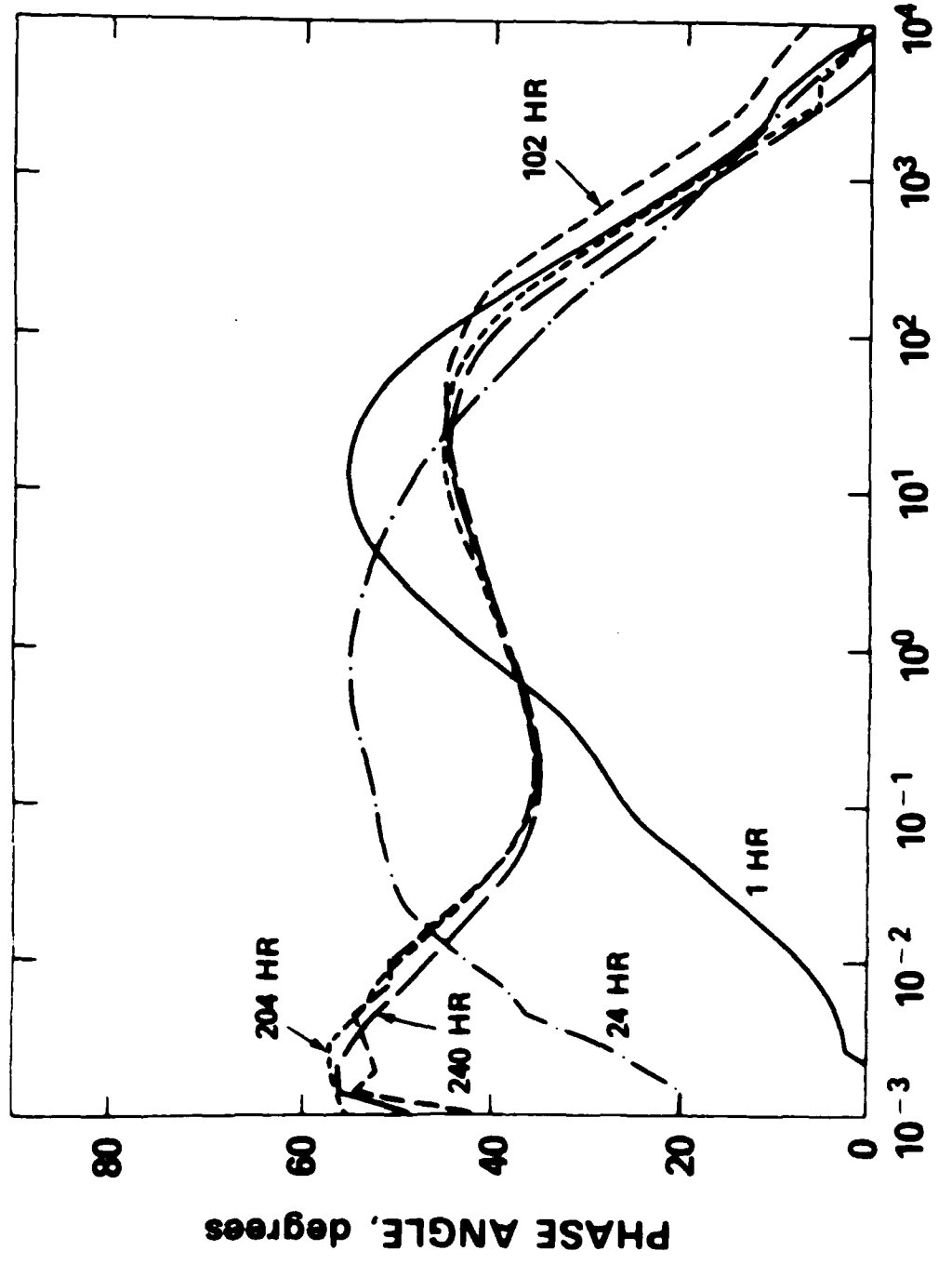

Figure 28.
Effect of Time on Bode Curves for 90-10 Copper-Nickel

over 200 kohm-cm^2. The intercepts after various exposure periods are consistent with those found by other investigators.[17,57,58] The shape of the curves at high frequencies (low impedances) indicates a deviation from a semicircular shape at about 2 kohm-cm^2, indicating a possible second time constant, as found by others.[17] The phase data indicates that a second, low frequency, phase peak developed at longer exposure times. This would indicate that two overlapping semicircles are contributing to the Nyquist data, thus explaining the curve shape. The second phase peak was centered at a very low frequency, about 0.002 Hz, which is the reason why the lowest frequency of test was unable to record a real value of polarization resistance.

The effects of rotation speed and DC bias for 90-10 copper-nickel are presented in Figures 29 and 30. The low frequency peak in this test exposure was much higher in frequency than that of the exposure shown in Figure 28, however the behavior was qualitatively similar. Rotation speed had little effect, indicating reaction control by a process on the surface. Both anodic and cathodic bias had some effect on the shape of the Nyquist curves. Since an accurate polarization resistance cannot be obtained from these curves because they do not intersect the real axis a second time, it is not known which direction of bias would affect the polarization resistance. In the area of the curves that can be seen, the shape changes were similar to

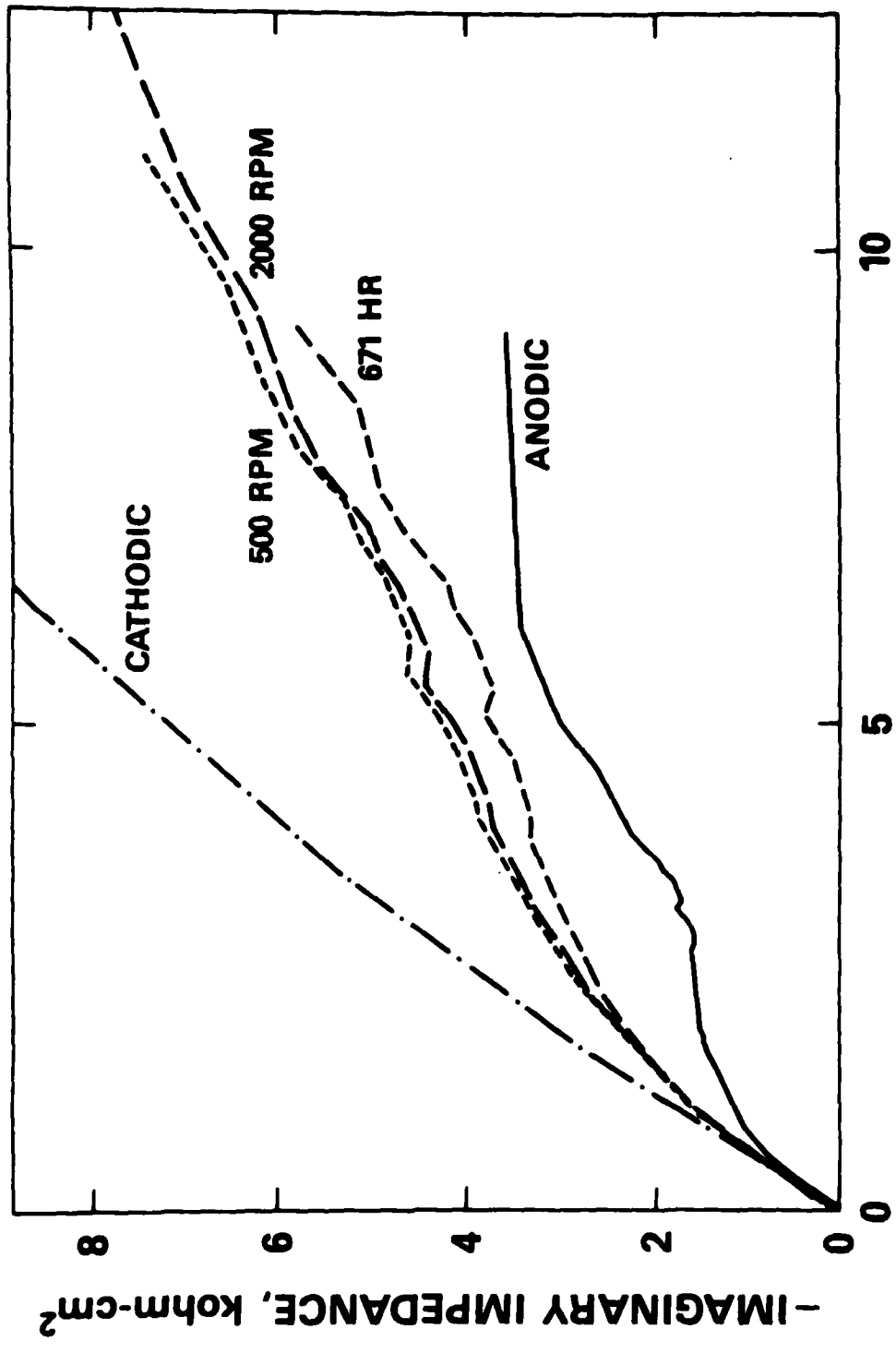

Figure 29.
Effect of Rotation and Bias on Nyquist Curves for 90-10 Copper-Nickel

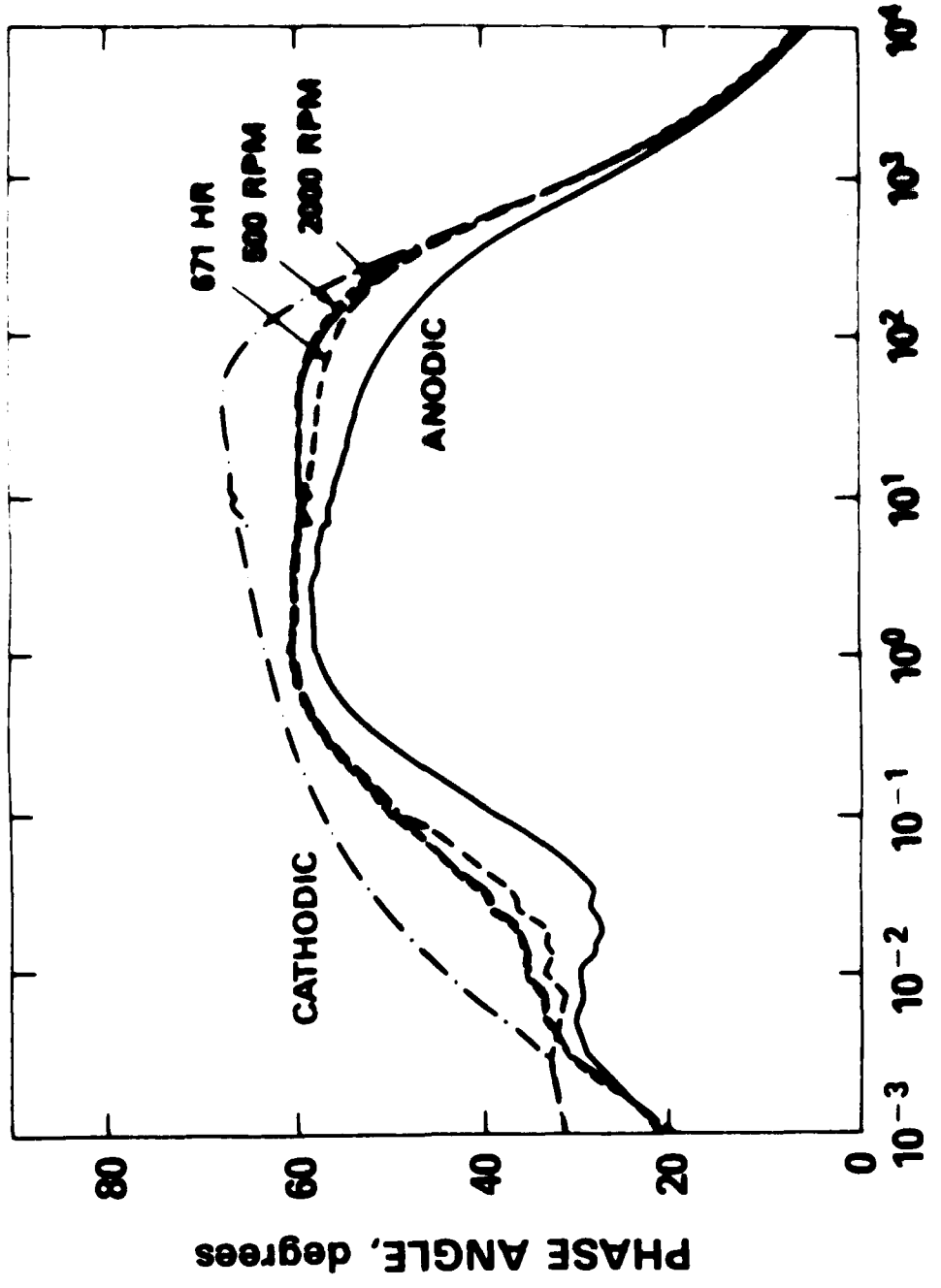

Figure 30.
Effect of Rotation and Bias on Bode Curves for 90-10 Copper-Nickel

those of the second pure copper exposure. In addition, the behavior on the Bode plot was also similar to the second copper exposure. It is therefore likely that the cathodic reaction also controls the corrosion process in this alloy as well.

Figures 31 and 32 illustrate the effect of stripping and palladium coating. Stripping of the corrosion product film after 672 hours exposure reduced the polarization resistance to 2 kohm-cm^2, a value closer to 1 hour exposure values, and removed the second time constant. This is consistent with rotating disk data by Kato and Pickering.[14] Thus, the very high resistance and the second time constant appear to be related to the formation of the loosely adherent outer layers. Consequently these outer layers must be the reason for the good corrosion performance of the 90-10 alloy as compared to copper. Palladium coating prior to stripping also dramatically reduced the polarization resistance and removed the second time constant. Thus, the film must control corrosion by its poor catalytic surface for the oxygen reduction reaction, which is subsequently improved by the palladium coating. This is in agreement with potentiodynamic work performed by other investigators[9,10,14,15].

Composite potentiodynamic curves for 90-10 copper-nickel are shown in Figure 33. These data are consistent with the behavior indicated by the impedance data. The one hour exposure resulted in a current density

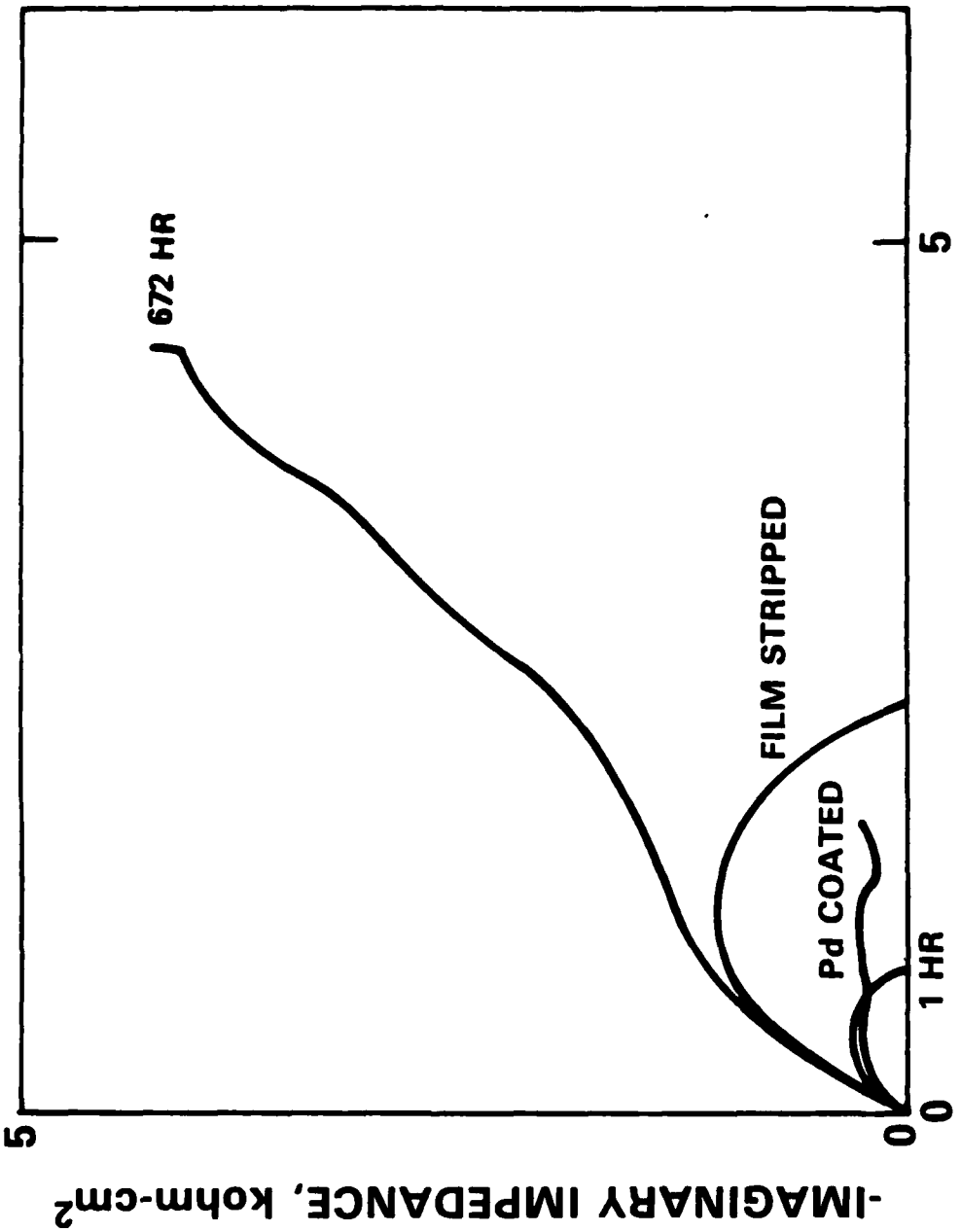

Figure 31.
Effect of Palladium Coating and Stripping on Nyquist Curves for 90-10 Copper-Nickel

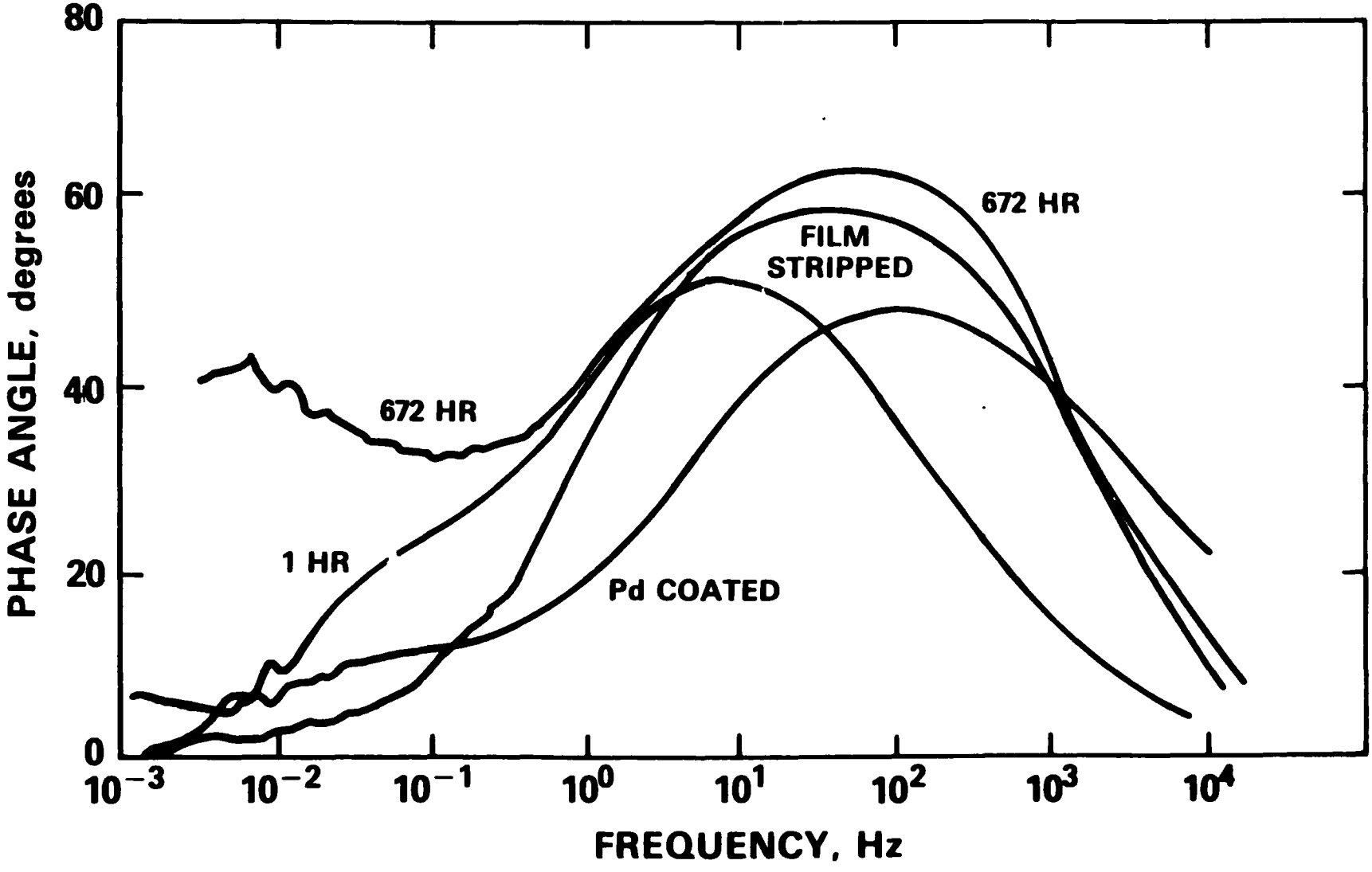

Figure 32.
Effect of Palladium Coating and Stripping on Bode Curves for 90-10 Copper-Nickel

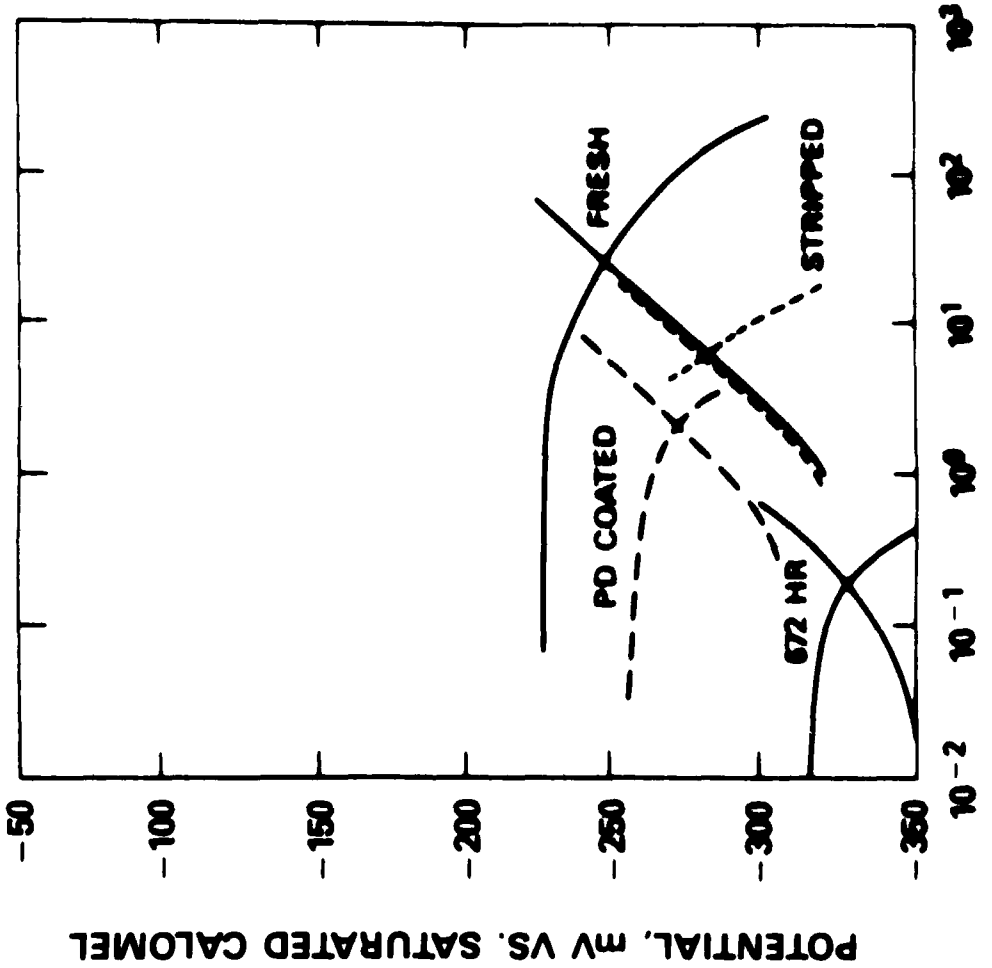

Figure 33.
Polarization Behavior of 90-10 Copper-Nickel

of 30 uA-cm^{-2}, whereas this corrosion current dropped to around 0.2 uA-cm^{-2} after 672 hours of exposure. This is equivalent to a corrosion rate of about 0.2 mils per year, which is consistent with the corrosion rates published for 90-10 copper-nickel in seawater[88]. Palladium coating increased the current to 3 uA-cm^{-2}, a value approaching that of freshly exposed material, and stripping of the outer layer increased the current slightly more, to 6 uA-cm^{-2}.

4.3 70-30 Copper-Nickel

Figure 34 is potentiodynamic data from a slow scan on freshly exposed 70-30 copper-nickel in de-aerated saltwater. At low overpotentials Tafel behavior is exhibited, with a slope of 53 mV per decade at 1000 RPM. The effect of rotation speed cannot be easily determined above the moderate scatter. At higher overpotentials, passivity is seen in some of the curves, and a change of slope in others. Occurrence of passivity does not seem to be related to rotation speed, but is instead somewhat random. Except for this last observation, the behavior of 70-30 copper-nickel is similar to that of the 90-10 alloy described above.

Figures 35 and 36 show the time-dependent behavior of impedance for 70-30 copper-nickel. The Nyquist plot for this material appears to be one semicircle that almost closes on the real axis at all exposure durations. The value of polarization resistance increases from about 1

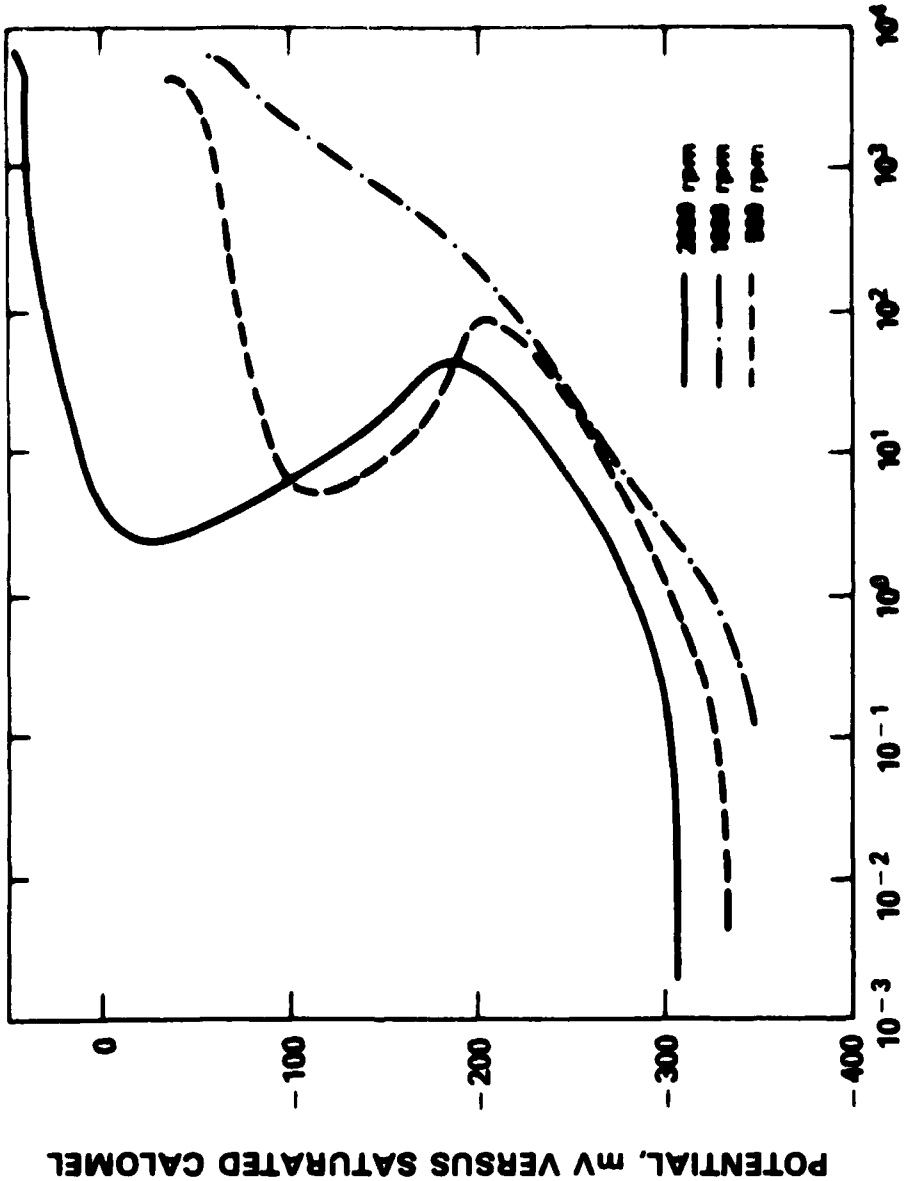

Figure 34.
Potentiodynamic Scan for 70-30 Copper-Nickel in Deaerated Saltwater

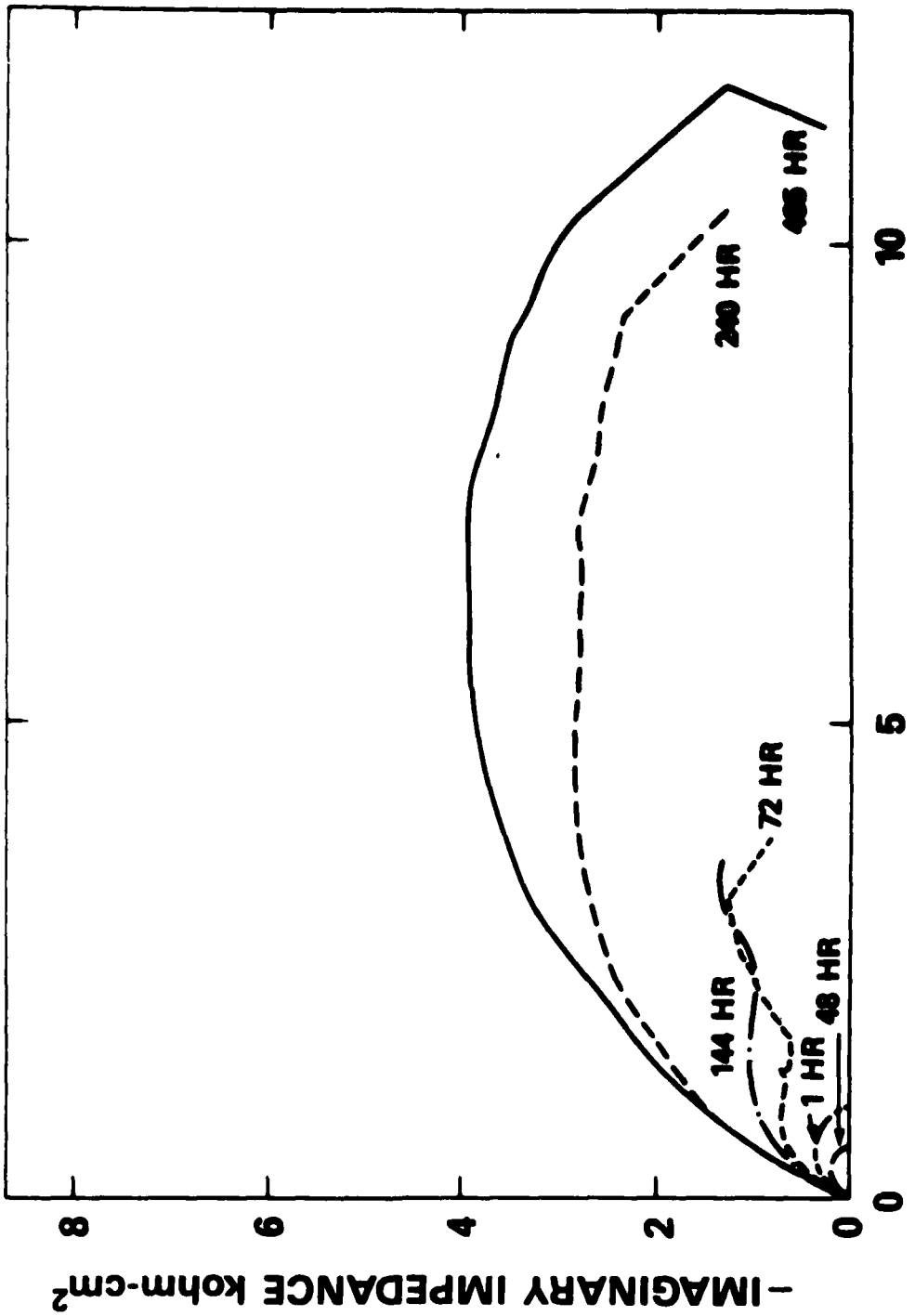

Figure 35.
Effect of Time on Nyquist Curves for 70-30 Copper-Nickel

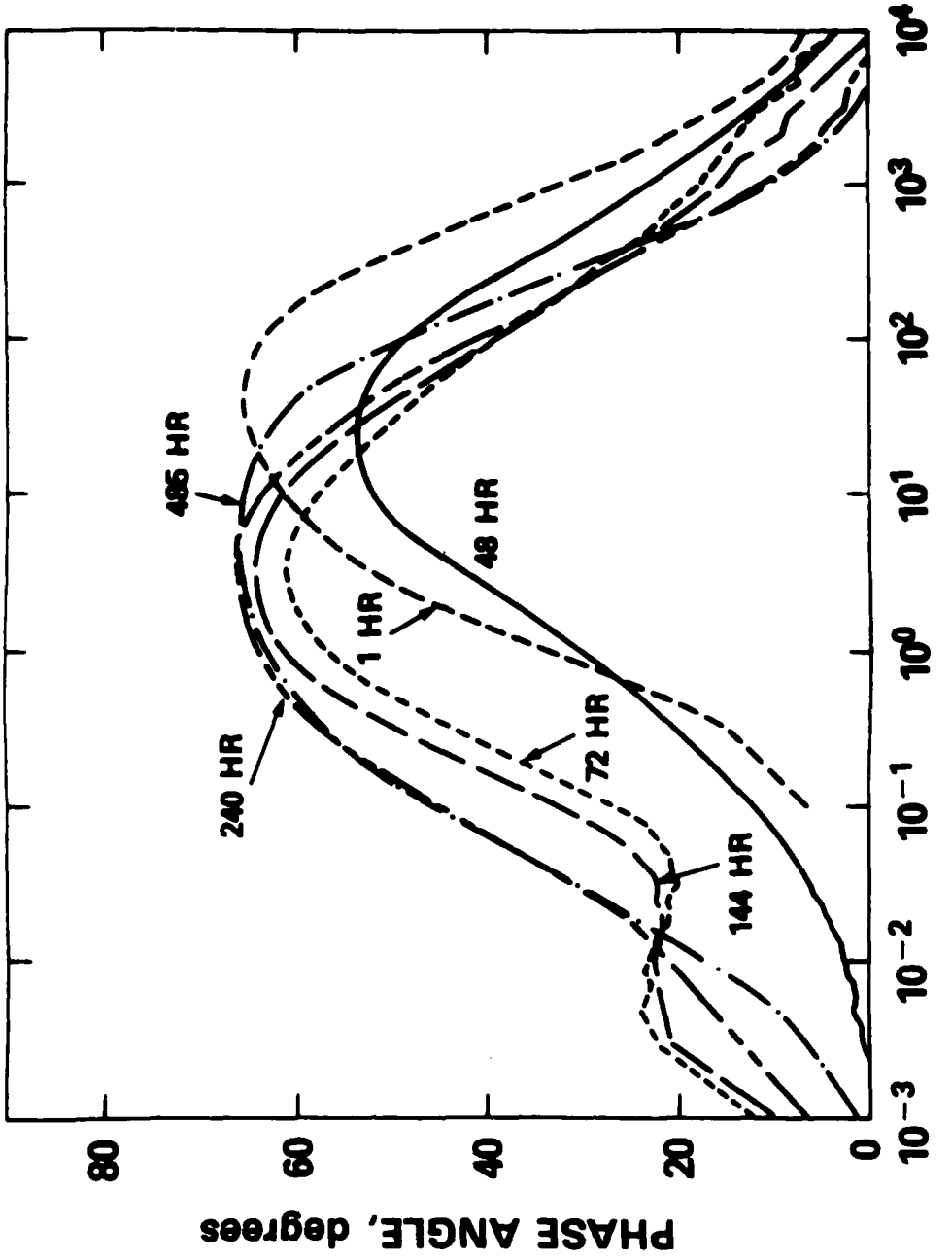

Figure 36.
Effect of Time on Bode Curves for 70-30 Copper-Nickel

kohm-cm^2 after one hour to about 20 kohm-cm^2 after 485 hours. This final resistance is lower than that found by others[17], but is still reasonable considering the wide range in reported corrosion rates for this alloy. The intermediate exposure durations show indications of two time constants (two semicircles). Although the phase data show only one peak, the width of this peak is too great for a simple one-time-constant model. These data are likely due to the presence of two, overlapping time constants, one centered at about 50 Hz and the other becoming visible only after longer exposure durations and centered at about 2 Hz. Thus, the apparent single semicircles on the Nyquist plot are, in fact, two closely overlapping semicircles. An identical conclusion has been reached by others.[17]

The rotation speed and DC bias data for 70-30 copper-nickel are presented in Figures 37 and 38. Rotation speed had little effect, just as on 90-10 copper-nickel, indicating reaction control by a process on the surface. Cathodic bias changed the shape of the Nyquist curve and increased the peak height of the Bode curve just as on the other materials. No data are available for an anodic bias for this material, and thus no conclusions can be made about the controlling reaction.

Impedance results for palladium coating and corrosion product stripping of the 70-30 copper-nickel alloy are shown in Figures 39 and 40. Although the impedance of filmed material is high, about 38 kohm-cm^2, it is not as high as

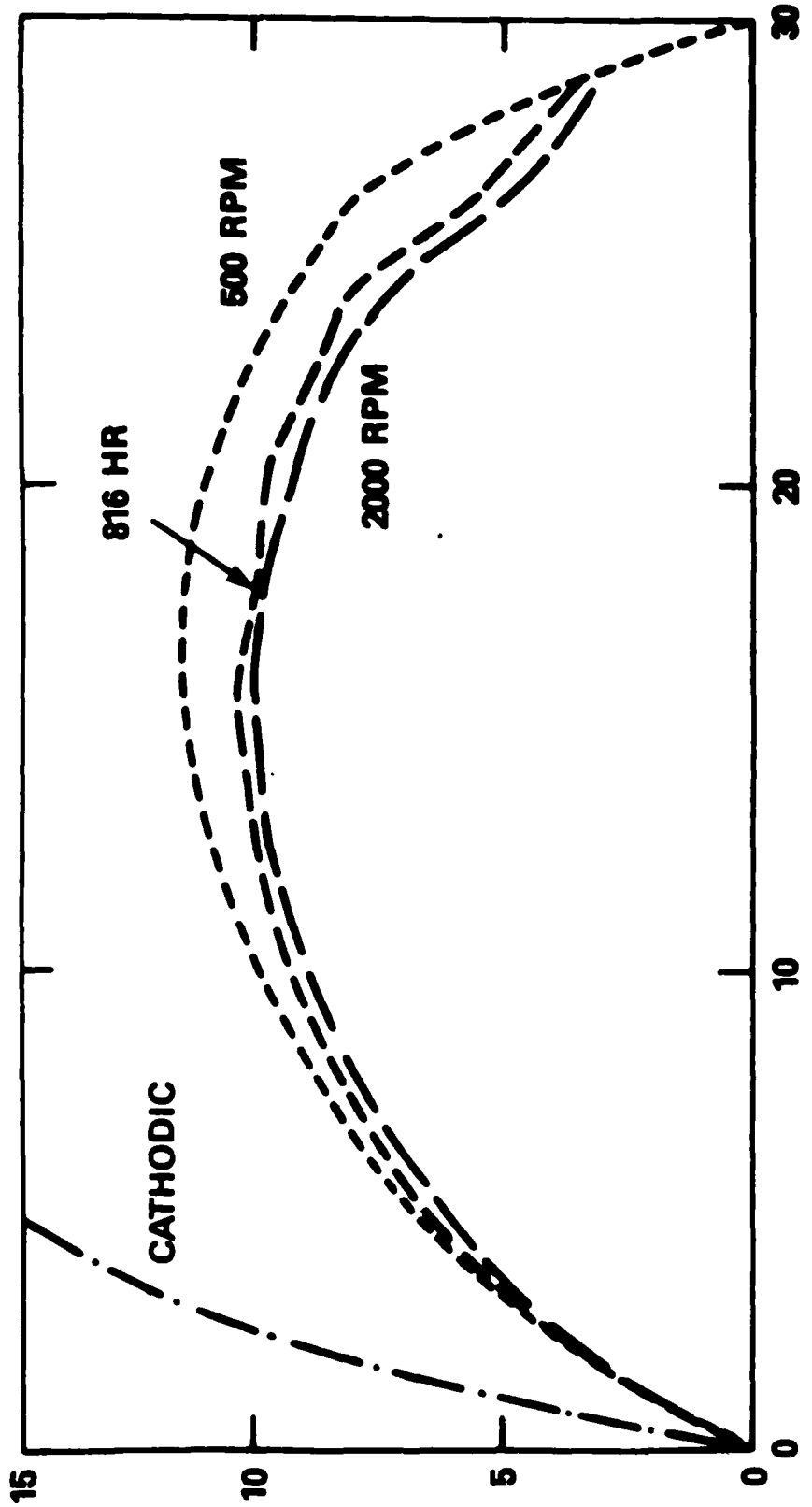

Figure 37.
Effect of Rotation and Bias on Nyquist Curves for 70-30 Copper-Nickel

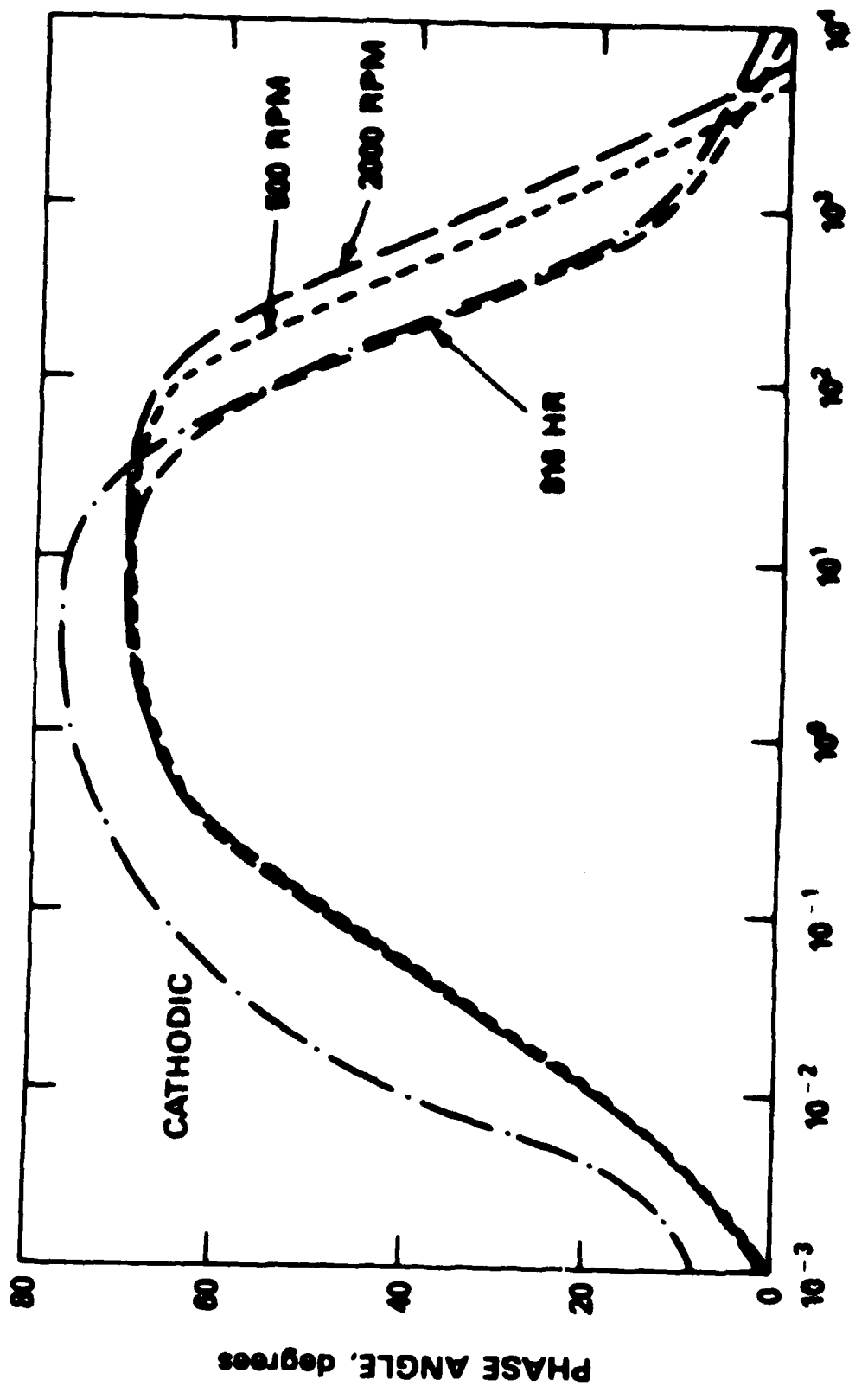

Figure 38.
Effect of Rotation and Bias on Bode Curves for 70-30 Copper-Nickel

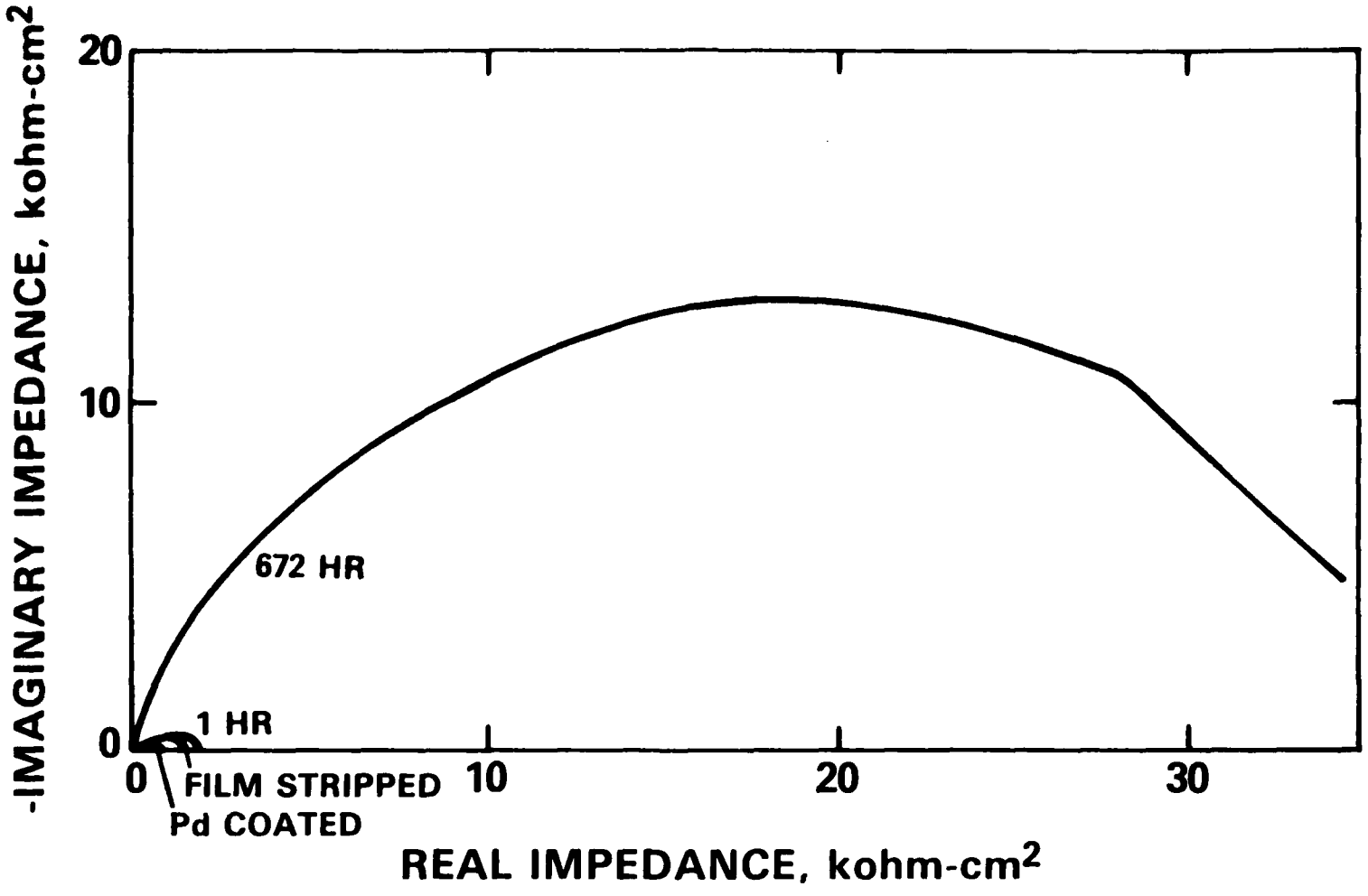

Figure 39.
Effect of Palladium Coating and Stripping on Nyquist Curves for 70-30 Copper-Nickel

AD-A189 884 ROLE OF THE CORROSION PRODUCT FILM IN THE CORROSION PROTECTION OF CU-NI A (U) DAVID W TAYLOR NAVAL SHIP RESEARCH AND DEVELOPMENT CENTER ANN H P HACK NOV 87 2/2

UNCLASSIFIED DTNSRDC/SME-87-22 F/G 11/6.1 NL

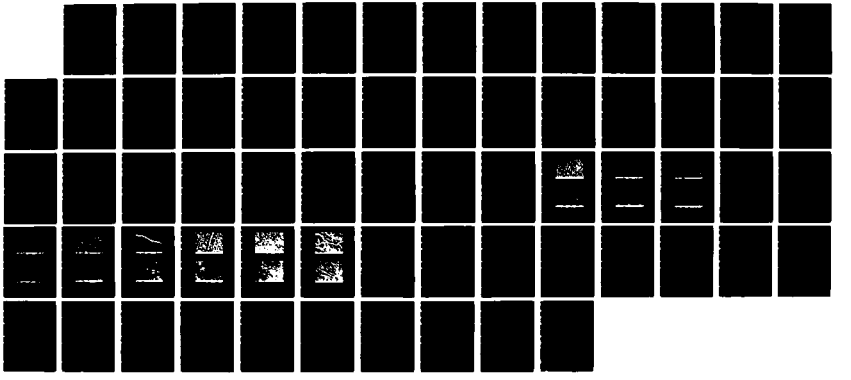

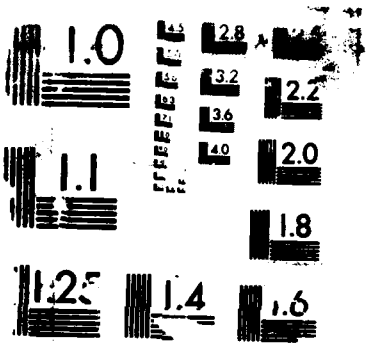

MICROCOPY RESOLUTION TEST CHART

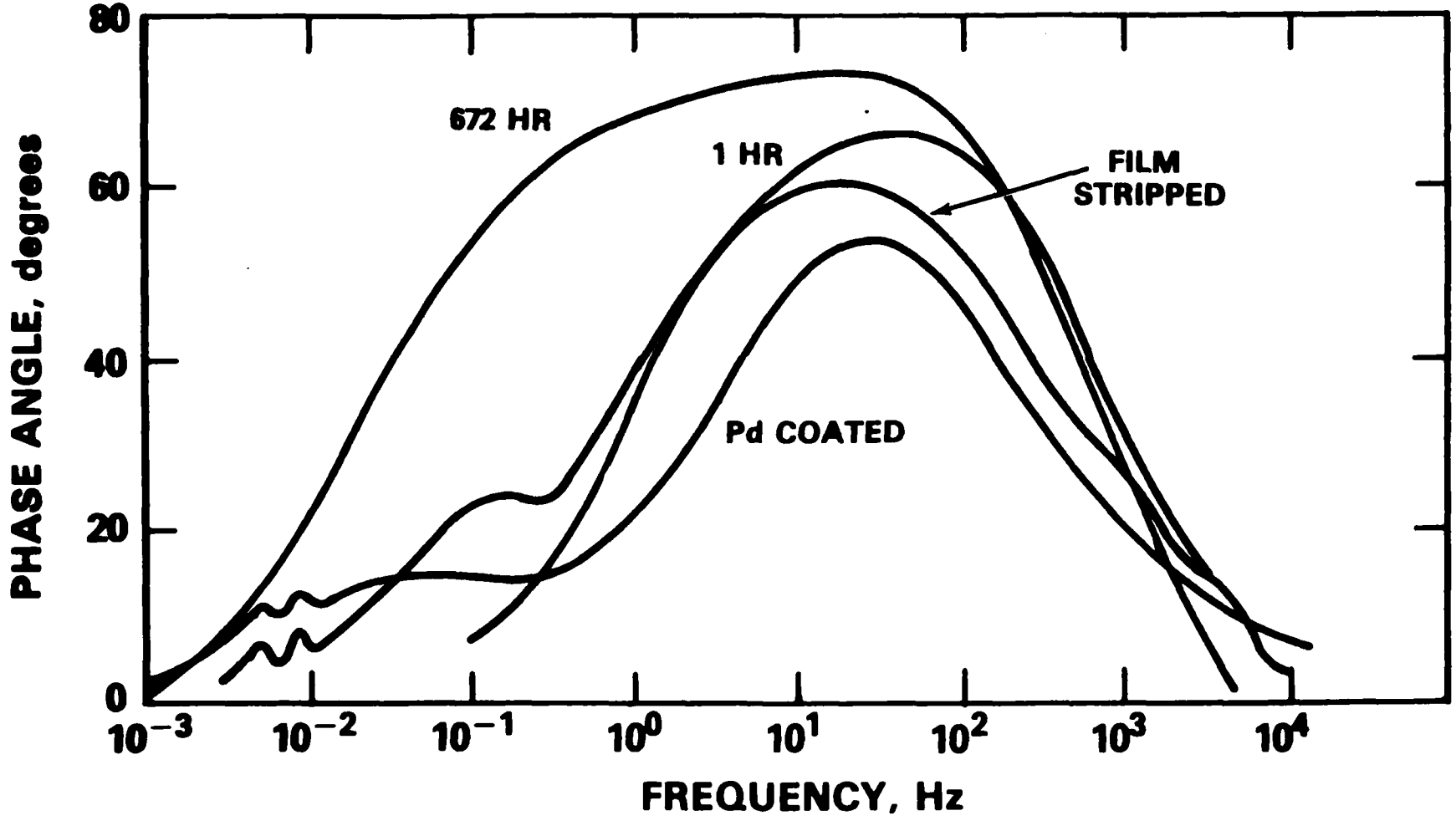

Figure 40.
Effect of Palladium Coating and Stripping on Bode Curves for 70-30 Copper-Nickel

the 90-10 alloy, an observation which is at odds with this material's better corrosion resistance under conditions of turbulent flow, and with other measurements on these alloys at 360 hours by the small amplitude cyclic voltammetry (SACV[90]) technique[91], but is supportable based on corrosion rates under low flow conditions.[88] Like the 90-10 alloy, either palladium coating or stripping of the outer corrosion product layers greatly reduces the impedance to a level roughly equivalent to freshly exposed material, about 1 kohm-cm^2. In addition, the lower overlapping frequency peak is also removed by palladium coating or stripping of the outer layers.

Composite potentiodynamic curves for 70-30 copper-nickel are shown in Figure 41. Material exposed for 672 hours had a corrosion current of 0.7 uA-cm^{-2}, as compared to 3 uA-cm^{-2} for freshly exposed material. The 672 hour data are equivalent to 0.7 mils per year, which compares favorably to 0.3 mils per year for one year seawater exposure[88]. The current was increased somewhat by stripping, indicating that the outer layers are part of the barrier, and by palladium coating, indicating that a low catalysis rate is the rate controlling step for oxygen reduction on the film. This is in agreement with the impedance data, and is similar to the behavior of the 90-10 copper-nickel alloy.

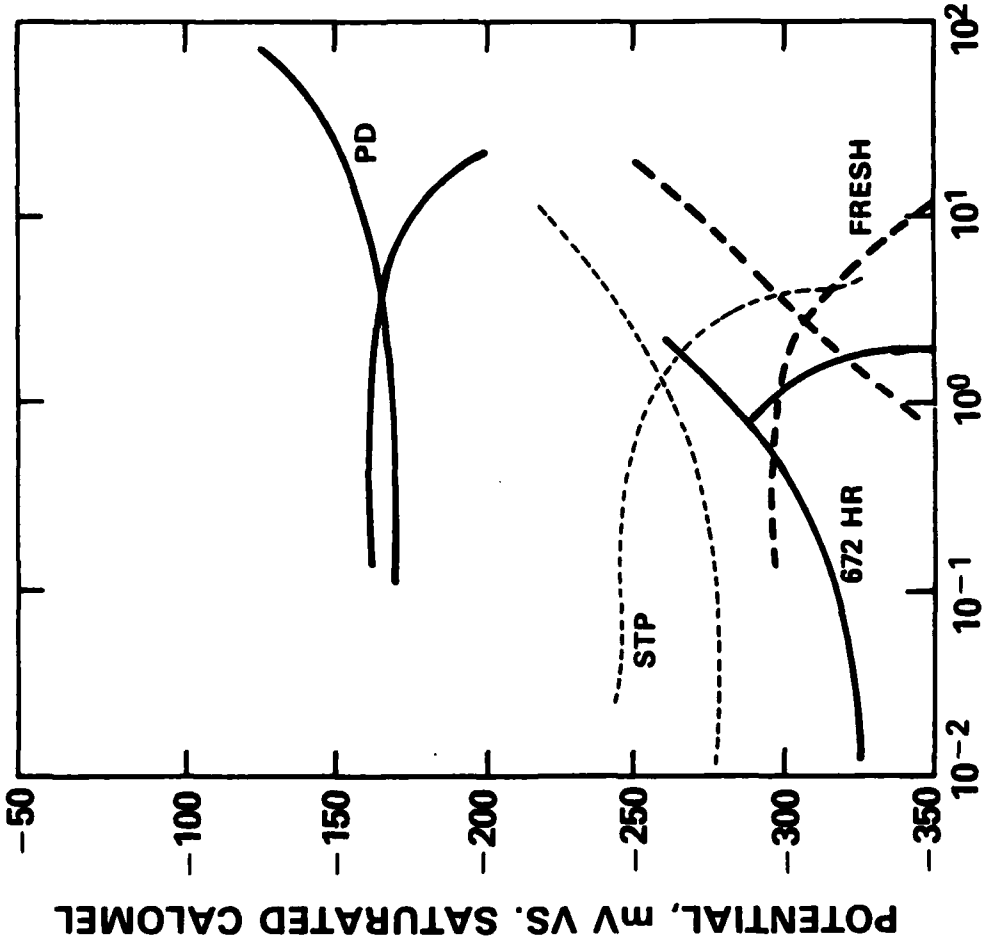

Figure 41.
Polarization Behavior of 70-30 Copper-Nickel

5. CONCLUSIONS

Under circumstances where a cupric hydroxy-chloride corrosion product forms, copper experiences an increase in corrosion resistance with time which can not be correlated with a specific growth law. When the hydroxy-chloride is not present, the corrosion rate of copper is constant over time. Copper-nickel alloys experience increasing corrosion resistance with increased exposure time. On all of the alloys tested, the enhanced corrosion resistance is due to a process associated with the specimen surface, such as diffusion through the corrosion product layer or limited catalysis of the cathodic reaction, rather than by diffusion through a Nernst-like fluid boundary layer. This is evidenced by a lack of rotation speed dépendence of the polarization resistance. DC bias tests indicated that the corrosion of copper is controlled by the cathodic reaction, and all data were consistent with the assumption that this is also the case for the copper-nickel alloys.

The effect of exposure duration on the alloys can be explained by assuming initially a similar behavior on all materials, resulting from double-layer capacitance and faradaic resistance, that results in a semicircular Nyquist behavior with a polarization resistance of 0.5 to 1 kohm-cm^2. As a corrosion product forms, an alloy-dependent second time constant is evidenced, due to the cupric hydroxy-chloride layer of the corrosion product. This

second time constant results in a systematic increase in the polarization resistance of the material, with the effect being less [illegible] pure copper, where the hydroxy-chloride layer only forms intermittently.

The corrosion rate of [illegible] copper-nickel alloys is controlled by the cathodic reaction, generally assumed to be oxygen reduction under these conditions in saltwater. The inner cuprous oxide provides protection for pure copper. Additional protection is provided to copper during the precipitation under some circumstances of a hydroxy-chloride compound. A palladium coating does not increase the reaction rate on this layer. The greater corrosion resistance of the copper-nickel alloys, 90-10 copper-nickel and 70-30 copper-nickel, appears to be due to the outer, loosely adherent corrosion product layers, since the rate increases when these layers are removed. Since palladium coating prior to removal of these outer layers significantly increases the reaction rate, the rate must be limited by the poor catalytic nature of the corrosion product surface for the oxygen reduction reaction.

In summary, the copper-nickel alloys are protected from corrosion by a loosely adherent copper hydroxy-chloride outer corrosion product layer which is a poor catalyst for the oxygen-reduction reaction. The presence of nickel in the alloy is necessary for this protective layer to form.

REFERENCES

1. Gudas, J. P. et al, "Accelerated Corrosion of Copper-Nickel Alloys in Polluted Water," Paper No. 76, Corrosion/76, NACE, Houston, TX, March 1976.

2. Gudas, J. P. and H. P. Hack, "Sulfide Induced Corrosion of Copper Nickel Alloys," Corrosion, 35(2), p 67, February 1979.

3. Hack, H. P. and J. P. Gudas, "Inhibition of Sulfide-Induced Corrosion of Copper-Nickel Alloys with Ferrous Sulfate," Materials Performance, 18(3), p 25, March 1979.

4. Hack, H. P., T. S. Lee, and D. G. Tipton, "The Effect of Ferrous Sulfate on Sulfide-Induced Corrosion of Copper-Base Condenser Alloys in Aerated Seawater," Proceedings of the 5th International Congress on Marine Corrosion and Fouling, Barcelona, Spain, 1981.

5. Hack, H. P. and T. S. Lee, "The Effect of Ferrous Sulfate on Sulfide Induced Corrosion of Copper-Base Condenser Alloys in Aerated Seawater," Report SME 81/91, David Taylor Naval Ship Research and Development Center, Bethesda, MD, January 1982.

6. Hack, H. P. and J. P. Gudas, "Inhibition of Sulfide-Induced Corrosion of Copper-Nickel Alloys With a Stimulated Iron Anode," Materials Performance, 19(4), p 49, April 1980.

7. Syrett, B. C., "Some Thoughts on Cathodic Protection and Other Methods of Protecting Copper Alloys from Corrosion in Sulfide-Polluted Seawater," Paper No. 196, Corrosion/81, NACE, Toronto, Canada, March 1981.

8. Hack, H. P. Shih, H., and H. W. Pickering, "Role of the Corrosion Product Film in the Corrosion Protection of Cu-Ni Alloys in Seawater," in Surfaces, Inhibition, and Passivation, E. McCafferty and R. J. Brodd Eds., Proceedings Volume 86-7, The Electrochemical Society, Inc., Pennington, NJ, pp 355-367, 1986.

9. Kato, C., B. G. Ateya, J. E. Castle, and H. W. Pickering, "On the Mechanism of Corrosion of Cu-9.4Ni-1.7Fe Alloy in Air Saturated Aqueous NaCl Solution, I. Kinetic Investigations," J. Electrochem. Soc., 127(9), p 1890, September 1980.

10. Kato, C., J. E. Castle, B. G. Ateya, and H. W. Pickering, "On the Mechanism of Corrosion of Cu-9.4Ni-1.7Fe Alloy in Air Saturated Aqueous NaCl Solution, II. Composition of the Protective Surface Layer," J. Electrochem. Soc., 127(9), p 1897, September 1980.

11. North, R. F. and M. J. Pryor, "The Influence of Corrosion Product Structure on the Corrosion Rate of Cu-Ni Alloys," Corrosion Science, 10, p 297, October 1970.

12. Popplewell, J., R. Hart and J. Ford, Corrosion Science, 13(4), p 295, April 1973.

13. Kubschenski, O., and B. Hopkins, Oxidation of Metals and Alloys, Buttersworth, London, p 21, 1967.

14. Kato, C. and H. W. Pickering, "A Rotating Disk Study of the Corrosion Behavior of Cu-9.4Ni-1.7Fe Alloy in Air Saturated Aqueous NaCl Solution," J. Electrochem. Soc., 131(6), p 1219, June 1984.

15. Kato, C., H. W. Pickering and J. E. Castle, "Effect of Sulfide on the Corrosion of Cu-9.4Ni-1.7Fe Alloy in Aqueous NaCl Solution," J. Electrochem. Soc., 131(6), p 1225, June 1984.

16. North, R. F. and M. J. Pryor, "The Nature of Protective Films Formed on a Cu-Ni Alloy," Corrosion Science, 9(7), pp 509-517, July 1969.

17. MacDonald, D. D., B. C. Syrett, and S. S. Wing, "The Corrosion of Copper-Nickel Alloys 706 and 715 in Flowing Sea Water I. Effect of Oxygen," Corrosion, 34(9), pp 289-301, September 1978.

18. Stewart, W. C. and F. L. LaQue, "Corrosion Resisting Characteristics of Iron Modified 90:10 Cupro Nickel Alloy," Corrosion, 8(8), pp 259-277, August 1952.

19. Syrett, B. C. and D. D. MacDonald, "The Validity of Electrochemical Methods for Measuring Corrosion Rates of Copper-Nickel Alloys in Sea Water," Corrosion, 35(11), pp 505-509, November 1979.

20. Efird, K. D., "Potential-pH Diagrams for 90-10 and 70-30 Cu-Ni in Sea Water," Corrosion, 31(3), pp 77-83, March 1975.

21. Parvizi, M. S., A. Aladjem, and J. E. Castle, Behavior of 90/10 Cupronickel in Seawater, INCRA Project 254D, INCRA, N. Y., NY, 1985.

22. Osterwald, J. and H. H. Uhlig, "Anodic Polarization and Passivity of Ni and Ni-Cu Alloys in Sulfuric Acid," J. Electrochem. Soc., 108(6), pp 515-519, June 1961.

23. Koizumi, T. and H. H. Uhlig, "Passivity and Pitting of Ni-Cu Alloys in NaCl Solutions," J. Electrochem. Soc, 121(9), pp 1137-1141, September 1974.

24. Mansfeld, F. and H. H. Uhlig, "Effect of Electron Donor and Acceptor Elements on Passivity of Copper-Nickel Alloys," J. Electrochem. Soc., 117(4), pp 427-432, April 1970.

25. Nobe, K. and G. L. Bauerle, "Effects of Chloride Ions on the Anodic Dissolution of 90/10 and 70/30 Cu-Ni Alloys in H_2SO_4," Corrosion, 37(7), pp 426-427, July 1981.

26. Nobe, K., L. L. C. Sorenson, W. D. Bjorndahl, and P. N. Pintauro, "Oxygen and Chloride Corrosion of Copper," in Equilibrium Diagrams Localized Corrosion, R. P. Frankenthal and J. Kruger Eds., Proceedings Volume 84-9, The Electrochemical Society, Inc., Pennington, NJ, p 350, 1984.

27. Shen, W. and K. Nobe, "Rotating Ring Disk Electrode Studies of Cu and Cu-Ni(90/10) Alloy Electrodissolution in H_2SO_4. Effect of Benzotriazole and Low Cl^-," in Surfaces, Inhibition, and Passivation, E. McCafferty and R. J. Brodd Eds., Proceedings Volume 86-7, The Electrochemical Society, Inc., Pennington, NJ, pp 82-87, 1986.

28. Ghandehari, M. H., T. N. Anderson, and H. Eyering, "The Electrochemical Reduction of Oxygen on Copper in Dilute Sulphuric Acid Solutions," Corr. Sci., 16(3), pp 123-135, March 1976.

29. Ashworth, V. and D. Fairhurst, "The Anodic Formation of Cu_2O in Alkaline Solutions," J. Electrochem. Soc., 124(5), pp 506-517, April 1977.

30. Ambrose, J., R. G. Barradas, and D. W. Shoesmith, "Rotating Copper Disk Electrode Studies of the Mechanism of the Dissolution-Passivation Step on Copper in Alkaline Solutions," Electroanalytical Chemistry and Interfacial Electrochemistry, 47, pp 65-80, 1973.

31. Ives, D. J. G. and A. E. Rawlings, "Copper Corrosion II. Kinetic Studies," J. Electrochem. Soc., 109(6), pp 452-457, June 1962.

32. Ives, D. J. G. and A. E. Rawlings, "Copper Corrosion III. Electrochemical Theory of General Corrosion," J. Electrochem. Soc., 109(6), pp 458-462, June 1962.

33. Kruger, J., "Use of Ellipsometry in the Study of Corrosion," Corrosion, 22(4), p 88, April 1966.

34. Kruger, J., "The Oxide Films Formed on Copper Single Crystal Surfaces in Pure Water I. Nature of the Films Formed at Room Temperature," J. Electrochem. Soc., 106(10), p 847, October 1959.

35. Bonfiglio, C. H., H. C. Albaya, and O. A. Cobo, "The Kinetics of the Anodic Dissolution of Copper in Acid Chloride Solutions," Corros. Sci., 13(10), pp 717-724, October 1973.

36. Braun, M. and K. Nobe, "Electrodissolution Kinetics of Copper in Acidic Chloride Solutions," J. Electrochem. Soc., 126(10), pp 1666-1670, October 1979.

37. Lee, H. P. and K. Nobe, "Rotating Ring-Disk Electrode Studies of Cu-Ni Alloy Electrodissolution in Acidic Chloride Solution I. A Commercial Cu-Ni(90-10) Alloy," J. Electrochem. Soc., 131(6), pp 1236-1242, June 1984.

38. Smyrl, W. H., "Digital Impedance for Faradaic Analysis II. Electrodissolution of Cu in HCl," J. Electrochem. Soc., 132(7), pp 1555-1562, July 1985.

39. Bockris, J. O'M., B. T. Rubin, A. Despic, and B. Lovrecek, "The Electrodissolution of Copper-NIckel Alloys," Electrochimica Acta, 17, pp 973-999, 1972.

40. Walton, M. E. and P. A. Brook, "The Dissolution of Cu-Ni Alloys in Hydrochloric Acid - I. Rotating Disc Electrode Measurements," Corrosion Science, 17(4), pp 317-328, April 1977.

41. Hurlen, T., "Electrochemical Behavior of Copper in Acid Chloride Solution," Acta Chemica Scandinavica, 15(6), pp 1231-1238, June 1961.

42. Hurlen, T., "Dissolution of Copper by Oxydation Agents in Acid Chloride Solution," Acta Chemica Scandinavica, 15(6), pp 1239-1245, June 1961.

43. Stephenson, L. and J. H. Bartlett, "Anodic Behavior of Copper in HCl," J. Electrochem. Soc., 101(11), pp 571-581, November 1954.

44. Smyrl, W. H. and L. L. Stephenson, "Digital Impedance for Faradaic Analysis III. Copper Corrosion in Oxygenated 0.1N HCl," J. Electrochem. Soc., 132(7), pp 1563-1567, July 1985.

45. Pourbaix, M., "Some Applications of Potential-pH Diagrams to the Study of Localized Corrosion," J. Electrochem. Soc.: News and Reviews, 123(2), pp25C-36C, February 1976.

46. Blanchi and Longhi, "Copper in Sea-Water, Potential-pH Diagrams," Corros. Sci., 13(11), pp 853-864, November 1973.

47. Ives, D. J. G. and A. E. Rawson, "Copper Corrosion I. Thermodynamic Aspects," J. Electrochem. Soc., 109(6), pp 447-451, June 1962.

48. Blundy, R. G. and M. J. Pryor, "The Potential Dependence of Reaction Product Composition on Copper-Nickel Alloys," Corros. Sci., 12(1), pp 65-75, January 1972.

49. McGuire, G. E., A. L. Bacarella, J. C. Griess, Jr., R. E. Clausing, and L. D. Hulett, "Analysis of Protective Oxide Films on Copper-Nickel Alloys by Auger Spectroscopy," J. Electrochem. Soc., 125(11), pp 1801-1804, November 1978.

50. Gilbert, P. T., "A Review of Recent Work on Corrosion Behavior of Copper Alloys in Sea Water," Materials Performance, 21(2), pp 47-53, February 1982.

51. Ives, D. J. G. and A. E. Rawlings, "Copper Corrosion IV. The Effects of Saline Additions," J. Electrochem. Soc., 109(6), pp 462-466, June 1962.

52. Bailey, G. L., "Copper-Nickel-Iron Alloys Resistant to Sea-Water Corrosion," J. Inst. Metals, 79, pp 243-292, 1951.

53. North, R. F. and M. J. Pryor, "The Influence of Corrosion Product Structure on the Corrosion Rate of Cu-Ni Alloys," Corrosion Science, 10(5), pp 297-311, May 1971.

54. Popplewell, J. M., R. J. Hart, and J. A. Ford, "The Effect of Iron on the Corrosion Characteristics of 90-10 Cupro Nickel in Quiescent 3.4% NaCl Solution," Corrosion Science, 13(4), pp 295-309, April 1973.

55. Dhar, H. P., R. E. White, R. Darby, L. R. Cornwell, R. B. Griffin, and G. Burnell, "Corrosion Behavior of 70Cu-30-Ni Alloy in 0.5M NaCl and in Synthetic Seawater," Corrosion, 41(4), pp 193-196, April 1985.

56. Castle, J. E. and M. S. Parvizi, "Protective Surface Film Characteristics of Copper Alloys in Seawater," Corrosion Prevention and Control, 17(1), pp 1-17, January 1986.

57. IJsseling, F. P., L. P. J. Drolenga, and B. H. Kolster, "Influence of Temperature on Corrosion Product Film Formation on CuNi10Fe in the Low Temperature Range I. Corrosion Rate as a Function of Temperature in Well Aerated Sea Water," Br. Corr. J., 17(4), pp 162-167, April 1982.

58. Drolenga, L. P. J., F. P. IJsseling, and B. H. Kolster, "The Influence of Alloy Composition and Microstructure on the Corrosion Behaviour of Cu-Ni Alloys in Seawater," Werkstoffe und Korrosion, 34, pp 167-178, 1983.

59. Admiral, L., F. P. IJsseling, B. H. Kolster, and J. Van Der Veer, "Influence of Temperature on Corrosion Product Film Formation on CuNi10Fe in the Low Temperature Range Part 2: Studies on Corrosion Product Film Formation and Properties in Relation to Microstructure and Iron Content," Br. Corr. J., 21(1), pp 33-43, January 1986.

60. Bacarella, A. L. and J. C. Griess, Jr., "The Anodic Dissolution of Copper in Flowing Sodium Chloride Solutions Between 25° and 175 °C," J. Electrochem. Soc., 120(4), pp 459-465, April 1973.

61. Boden, P. J., "Corrosion of Cu and Cu-Base Alloys Under Conditions of Boiling Heat Transfer - I. Corrosion of Cu," Corrosion Science, 11(6), pp 353-362, June 1971.

62. Ali, J. A. and J. R. Ambrose, "Corrosion Kinetics of Nickel/Copper Alloy in Flowing Sea Water," Corrosion Research in Progress, Corrosion/82, NACE, Houston, TX, March 1982.

63. Taylor, A. H., "The Corrosion Behavior of Cu and Naval Brass in 0.5M NaCl Solution at Ambient Temperature," J. Electrochem. Soc., 118(6), pp 854-859, June 1971.

64. Bomberger, H. B., F. H. Beck, and M. G. Fontana, "Polarization Studies of Copper, Nickel, Titanium, and Some Copper and Nickel Alloys in Three Per Cent Sodium Chloride," J. Electrochem. Soc., 102(2), pp 693-695, December 1955.

65. Bjorndahl, W. D. and K. Nobe, "Copper Corrosion in Chloride Media. Effect of Oxygen," Corrosion, 40(2), pp 82-87, February 1984.

66. Boden, P. J., "Corrosion of Cu and Cu-Base Alloys Under Conditions of Boiling Heat Transfer - II. Corrosion of Cu-Base Alloys," Corrosion Science, 11(6), pp 363-370, June 1971.

67. Melton, D. G., R. M. McGowan, and M. W. Joseph, "Evaluations of Erosion-Corrosion of Copper Nickel in Seawater under Transient Velocity Conditions Using a Split Electrode," Paper No. 276, Corrosion/86, NACE, Houston, TX, March 1986.

68. Cahan, B. D. and C. T. Chen, "Questions on the Kinetics of O_2 Evolution on Oxide-Covered Metals," J. Electrochem. Soc., 129(4), pp 700-705, April 1976.

69. Gabrielli, C., Identification of Electrochemical Processes by Frequency Response Analysis, Monograph SI/Dym/001/Issue 1/10.80, The Solartron Electronic Group Limited, Irvine, CA, 1980.

70. MacDonald, D. D. and M. C. H. McKubre, "Impedance Measurements in Electrochemical Systems," in Treatise on Modern Electrochemistry, Yeager, Ed, 1984.

71. Mansfeld, F., M. W. Kendig, and S. Tsai, "Recording and Analysis of AC Impedance Data for Corrosion Studies II. Experimental Approach and Results," Corrosion, 38(11), pp 570-580, November 1982.

72. Gad Allah, A. G., A. A. Mazhar, and M. S. El-Basiouny, "Impedance Properties of the Passive Layer on a Titanium Electrode in a Phosphoric Acid Electrolyte," Corrosion, 42(12), pp 740-744, December 1986.

73. Mansfeld, F. B. and M. W. Kendig, "Impedance Measurement for the Analysis of Corrosion Induced Failures," Report NADC-80102-60, Naval Air Development Center, Warminster, PA, February 1982.

74. Bonnel, A., F. Dabosi, C. Deslouis, M. Duprat, M. Keddam, and B. Tribollet, "Corrosion Study of a Carbon Steel in Neutral Chloride Solutions by Impedance Techniques," J. Electrochem. Soc., 130(4), pp 753-761, April 1983.

75. Mansfeld, F., "Recording and Analysis of AC Impedance Data for Corrosion Studies I. Background and Methods of Analysis," Corrosion, 36(5), pp 301-307, May 1981.

76. "Basics of AC Impedance Measurements," Application Note AC-1, E G + G Princeton Applied Research, Princeton, NJ, 1984.

77. Hepburn, B. J., K. R. Gowers, and J. D. Scantlebury, "Interpretation of Low Frequency AC Impedance Data for Organic Coatings on Mild Steel," Br. Corros. J., 21(2), pp 105-108, February 1986.

78. Scully, J. R., "Electrochemical Impedance Spectroscopy for Evaluation of Organic Coating Deterioration and Under Film Corrosion--A State of the Art Technical Review," Report DTNSRDC/SME-86/006, David Taylor Naval Ship Research and Development Center, Bethesda, MD, September 1986.

79. Kendig, M., S. Tsai, and F. Mansfeld, "Influence of Steel Surface Preparation on Coating Performance and Cathodic Delamination," Materials Performance, 23(6), pp 37-40, June 1984.

80. Mansfeld, F., M. W. Kendig, and S. Tsai, "Evaluation of Corrosion Behavior of Coated Metals with AC Impedance Measurements," Paper 182, Corrosion/82, NACE, Houston, TX, March 1982.

81. Mansfeld, F. and M. Kendig, "Evaluation of Protective Coatings with Impedance Measurements," Proc. Int. Cong. Metal. Corr., Toronto, Canada, p 74, June 1984.

82. IJsseling, F. P., "Application of Electrochemical Methods of Corrosion Rate Determination to Systems Involving Corrosion Product Layers," Br. Corros. J., 21(2), pp 95-102, February 1986.

83. MacDonald, D. D., B. C. Syrett, and S. S. Wing, "The Corrosion of Cu-Ni Alloys 706 and 715 in Flowing Sea Water II. Effect of Dissolved Sulfide," Corrosion, 35(8), pp 367-378, August 1979.

84. Eiselstein, L. E., R. D. Caligiuri, S. S. Wing, and B. C. Syrett, "Mechanisms of Corrosion of Copper-Nickel Alloys in Sulfide-Polluted Seawater," Report PYU 6077, SRI International, prepared under ONR Contract N00014-77-C-0046, NR 036-116, February 1981.

85. Levich, V. G., Physicochemical Hydrodynamics, Prentice-Hall,Inc., Englewood Cliffs, NJ, pp 345-357, 1962.

86. Riddiford, A. C., "The Rotating Disk System," in Advances in Electrochemistry and Electrochemical Engineering, Volume 4-Electrochemistry, Paul Delahay, Ed., John Wiley and Sons, NY, ,pp 46-116, 1965.

87. Leimkuhler, A., "Structural Homogeneity, Crystallization, and Embrittlement Behavior of $Fe_{81}B_{13.5}Si_{3.5}C_2$," Ph.D. Dissertation, The Johns Hopkins University, May 1983.

88. Uhlig, H. H., The Corrosion Handbook, John Wiley and Sons, New York, NY, p 394, 1948.

89. Hack, H. P., "Exposure Time Effects on Current Densities of Polarized Marine Materials," Paper No. 210, Corrosion/83, NACE, Anaheim, CA, April 1983.

90. Shih, H. and H. W. Pickering, "Analysis of the Small Amplitude Cyclic Voltammetry Technique for Measuring Polarization Resistance and Interfacial Capacitance," submitted to the J. Electrochem. Soc.

91. Shih, H. and H. W. Pickering, "SACV Measurement of the Polarization Resistance and Capacitance of Copper Alloys in 3.4 wt.% NaCl Solution," submitted to the J. Electrochem. Soc.

APPENDIX

A. MATHEMATICAL MODEL FOR IONIC FLUXES ON COPPER IN HCL

The corrosion mechanism for copper in chloride-containing acid electrolytes such as HCl has been shown to be as illustrated in Figure A-1[A-1]. The first steps in the reaction process result in the combination of a copper atom with two chlorides to produce an adsorbed, negatively charged, copper chloride complex. The next step is rate-determining and is the diffusion of this complex away from the surface, noted as II in the figure. From the Nernst equation and diffusion through a Nernst boundary layer it was predicted that the derivative of overpotential against log of current should be 60 mV per decade, and that the derivative of the log of current against the log of chloride ion content be 2. Both of these values were actually observed[A-1], making this a powerful argument in favor of this mechanism.

The rotating disk electrode is a perfect device for studying diffusion-controlled reactions such as this one. This is due to the "uniform accessibility", or constant diffusion layer thickness, achieved in this apparatus. From the standpoint of a mathematical model, this allows the diffusion problem to be modelled in one dimension. Such a model is described below.

A mathematical model is shown in Figure A-2 where a diffusion layer of thickness L is placed adjacent to an

I. $$Cu + 2Cl^- = (CuCl_2^-)_{ads} + e^-$$

II. $$(CuCl_2^-)_{ads} \xrightarrow{r.d.s.} (CuCl_2^-)_{Soln}$$

From I: $$E = E^\circ + \frac{RT}{F} \ell n \frac{(CuCl_2^-)_{ads}}{(Cl^-)^2}$$

Therefore $$(CuCl_2^-)_{ads} = (Cl^-)^2 \exp\left(\frac{F(E-E^0)}{RT}\right)$$

From II: $$i = \frac{ZFD\,(CuCl_2^-)_{ads}}{\delta} = \frac{ZFD}{\delta}(Cl^-)^2 \exp\left(\frac{F(E-E^0)}{RT}\right)$$

$$\frac{d(E-E^0)}{d \log i} = \frac{2.3\,RT}{F} = 60 \text{ mV/decade } \underline{\text{AS OBSERVED}}$$

$$\frac{d \log i}{d \log (Cl^-)} = 2 \qquad \underline{\text{AS OBSERVED}}$$

Figure A1.
Copper Corrosion Mechanism in HCl

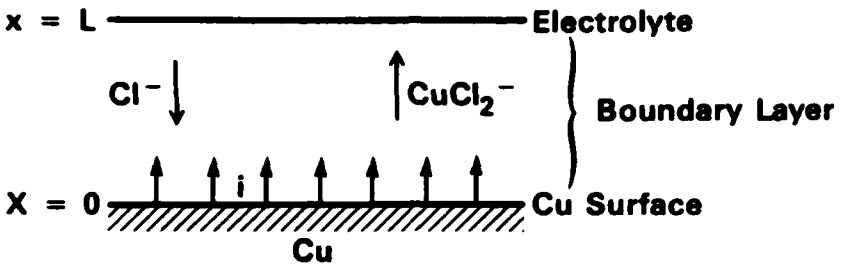

At X = 0 $\quad Cu + 2\,Cl^- \Rightarrow CuCl_2^- + e^-$

At X = L $\quad C_{CuCl_2^-} = \phi = 0$

$C_{H^+} = C_{Cl^-} = C^\circ$

Assumptions: In HCl, no hydrolysis

Only $CuCl_2^-$ formed, instantly & completely

Dilute solutions, no precipitation or constrictions

Steady State, ID transport

Fluxes:

$$(1)\quad J_{H^+} = -D_{H^+}\left(\frac{\delta C_{H^+}}{\delta x} + C_{H^+}\frac{F}{RT}\frac{d\phi}{dx}\right) = 0$$

$$(2)\quad J_{CuCl_2^-} = -D_{CuCl_2^-}\left(\frac{\delta C_{CuCl_2^-}}{\delta x} - C_{CuCl_2^-}\frac{F}{RT}\frac{d\phi}{dx}\right) = \frac{i}{F}$$

$$(3)\quad J_{Cl^-} = -D_{Cl^-}\left(\frac{\delta C_{Cl^-}}{\delta x} - C_{Cl^-}\frac{F}{RT}\frac{d\phi}{dx}\right) = -2J_{CuCl_2^-} = -\frac{2i}{F}$$

Electroneutrality:

$$(4)\quad C_{CuCl_2^-} + C_{Cl^-} - C_{H^+} = 0$$

Figure A2.
Math Model for Corrosion of Cu in HCl

anodically polarized copper electrode in an aqueous electrolyte containing hydrochloric acid. At this electrode, at position X=0, chloride ions react with copper to form a negatively-charged copper-chloride complex. It is assumed that the electrode is polarized sufficiently to suppress the cathodic reactions, that steady-state has been reached, and that there are no precipitates, constrictions of the current flow path, or hydrolysis. The copper-chloride complex formed is assumed to be the only complex formed and it is formed instantly and completely. For the rotating disk electrode, transport should be one-dimensional. The electrolyte acts as an infinite source of chloride ions at concentration C^o and sink of $CuCl_2^-$ ions at zero concentration, and is located at X=L, the edge of the diffusion boundary layer. The potential in the electrolyte is assumed to be zero outside the boundary layer where X is greater than L and the hydrogen ion concentration is assumed to be C^o. Equations 1 to 3 can then be set up to describe the fluxes of all of the ions involved, as caused by diffusion and migration in the electric field. Convective effects are assumed to be negligible. These equations are written under the assumption of dilute electrolyte behavior. This assumption may be invalid near the electrode. Hydrogen ion flux is zero at steady state as these ions are neither created nor destroyed. The flux of chloride ion complexes can be related to the anodic current density, since an electron is

generated in the formation of each complex. To maintain chlorine balance, the flux of chloride ions must be equal to twice that of the complex, and in the opposite direction. Finally, Equation 4 of Figure A-2 is an expression of charge neutrality, which must hold throughout the electrolyte.

Equations 1 to 4 may be solved simultaneously as follows:

Add 3 flux equations:

$$\frac{\delta C_{H^+}}{\delta x} + \frac{\delta C_{CuCl_2^-}}{\delta x} + \frac{\delta C_{Cl^-}}{\delta x} + (C_{H^+} - C_{CuCl_2^-} - C_{Cl^-})\frac{F}{RT}\frac{d\phi}{dx} = \frac{2i}{F}\left(\frac{1}{2D_{CuCl_2^-}} - \frac{1}{D_{Cl^-}}\right)$$

$$\int_{C_{H^+}}^{C^o} dC_{H^+} + \int_{C_{CuCl_2^-}}^{0} dC_{CuCl_2^-} + \int_{C_{Cl^-}}^{C^o} dC_{Cl^-} = \int_{x}^{L} \frac{2i}{DF}\,dx \qquad \frac{1}{D} \equiv \frac{1}{D_{Cl^-}} - \frac{1}{2D_{CuCl_2^-}}$$

$$2C^o - C_{H^+} - C_{CuCl_2^-} - C_{Cl^-} = \frac{2i}{DF}(L-x)$$

$$+ \quad - C_{H^+} + C_{CuCl_2^-} + C_{Cl^-} = 0$$

$$2C^o - 2C_{H^+} = \frac{2i}{DF}(L-x)$$

$$\boxed{C_{H^+} = C^o - \frac{i}{DF}(L-x)}$$

Substitute C_{H^+} into the H^+ flux equation:

$$\frac{i}{DF} + \{C^o - \frac{i}{DF}(L-x)\}\frac{F}{RT}\frac{d\phi}{dx} = 0$$

$$\int_0^{\phi} d\phi = -\frac{RT}{F}\int_L^x \frac{1}{\frac{DFC^o}{i} - (L-x)}\,dx$$

$$\phi = -\frac{RT}{F}\{\ln(\frac{DFC^o}{i} - (L-x)) - \ln(\frac{DFC^o}{i})\}$$

$$\boxed{\phi = -\frac{RT}{F}\{\ln 1 - \frac{i}{DFC^o}(L-x)\}}$$

Substitute potential into $CuCl_2^-$ flux equation:

$$\frac{\delta C_{CuCl_2^-}}{\delta x} - C_{CuCl_2^-}\frac{F}{RT}(\frac{RT}{F}\frac{i}{DFC^o - i(L-x)} = \frac{i}{D_{CuCl_2^-F}}$$

$$\frac{\delta C_{CuCl_2^-}}{\delta x} + PC_{CuCl_2^-} = Q \qquad P \equiv \frac{i}{DFC^o - i(L-x)} \qquad Q \equiv \frac{-i}{D_{CuCl_2^-F}}$$

$$C_{CuCl_2^-} = \exp(-\int_0^x P dx)\{-\int Q\exp(\int_0^x P dx)dx + K\}$$

$$= \exp\int_0^x -\frac{i dx}{DFC^o - i(L-x)}\{-\int\frac{i}{D_{CuCl_2^-F}}\exp\int_0^x\frac{i dx}{DFC^o - i(L-x)}dx + K\}$$

$$= \exp\frac{\frac{DFC^o}{i} - (L-x)}{\frac{DFC^o}{i} - L}\{\frac{-i}{D_{DuCl_2^-}}\int\exp(\ln\frac{\frac{DFC^o}{i} - (L-x)}{\frac{DFC^o}{i} - L})dx + K\}$$

$$= \frac{DFC^o - iL}{DFC^o - i(L-x)}\{\frac{-i}{D_{CuCl_2^-F}}\int(1 + \frac{x}{\frac{DFC^o}{i} - L})dx + K\}$$

$$C_{CuCl_2^-} = \frac{DFC^o - iL}{DFC^o - i(L-x)} \left\{ - \frac{i}{D_{CuCl_2^-F}} \left(x + \frac{x^2}{2\left(\frac{DFC^o}{i} - L\right)} \right) + K \right\}$$

At $x=L$ $C_{CuCl_2^-} = 0$, therefore:

$$K = \frac{iL}{D_{CuCl_2^-F}} \left(1 + \frac{iL}{2(DFC^o - iL)} \right)$$

$$C_{CuCl_2^-} = \frac{DFC^o - iL}{DFC^o - i(L-x)} \left\{ \frac{-ix}{D_{CuCl_2^-F}} \left(1 + \frac{ix}{2(DFC^o - iL)}\right) + \frac{iL}{D_{CuCl_2^-F}} \left(1 + \frac{iL}{2(DFC^o - iL)}\right) \right\}$$

$$= \frac{i}{D_{CuCl_2^-F}} \frac{DFC^o - iL}{DFC^o - i(L-x)} \left\{ (L-x) + \frac{i(L^2 - x^2)}{2(DFC^o - iL)} \right\}$$

$$= \frac{i}{D_{CuCl_2^-F}} \frac{DFC^o - iL}{DFC^o - i(L-x)} (L-x) \left\{ 1 + \frac{i(L-x)}{2(DFC^o - iL)} \right\}$$

$$\boxed{C_{CuCl_2^-} = \frac{i(L-x)}{2D_{CuCl_2^-F}(DFC^o - i(L-x))} (2DFC^o - i(L-x))}$$

$$C_{Cl^-} = C_{H^+} - C_{CuCl_2^-}$$

$$C_{Cl^-} = C^o - \frac{i}{DF}(L-x) - \frac{i(L-x)}{2D_{CuCl_2^-F}(DFC^o - i(L-x))} (2DFC^o - i(L-x))$$

$$\boxed{C_{Cl^-} = C^o - \frac{i(L-x)}{F} \left\{ \frac{1}{D} + \frac{DFC^o - \frac{i}{2}(L-x)}{D_{CuCl_2^-}(DFC^o - i(L-x))} \right\}}$$

The final solutions are expressed as ion concentrations or potential as a function of distance in the electrolyte, and are summarized in Figure A-3. The distance X always appears in these equations subtracted from the diffusion boundary layer thickness, L, and multiplied by the anodic current density i. Thus, the plots of these concentrations and potentials presented below use the product i times L-X as the independent variable.

Figure A-4 is a plot of potential versus i times L-X divided by the bulk HCl concentration, C^o, assuming the diffusion constant for the chloride ion complex is the same as that for chloride ions, 2.03 X 10^{-5} cm^2/s. A positive value for the constant D was thus generated. Depending on the relative values of the diffusion constants for the chloride complex and the chloride ion, it is possible to get a negative value for the constant D. Positive shifts in potential are predicted, with the potential profile being roughly linear.

Figure A-5 is a plot of the concentration of ionic species, normalized by dividing by the bulk HCl concentration, versus i times L-X, also normalized by dividing by the bulk HCl concentration. All of the concentration profiles are roughly linear, although the cation profiles show a small amount of curvature. Since pure diffusion through a Nernst layer would predict a linear profile if diffusivity is not a function of position or concentration, the deviations from linearity must be due to

$$\phi = -\frac{RT}{F} \ell n \left(1 - \frac{i}{DFC^{\circ}} (L-X)\right)$$

$$C_{H^+} = C^{\circ} - \frac{i}{DF} (L-X)$$

$$C_{CuCl_2^-} = \frac{i\,(L-X)\,(2\,DFC^{\circ} - i(L-X))}{2\,D_{CuCl_2^-}\,F\,(DFC^{\circ} - i(L-X))}$$

$$C_{Cl^-} = C^{\circ} - \frac{i\,(L-X)}{F} \left[\frac{1}{D} + \frac{DFC^{\circ} - \frac{i}{2}(L-X)}{D_{CuCl_2^-}\,(DFC^{\circ} - i(L-X))}\right]$$

$$\frac{1}{D} \equiv \frac{1}{D_{Cl^-}} - \frac{1}{2D_{CuCl_2^-}}$$

Figure A3.
Solution for Mathematical Model

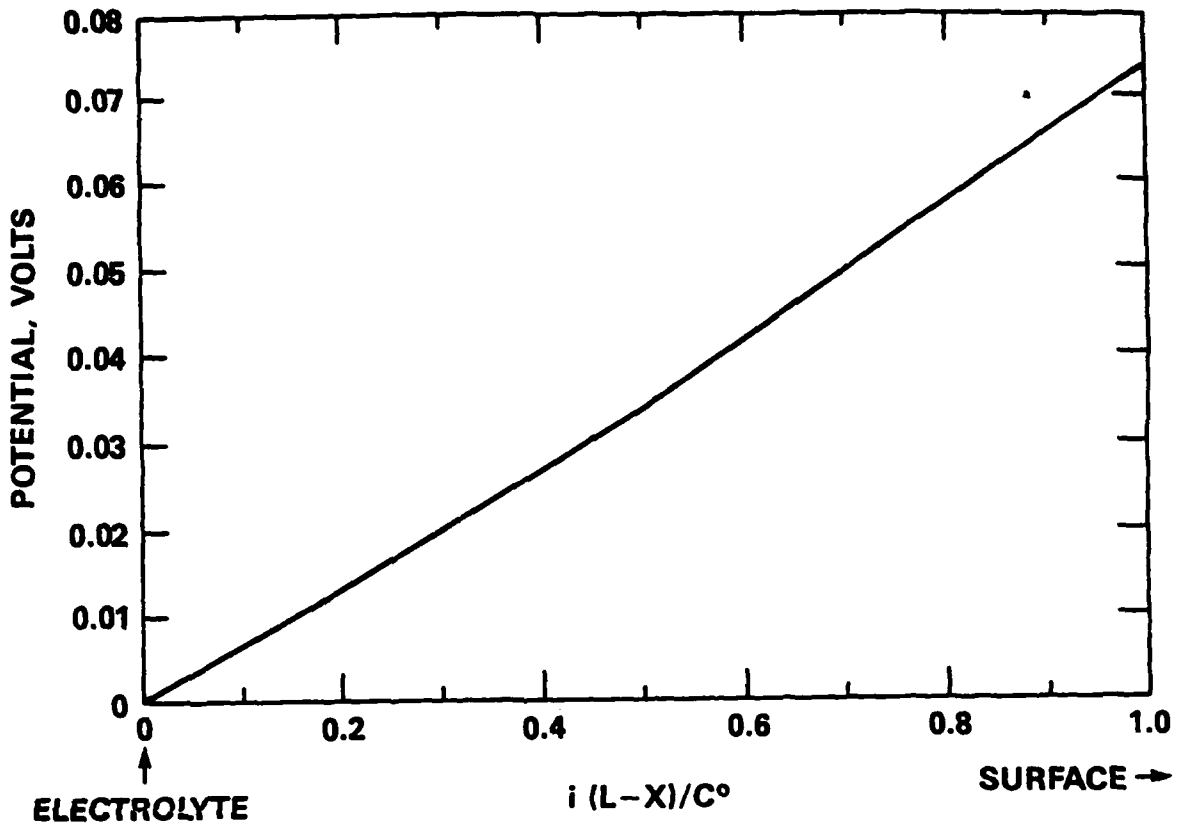

Figure A4.
Potential Profile

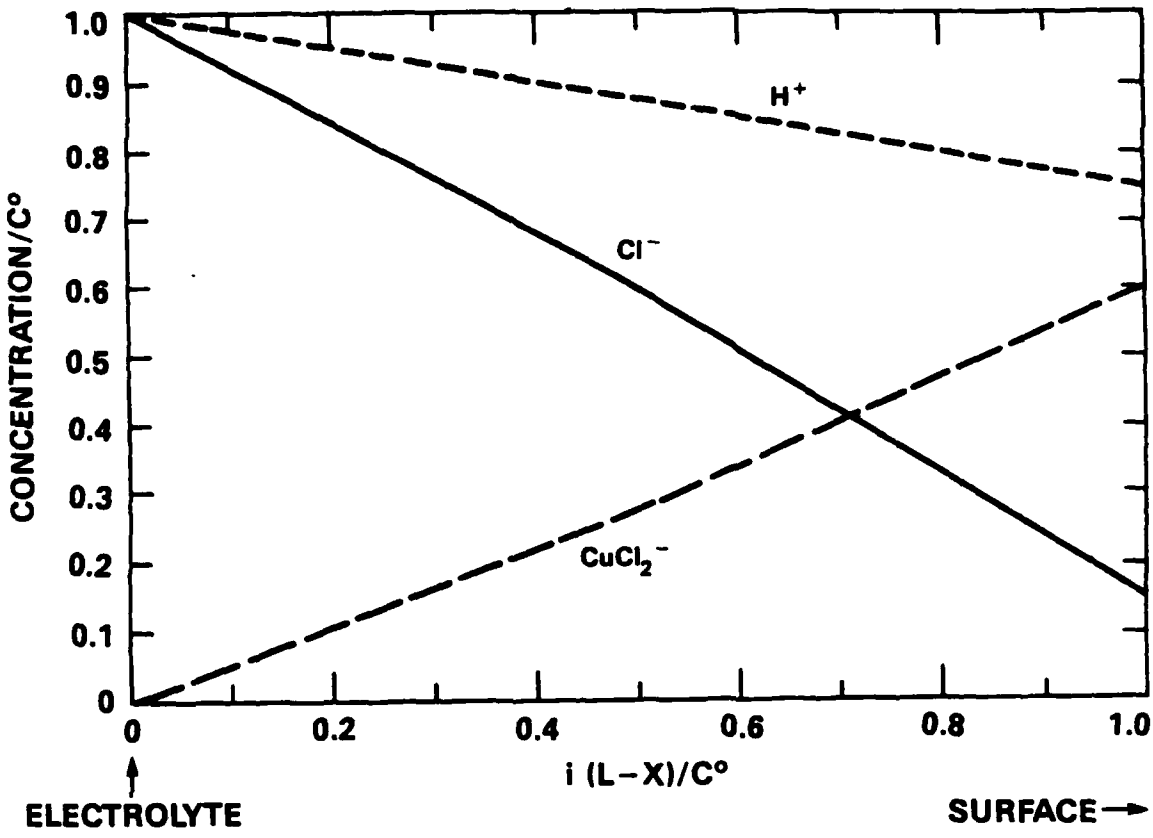

Figure A5.
Concentration Profiles

electro-migration effects. These effects must be comparitively small, since curvature is minimal. Hydrogen ion concentration decreases as the surface is approached, as expected from the potential gradient. Chloride ion concentration also decreases as the surface is approached, as expected since they are being used up at the surface, and finally goes to zero at a value for $i(L-X)/C^{o}$ of about 1.1. At this point the model breaks down, since negative values of concentration cannot physically exist. Thus, if the concentration of HCl is low enough to cause this condition before the surface is reached, then the assumed value of current is too large to support this corrosion mechanism. The concentration of the chloride ion complex increases as the surface is approached, as should be the case since these ions are generated there.

It is conceivable that the diffusivities of the chloride-containing ions may be such as to give a negative value to the constant D. The equations in Figure A-3 predict in this case a negative value for potential and negative concentrations, both of which are physically unrealistic in this situation. Thus, this value for the constant D is not permitted if this mechanism is valid.

In summary, this model predicts physically meaningful behavior only when the diffusivities of the chloride-containing ions are such that the constant D is positive. This is realistic based on the diffusivities used in the calculations. Near the electrode where the

concentration of the copper-chloride complex ion is large, the results of this model may not be accurate due to the dilute solution approximations used. Also, any time a negative concentration of chloride ions is predicted, a physically unrealistic situation exists, indicating that currents of the magnitude assumed cannot be supported by this corrosion mechanism.

Since this model is for steady-state conditions, it is interesting to surmise how these profiles develop. Since the concentration profiles of the chloride-containing ions are all essentially linear, they must be affected only minimally by the potential field in the solution, and must therefore be controlled by diffusion. The field does have an effect of redistributing the hydrogen ions, however. If the polarization of the copper is applied potentiostatically, the Nernst Equation predicts the concentration of the copper ion complex ions at the surface, and this is therefore invariant over time. A similar situation exists for the chloride ions. Thus, the depth of the diffusion boundary layer must be that predicted by diffusion into a semi-infinite plate, and be of the form[A-2]:

$$L = (\pi \times D \times t)^{1/2}$$

where: L = depth of diffusion boundary layer, cm

D = diffusivity of ionic species, cm^2/s

t = time, s

Conversely, if the polarization is developed galvanostatically (at constant current), the surface concentrations are not fixed, but the production rate of ions is a constant. Since ionic flux is related by Fick's Law to the slope of the concentration profile, the slope must be constant, and thus the depth of the diffusion boundary layer will increase as the ions are generated to fill in the "area" below the concentration profile curve. This leads to an equation of the form[A-2]:

$$L = (4/pi \times D \times t)^{1/2}$$

where: L = depth of diffusion boundary layer, cm

D = diffusivity of ionic species, cm^2/s

t = time, s

In both cases, the diffusion boundary layer increases as the square root of time until it is limited by the size of the hydrodynamic boundary layer, outside of which pure mixing takes place.

REFERENCES

A-1. Bacarella, A. L. and J. C. Griess, Jr., "The Anodic Dissolution of Copper in Flowing Sodium Chloride Solutions Between 25° and 175 °C," J. Electrochem. Soc., 120(4), pp 459-465, April 1973.

A-2. Bockris, J. O'M., and Reddy, A. K. N., Modern Electrochemistry, Plenum Press, New York, New York, 1970, pp. 1058-1059.

APPENDIX

B. DETERMINATION OF DIFFUSION CONTROL BY ANODIC ETCHING

The use of anodic polarization to etch rotating disk specimens of copper, 90-10 copper-nickel, and 70-30 copper-nickel has some interesting aspects related to the rate-controlling step of the anodic reaction. If the anodic reaction is under activation control, then the energy to remove the atoms should be dependent on the crystallographic orientation of the grains relative to the face of the specimen, or to the location of the atom relative to a kink, step, or terrace site. This should result in non-uniform attack, leading to the formation of crystallographic steps on the corroded surface. If the anodic reaction is controlled by reactants diffusing to the surface through a fluid boundary layer whose thickness is large compared to the grain size, then the rate of attack must be uniform. This is because the concentration of reactants is zero everywhere on the surface when this type of diffusion is controlling, resulting in a uniform concentration gradient of reactants at all points on the surface, which in turn means a uniform supply rate of reactants, which should result in uniform etching or polishing.

If the rate of the anodic reaction is controlled by diffusion of reaction products away from the surface, the result is more complex, as can be seen in Figure B-1. A constant anodic potential over the surface would initially

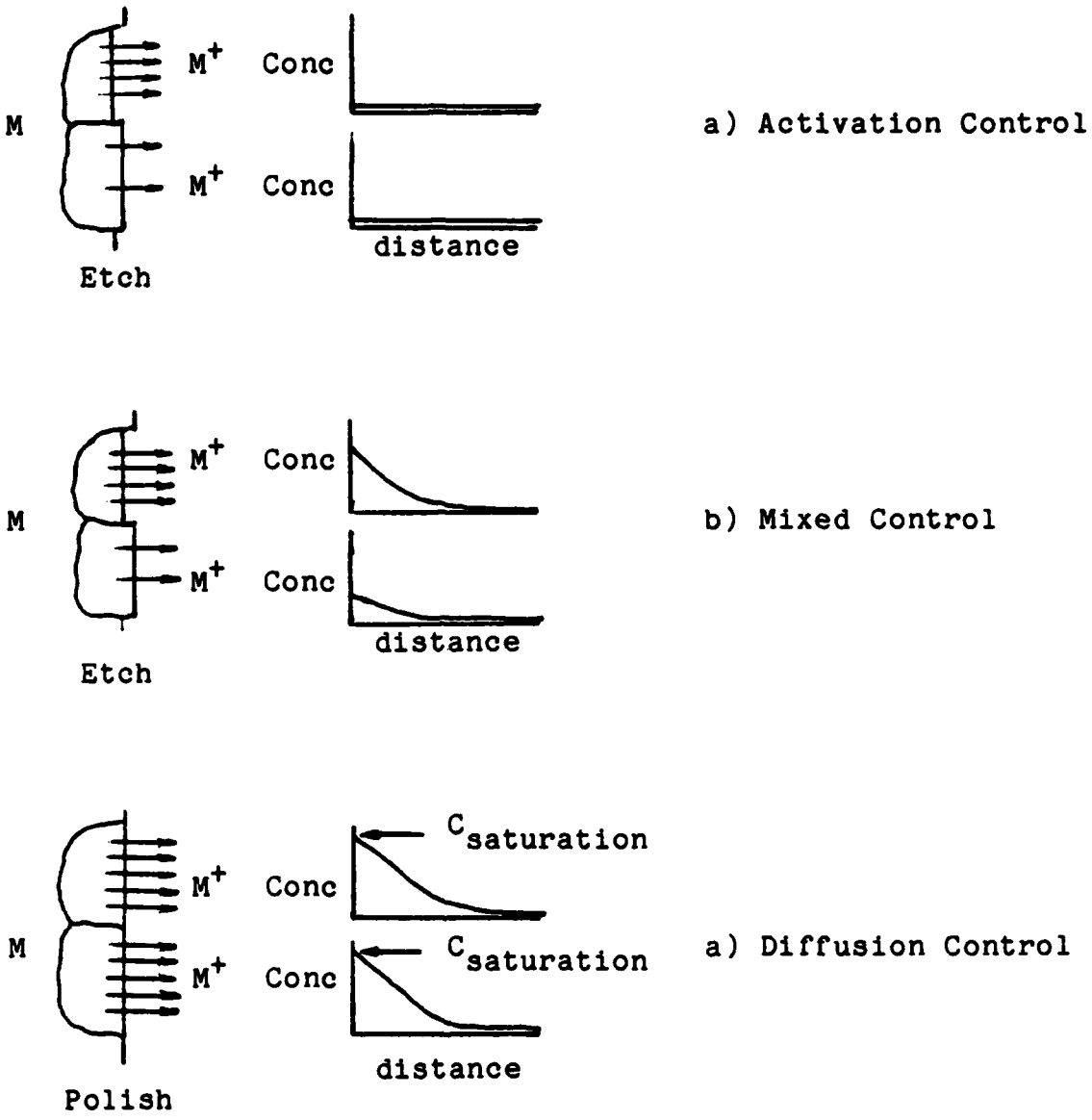

Figure B1.
Etching vs. Polishing for Diffusion Away from the Interface

result in activation control, as in Figure B-1a. As equilibrium is approached, the surface concentration of reaction products would increase to different levels at different points on the surface, resulting in an instantaneous form of mixed control. This would result in nonuniform concentration gradients which lead to nonuniform transport and nonuniform attack, as in Figure B-1b. This situation would not lead to diffusion control of the anodic reaction, since increasing anodic potentials would simply lead to a higher surface concentration of reactants, and thus to higher concentration gradients and corrosion rates. Diffusion control in this case can only occur if something happens to limit the concentration gradient. The likely limiting factor would be exceeding the solubility of the reaction product at the surface. This would limit the maximum concentration, and thus the concentration gradient, and result in diffusion control of the reaction and uniformity of the reaction over the surface due to uniformity of the removal rate of reaction products, as shown in Figure B-1c.

This hypothesis was tested by performing controlled anodic polarization in 10% H_2SO_4, where the corrosion rate is expected to be activation controlled, and in 10% HCl, where the attack is expected to be controlled by diffusion of a copper chloride ionic complex away from the surface. These results were compared to those for free corrosion in saltwater before formation of corrosion products, where the

anodic process is expected to be controlled by the same mechanism as in HCl, even though the overall corrosion rate is controlled by diffusion of oxygen to the surface. First, polarization curves of each material in each acid environment were made at 0.1 mV/s. For subsequent potentiostatic polarization, a potential in the Tafel region was chosen if it was apparent on these curves, otherwise a potential of about 100 mV from free corrosion was used to ensure suppression of the cathodic reactions on the specimen surface. Specimens of each material were metallographically polished, held potentiostatically in each solution while rotating at 1000 RPM, then examined using a scanning electron microscope. Additionally, the rotation dependence of the current needed to polarize each specimen was checked by decreasing rotation speed to 500 RPM for the second five minutes of each exposure. This provided an additional check on whether the reaction was controlled by diffusion through a fluid boundary layer.

Figure B-2 shows the anodic polarization behavior of the three copper-nickel alloys in de-aerated 10% H_2SO_4. Although having different corrosion potentials and differing degrees of passivity at 0 mV, all three curves were identical in the Tafel region. The three materials were polished, then held at the upper end of the Tafel region at about -25 mV versus saturated Calomel for 100 minutes in the acid. Although not expected for an activation-controlled process, a small rotation-speed dependence was noted.

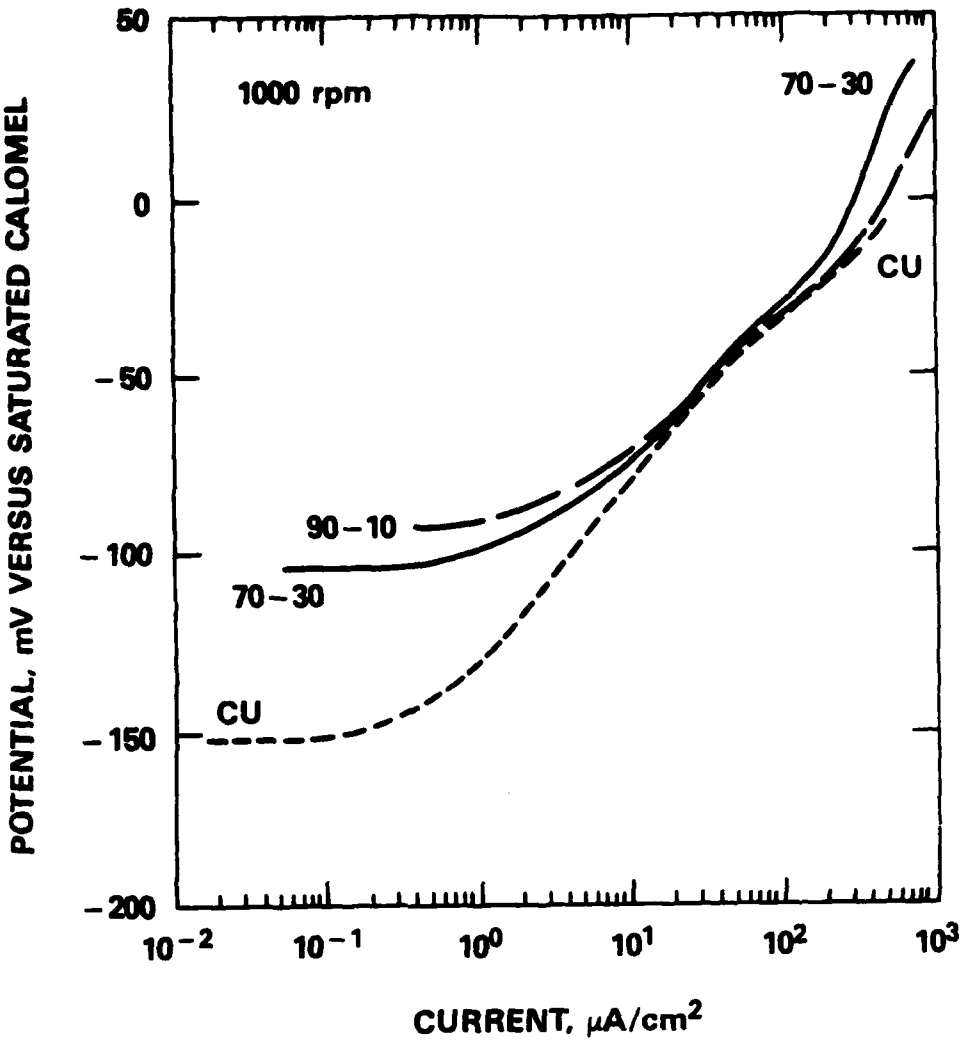

Figure B2.
Anodic Polarization in Deaerated 10% H_2SO_4

Current reductions were observed of 1.2 to 1.3 (as compared to 1.41 for ideal diffusion control) when going from 500 to 1000 RPM, indicating a slight departure from ideal activation-controlled behavior, with some contribution to reaction control by diffusion. SEM photographs of the surfaces are presented as Figures B-3 through B-5. Figure B-3 shows the copper surface. Crystallographic steps are evident and are on the order of 1-2 microns in size. These steps cannot be seen on 90-10 copper-nickel in Figure B-4 or on 70-30 copper nickel in Figure B-5. Attack on the alloys was so uniform that grain boundaries were not readily seen. It is possible that microsegregation effects in the alloys override the surface energy differences between crystallographic faces.

Figure B-6 shows the anodic polarization behavior of the three copper-nickel alloys in de-aerated 10% HCl. A distinct Tafel region is not seen, and the current at any given potential is lowered by the presence of nickel in the alloy, the effect being roughly proportional to the amount of nickel. After polishing, rotating specimens of the three alloys were held for 30 minutes in the acid at -275, -250, and -225 mV for copper, 90-10 copper-nickel, and 70-30 copper-nickel respectively. This gave roughly equal current densities for each alloy of about 1 mA/cm^2. As in the other acid, the currents showed a rotation speed dependence of 1.2 to 1.3 when going from 500 to 1000 RPM, indicating mixed control. SEM photographs for these alloys are shown in

a) Magnification 5400X

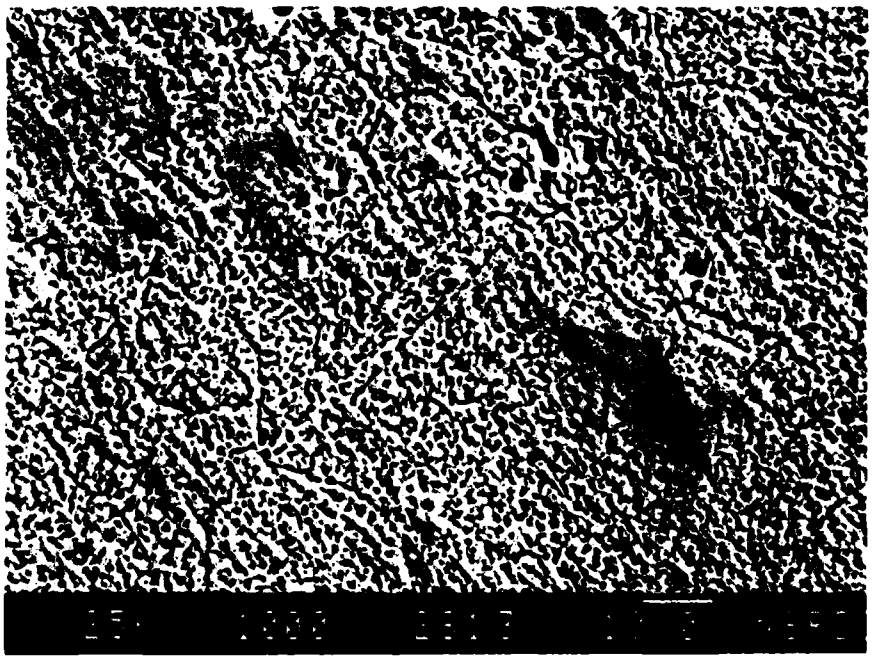

b) Magnification 1000X

Figure B3.
Copper Anodically Polarized in H_2SO_4

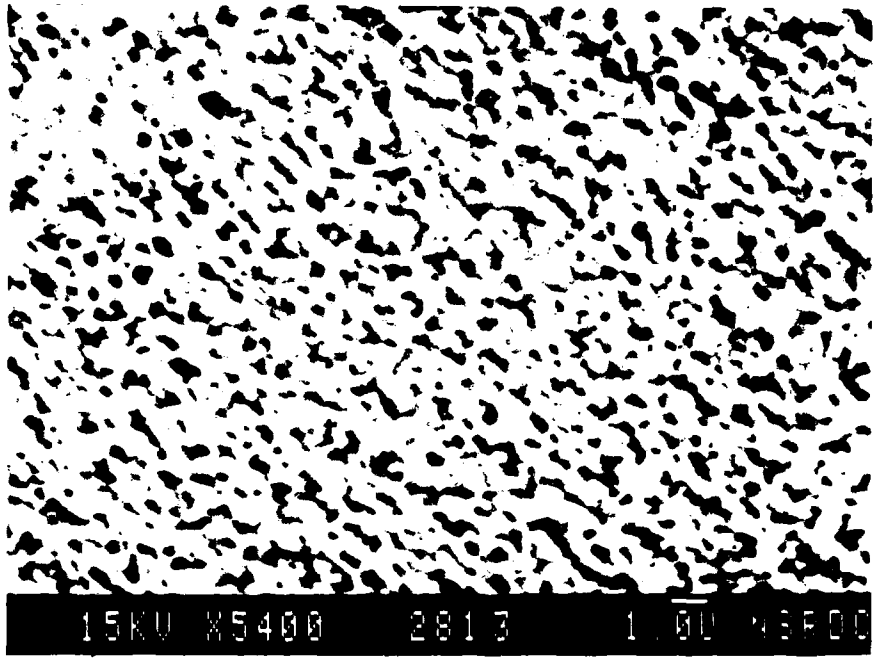

a) Magnification 5400X

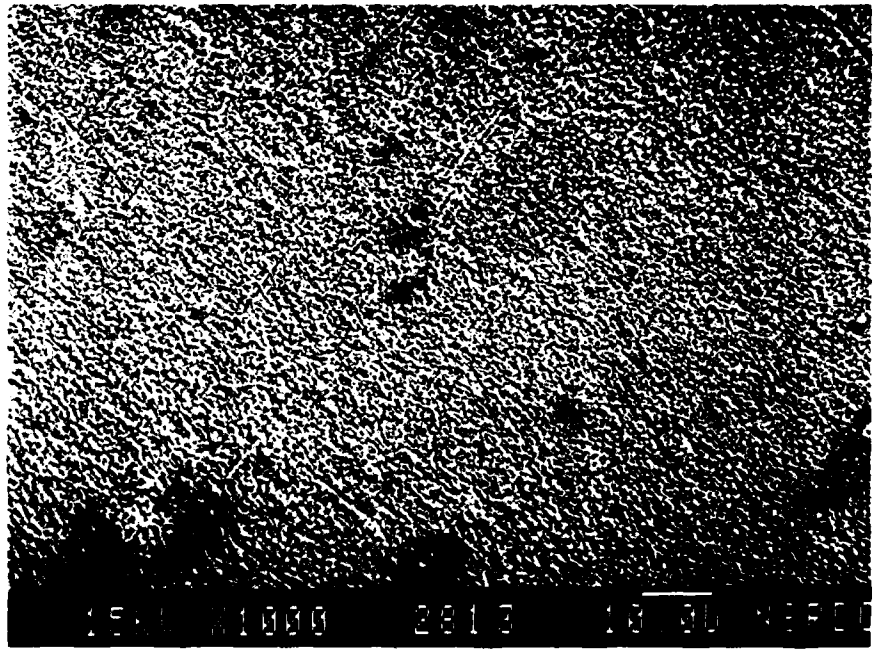

b) Magnification 1000X

Figure B4.
90-10 Copper-Nickel Anodically Polarized in H_2SO_4

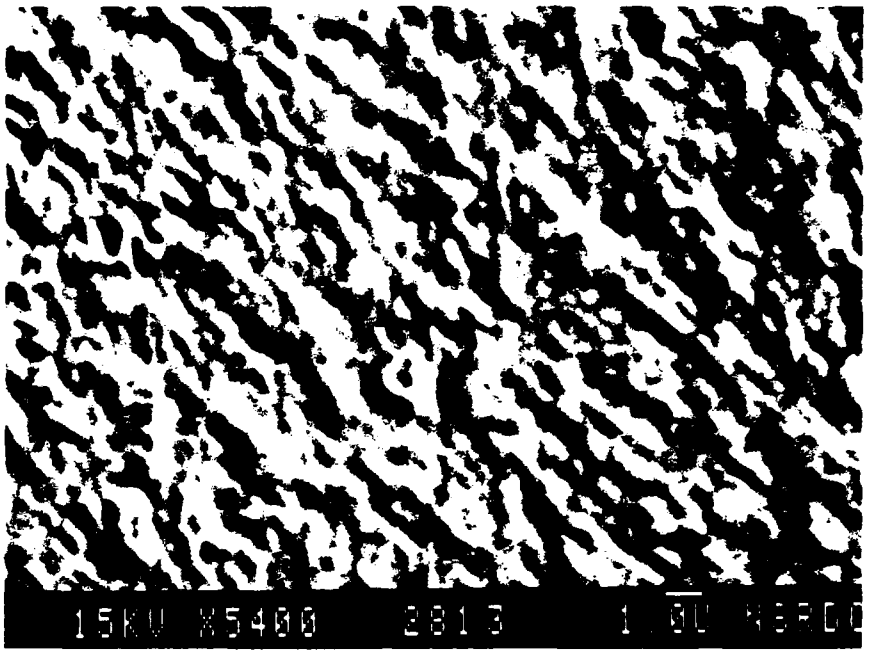

a) Magnification 5400X

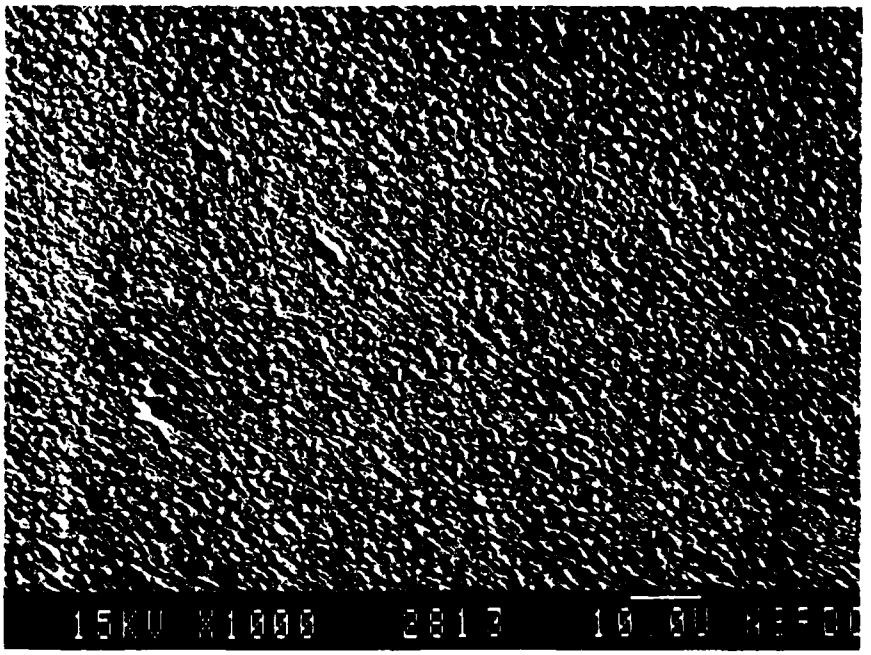

b) Magnification 1000X

Figure B5.
70-30 Copper-Nickel Anodically Polarized in H_2SO_4

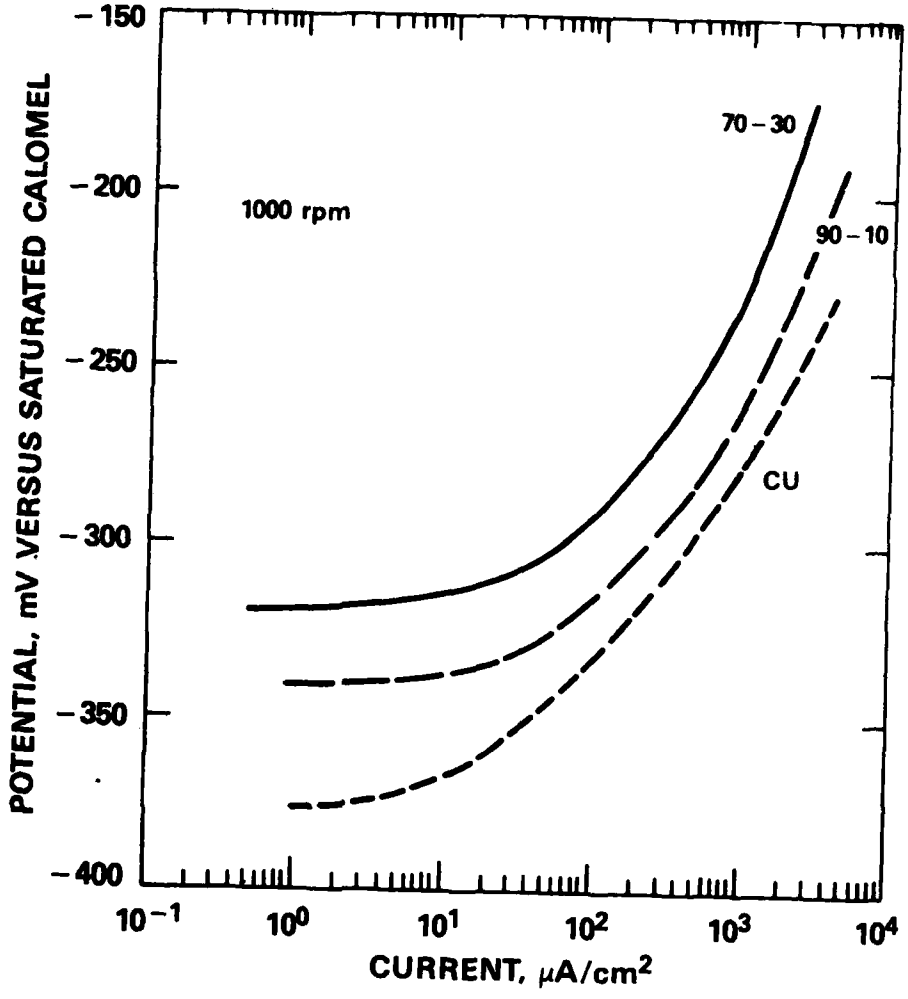

Figure B6.
Anodic Polarization in Deaerated 10% HCl

Figures B-7 to B-9. Figure B-7 shows the crystallographic steps for copper which are again on the order of 1-2 microns in size. The 90-10 alloy in Figure B-8 and the 70-30 alloy in Figure B-9 show no evidence of these steps, again probably due to microsegregation effects.

The three alloys were also polished and exposed to 3.4% NaCl solution for 8 hours under freely corroding conditions. SEM photographs of the specimen surfaces are shown in Figures B-10 to B-12. Crystallographic steps are seen for copper, although not for either alloy. At first, one might think that this exposure would result in polishing, since the overall corrosion reaction is controlled by diffusion of dissolved oxygen to the alloy surface. This may not be the case, however, since current from the cathodic partial reaction will redistribute so that the presence of etching or polishing will depend only on the controlling mechanism for the anodic partial reaction. Since oxygen diffusion is limiting the overall rate of reaction, the anodic partial reaction may not be proceeding at its maximum, diffusion-controlled rate, but may instead be operating under mixed control, resulting in etching.

The size of the diffusion boundary layer at 1000 RPM can be calculated from the Levich equation as follows:

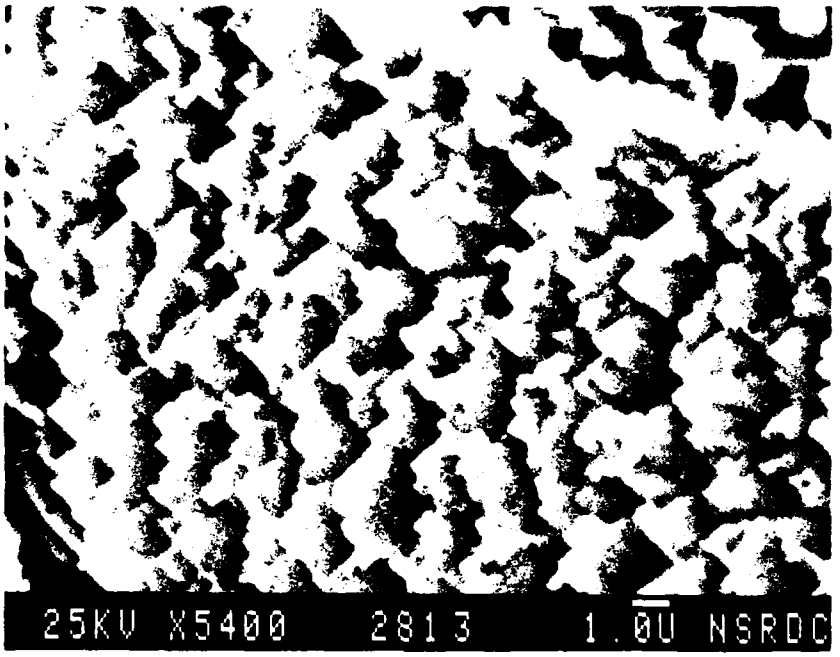

a) Magnification 5400X

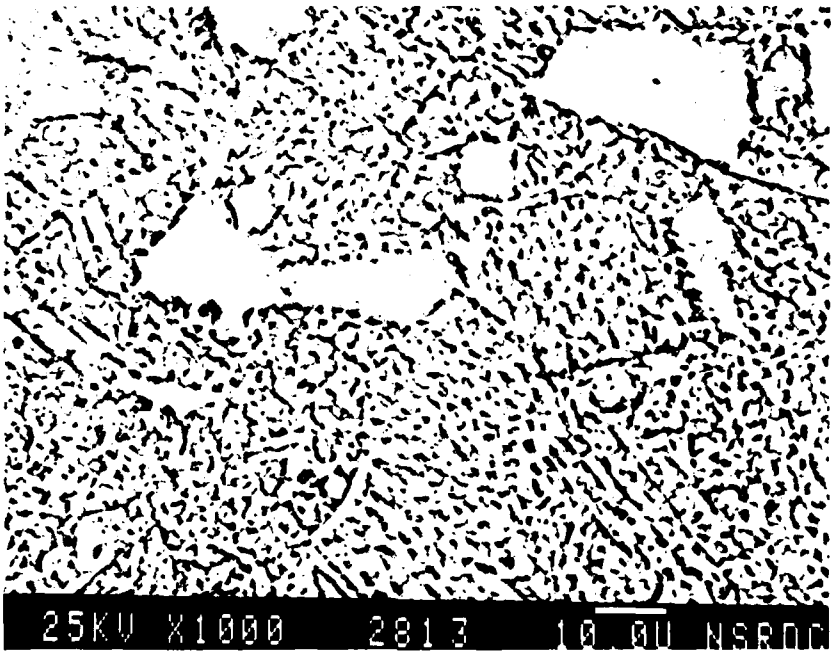

b) Magnification 1000X

Figure B7.
Copper Anodically Polarized in HCl

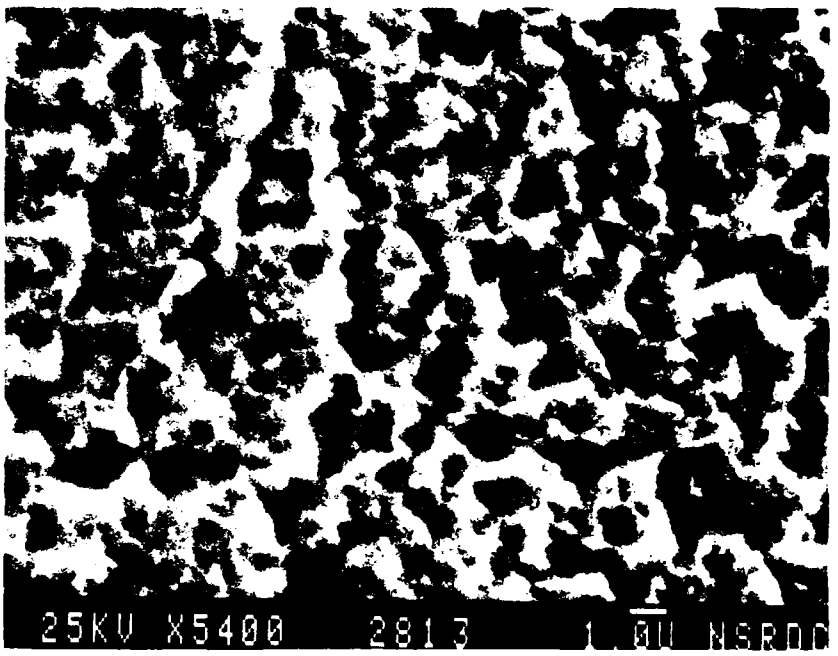

a) Magnification 5400X

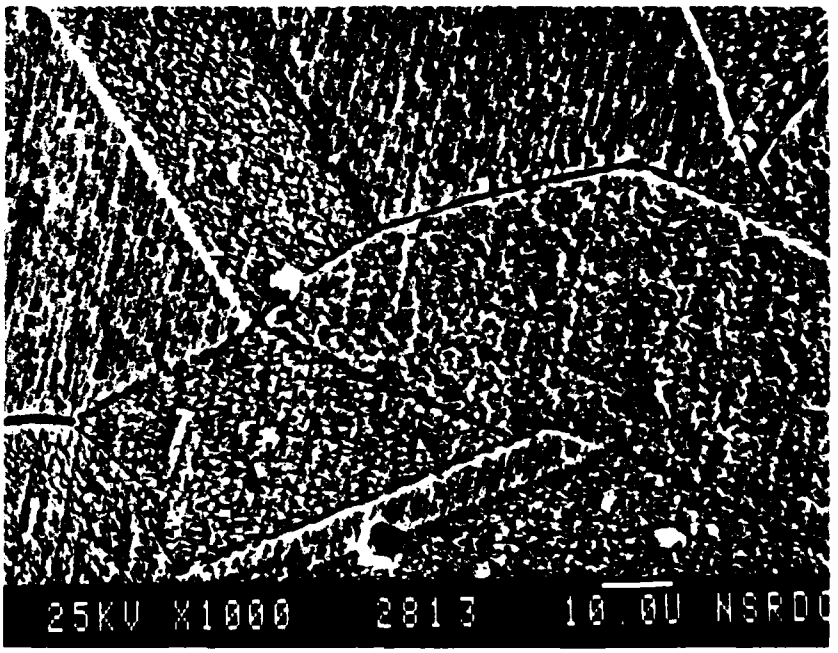

b) Magnification 1000X

Figure B8.
90-10 Copper-Nickel Anodically Polarized in HCl

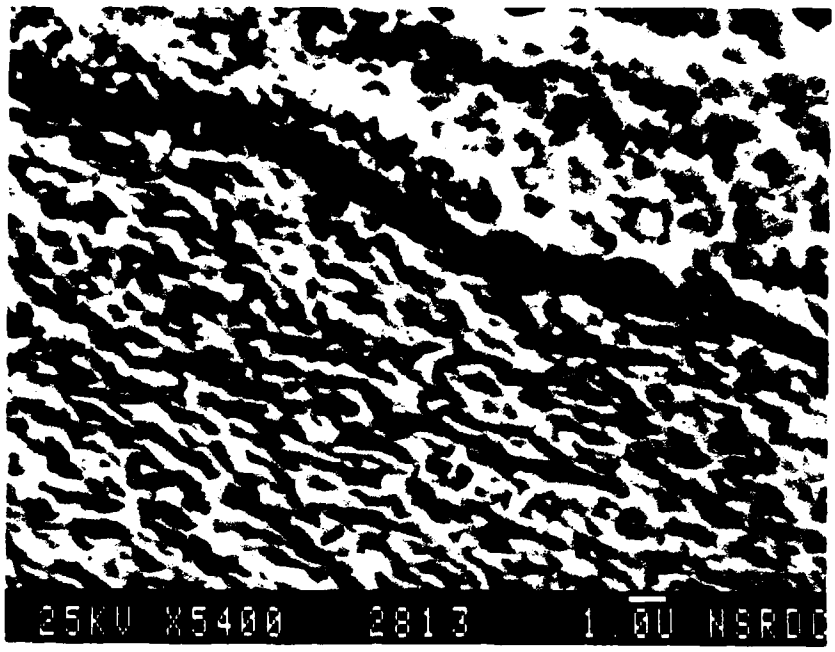

a) Magnification 5400X

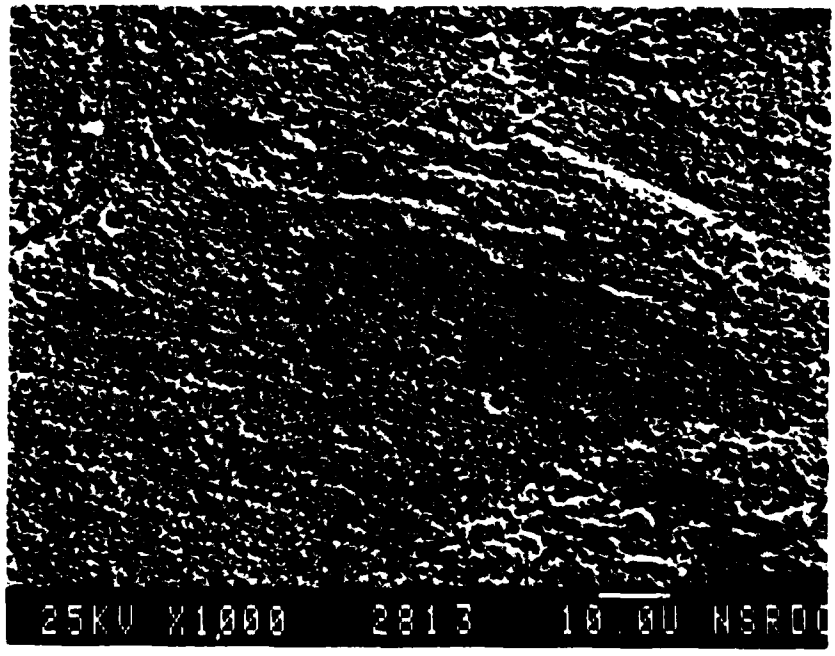

b) Magnification 1000X

Figure B9.
70-30 Copper-Nickel Anodically Polarized in HCl

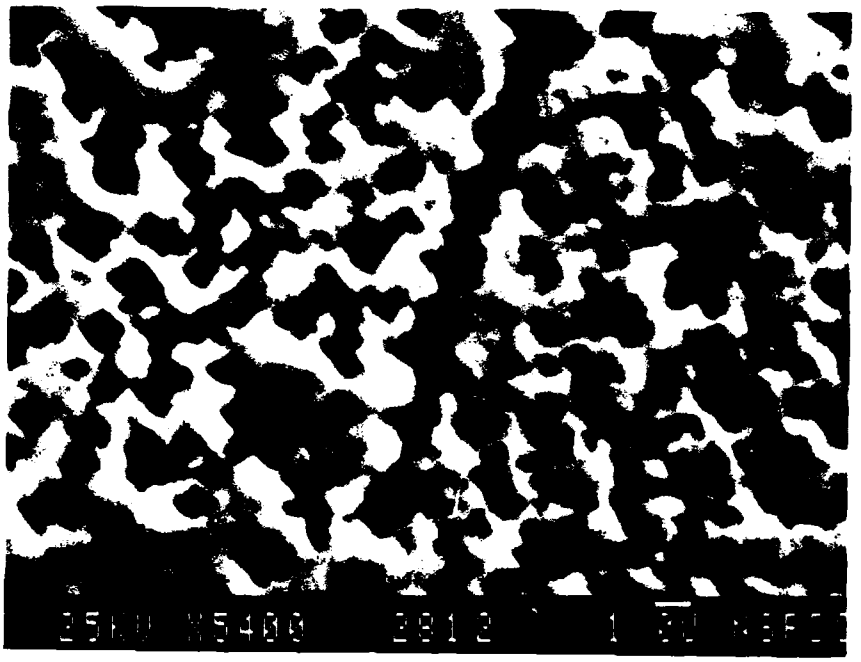

a) Magnification 5400X

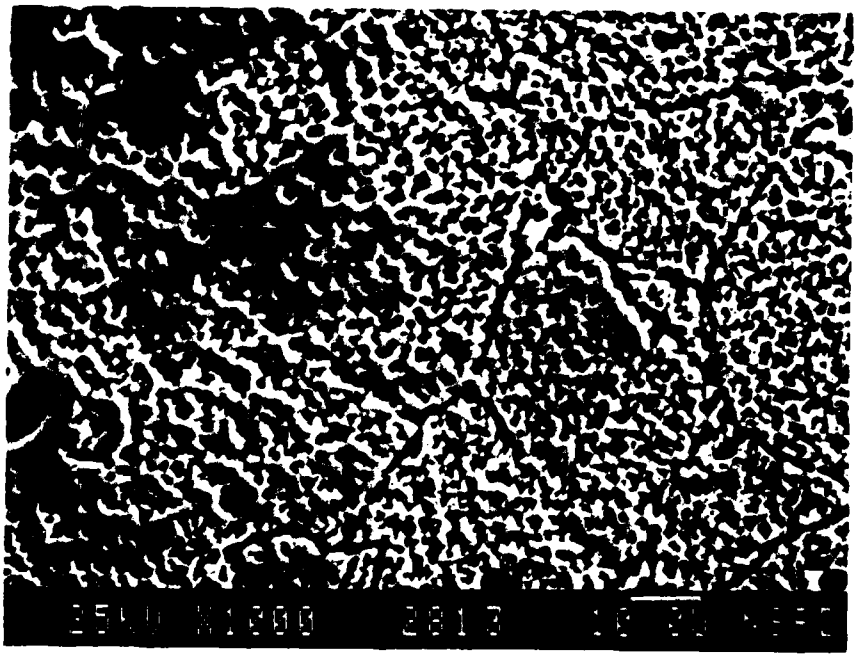

b) Magnification 1000X

Figure B10.
Copper Exposed to NaCl

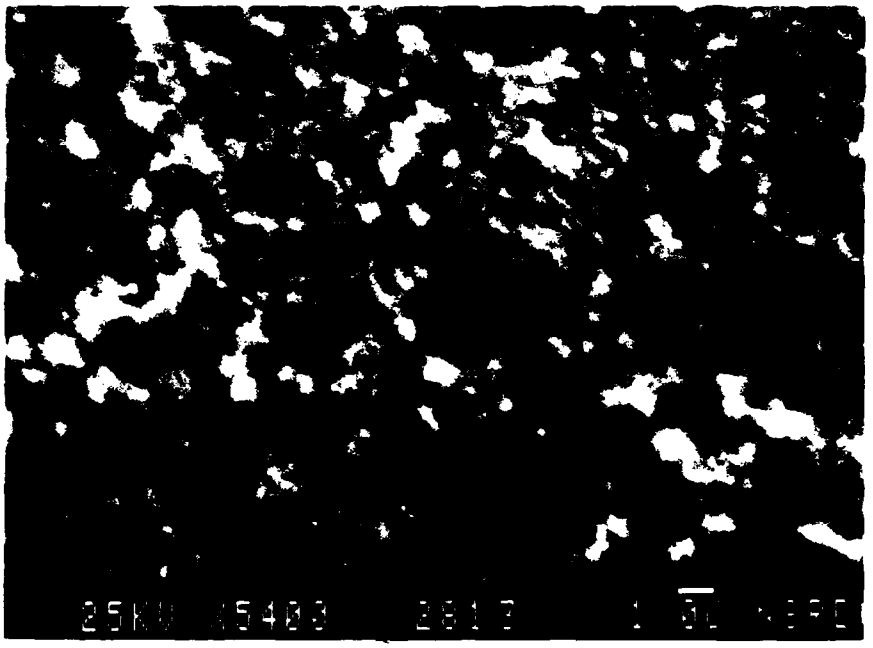

a) Magnification 5400X

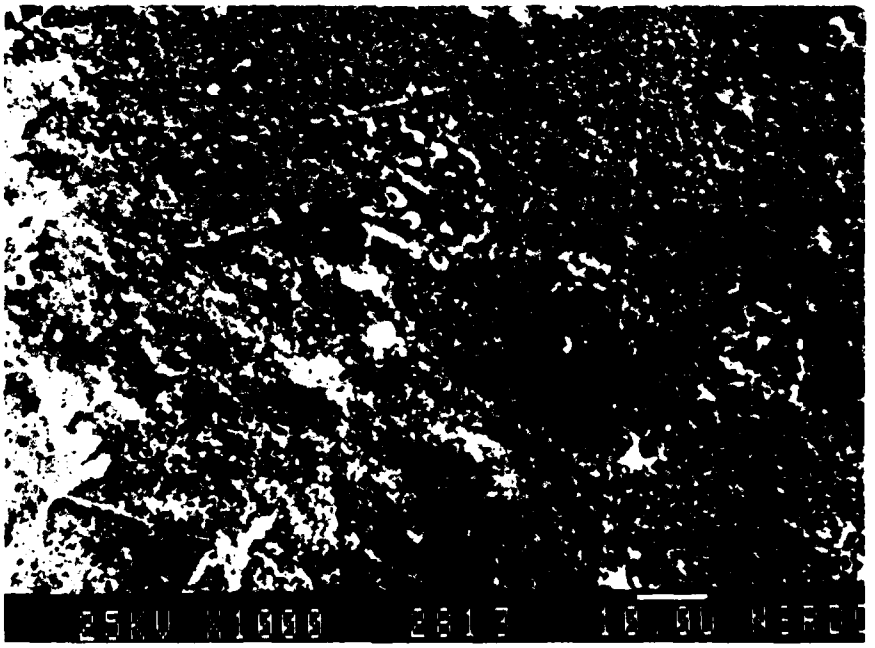

b) Magnification 1000X

Figure B11.
90-10 Copper-Nickel Exposed to NaCl

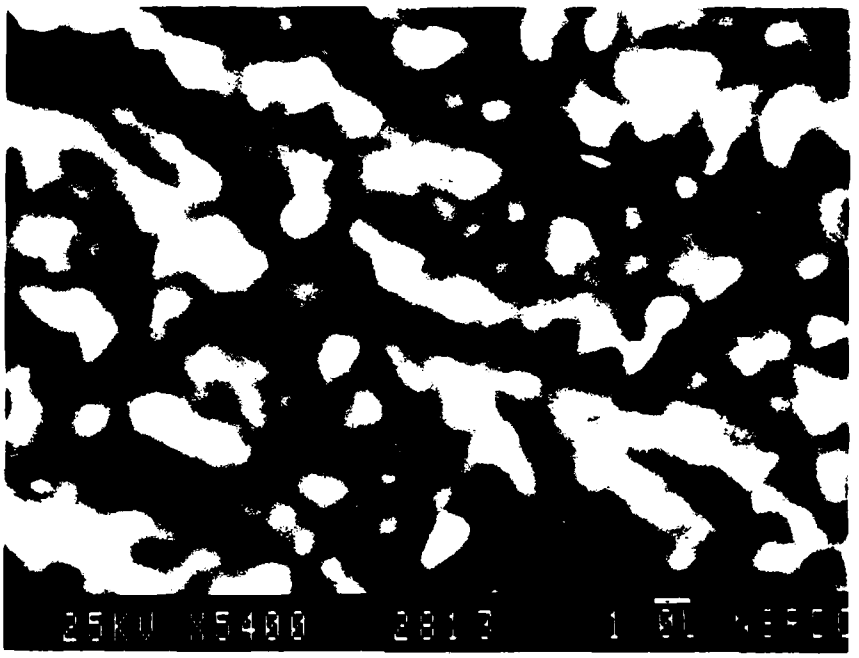

a) Magnification 5400X

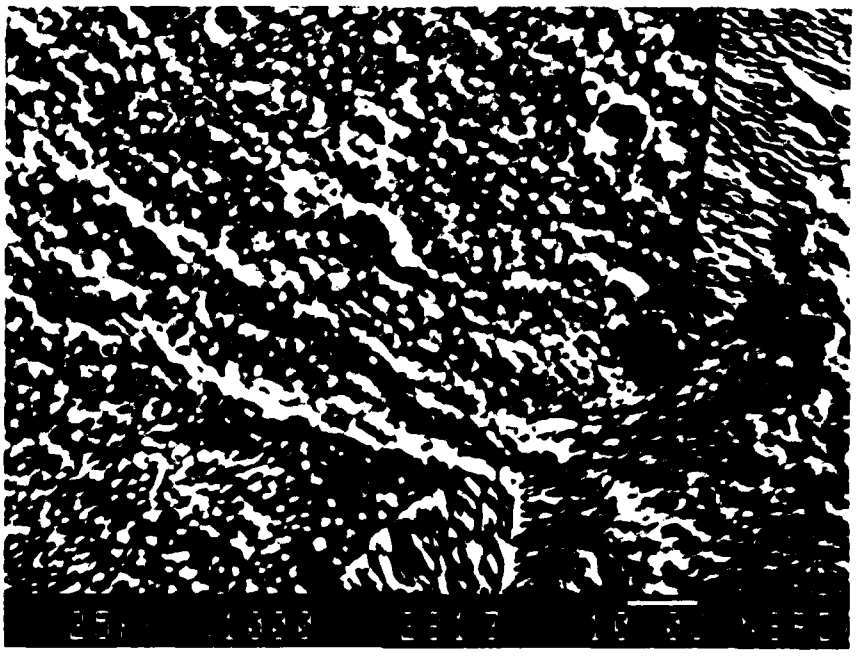

b) Magnification 1000X

Figure B12.
70-30 Copper-Nickel Exposed to NaCl

$$L = 1.61\ D^{1/3}\ w^{-1/2}\ v^{1/6}$$

where: L = diffusion boundary layer thickness, cm

D = diffusivity (1.9×10^{-5} cm^2/s for oxygen)

w = rotation speed (1000RPM X 2 X pi/60)

v = kinematic viscosity (0.008 cm^2/s)

which yields: L = 18.8 microns. This is much larger than the step size observed of 1-2 microns. If the diffusivity used is that for Cu^{2+} ions, 7.2×10^{-6} cm^2/s, the resulting boundary layer is only slightly thinner, 13.6 microns. For oxygen diffusion, to get a boundary layer of less than 1 micron thickness would require a rotation speed of 350,000 RPM, which is impractical.

In summary, etching occured on pure copper in acids and in saltwater, but not on any alloy in any environment, possibly due to the overriding effect of microsegregation on surface energy. For copper in sulfuric acid, pure activation control was not observed. The mixed control actually observed resulted in etching. In hydrochloric acid, the diffusion control usually pointed out in the literature was not rate controlling, but the reaction appeared instead to be under mixed control. Since diffusion control by the copper chloride complex ion movement away from the interface is difficult to achieve unless the reaction rate is high enough to exceed the solubility product for the reactant at the surface, the degree of

anodic polarization applied in this study may have been insufficient to move this reaction out of mixed control. In saltwater, the rate of the overall reaction was limited by diffusion of oxygen to the surface, which might well have kept the rate of the anodic partial reaction low enough to be under mixed activation/diffusion control. Etching appears to be a poor method of determining the rate-controlling step in the anodic reaction on copper-nickel alloys since it will occur only on pure copper, and then under a wide variety of circumstances.

APPENDIX

C. MODELLING OF IMPEDANCE DATA FOR 90-10 COPPER-NICKEL

Mathematical modelling of impedance data is useful for many reasons.[C-1] This type of modelling is usually accomplished by making assumptions about the electrochemical interface in order to construct the equivalent circuit of the interface out of components like resistors, capacitors, diffusional impedances, and in some cases, inductors. If the values of the circuit components can be selected such that the theoretical impedance generated by such a circuit is similar to the impedance actually measured, then a strong argument can be made about the validity of the equivalent circuit, and the magnitudes of parameters such as the double-layer capacitance, corrosion product layer resistance, and polarization resistance can be obtained. For this study, the polarization resistance is of the most importance, although corrosion product layer resistance is also of some interest.

In the simplist possible corrosion reaction, the separation of charge at the surface creates a capacitor. Corrosion at that surface causes charge to move across the charge separation, creating, in effect, a leaky capacitor, represented in an equivalent circuit model as a parallel resistor and capacitor. Since the resistor relates to a resistance to charge transfer resulting in loss of metal ions from the surface in a corrosion test, it is referred to

as a polarization resistance. Finally, the interface model must also include the resistance of the electrolyte between the sample surface and the reference electrode. Such a simple equivalent circuit is known as a Randles circuit[C-1,C-2] and is shown in Figure C-1. If one plots the theoretical current response of such a circuit to an applied sinusoidal voltage in a format where the in-phase, or real, component of impedance (obtained by dividing the applied voltage by the measured in-phase current) is on the horizontal axis and the negative of the out-of-phase, or imaginary, component of impedance (obtained from the out-of-phase component of current) is on the vertical axis, a representation known as a Nyquist plot results. For a simple Randles circuit, the Nyquist plot will appear to be a semicircle, with low frequency points falling on the real axis at a resistance equal to the sum of the solution and polarization resistances. This can be rationalized from the equivalent circuit by noting that at low frequencies the capacitor behaves as an open-circuit. As the frequency of the applied sinusoidal voltage increases, the measured impedances will trace out a semicircle from right to left until, at high frequencies, the real axis is again reached, at a value equal to the solution resistance. This can be rationalized by assuming the capacitor in the equivalent circuit acts like a short-circuit at high frequencies.

A second common type of plot used in impedance studies is the Bode plot, where the horizontal axis is the log of

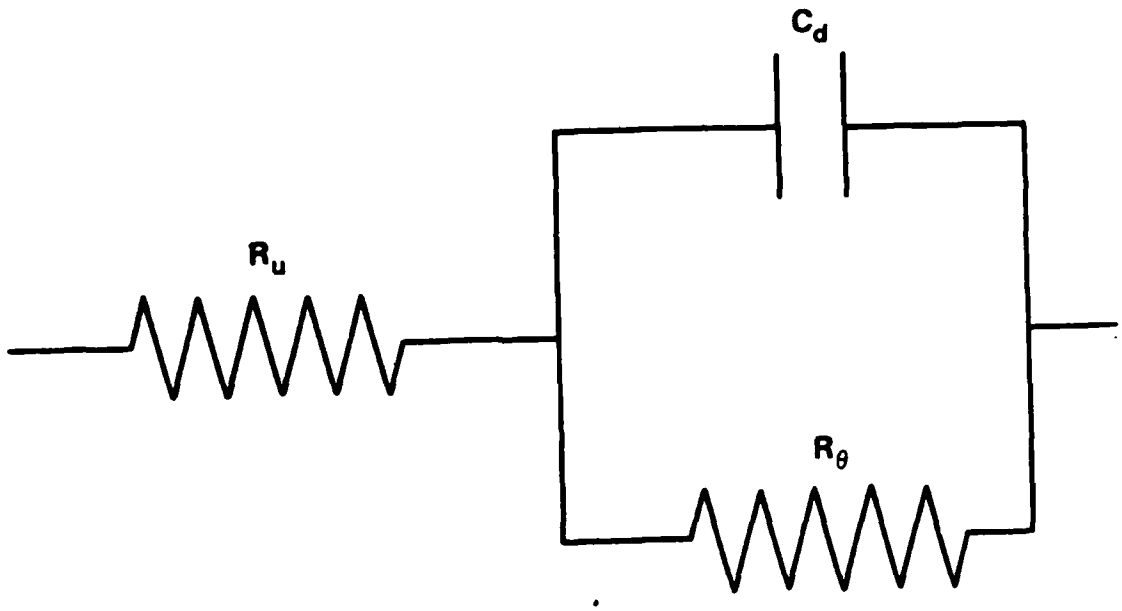

Figure C1.
Simple Electrochemical Equivalent Circuit

frequency and the vertical axis is either total impedance magnitude or phase angle between the applied voltage and the current response. In this study, only the Bode phase plots are shown. For the Randles circuit, the Bode phase plot will contain one peak, since there is one electrical time constant created by the resistor/capacitor network.

If a coating or corrosion product is present on the surface, one popular equivalent circuit which could apply is shown in Figure C-2[C-3]. The inner nested impedance can take a number of forms depending on whether finite diffusion is assumed through the corrosion product, infinite diffusion is assumed in the liquid, or whether the corrosion reaction is assumed to be a pure resistor/capacitor network with no diffusional character. In the simplist case, the Randles double-layer capacitance and polarization resistance are put in series with a resistance related to the coating, and the overall charge separation across the coating is represented by another capacitor. This type of circuit, where the inner nested impedance is simply the double layer capacitance in parallel with the polarization resistance, will generate two connected semicircles on a Nyquist plot and two peaks on a Bode phase plot, since two time constants are created by the two resistor/capacitor pairs. These two features on the curves may either be distinct, or overlapping, even to the point of impossibility of resolution, depending on the value for the various components in the circuit.

If diffusion of products or reactants through the

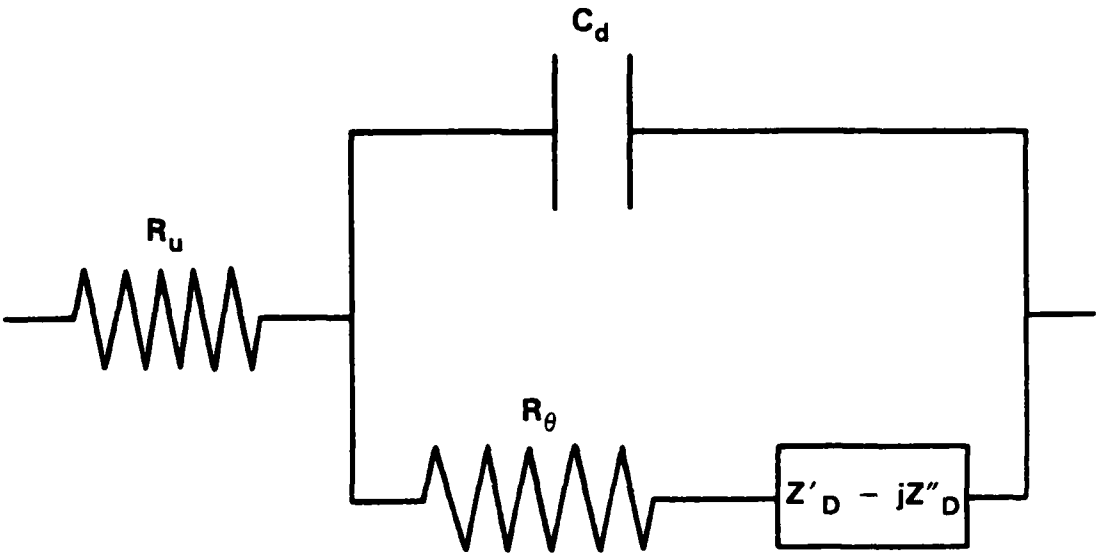

Figure C2.
Equivalent Circuit for Coating or Corrosion Product

solution is possible, the inner nested impedance is replaced with a special form specific to an infinite diffusion model, which is called a Warburg impedance and is shown in Figure C-3[C-4]. This type of impedance "looks" like a 45 degree line on the Nyquist plot extending to infinity, and like a flat line at 45 degrees on a Bode phase plot. If diffusion is over a finite distance, a modification of the diffusional impedance, as set forth by Dawson and Johns[C-5] can be used which causes the 45 degree line to eventually bend back to the real axis on a Nyquist plot and the phase angle to eventually fall to 0 degrees on a Bode plot.

In this study, a polarization resistance could be obtained fairly easily for copper and 70-30 copper-nickel by following the Nyquist semicircle back to the real axis at the lowest frequency. The 90-10 copper-nickel data did not intersect the real axis, and in fact did not usually even trace out a half of the Nyquist semicircle. Thus, it was not possible to obtain polarization resistance for that alloy from the impedance data directly. Mathematical modelling was attempted to obtain the desired data. The two cases modelled were the case of finite or "extended" diffusion as put forth by Dawson and Johns[C-5] and the pure two-time-constant case using two pure resistor/capacitor sets.

The first case discussed is the extended diffusion case. This involves a polarization resistance, double-layer capacitance, and diffusional impedance associated with a

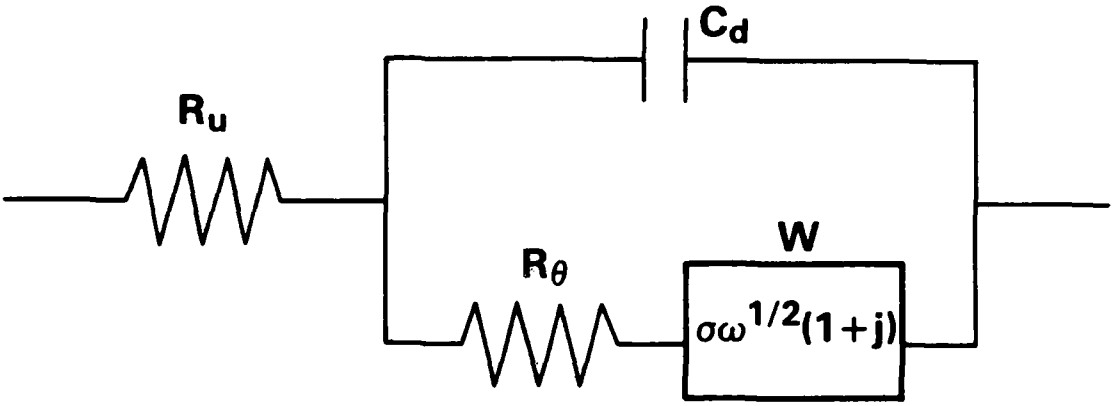

$$Z^{Real}_{Total} = R_u + \frac{R_\theta + \sigma\,\omega^{-1/2}}{(1+\sigma\omega^{1/2}\,C_d)^2 + \omega^2\,C_d^2\,(R_\theta + \sigma\omega^{-1/2})^2}$$

$$Z^{Imag}_{Total} = \frac{\omega C_d\,(R_\theta + \sigma\,\omega^{-1/2})^2 + \sigma\omega^{-1/2}\,(1+\sigma C_d\,\omega^{1/2})}{(1+\sigma\omega^{1/2}\,C_d)^2 + \omega^2\,C_d^2\,(R_\theta + \sigma\omega^{-1/2})^2}$$

Figure C3.
Extended Diffusion Electrical Analogue

finite diffusion distance, as shown in Figure C-3. The impedance behavior shown in the figure for this case is derived as follows:

For the general circuit in Figure C-2:

$$Z_T = R_u + \frac{1}{\frac{1}{R_\theta + Z_D' - jZ_D''} + j\omega C_d} = R_u + \frac{1}{\frac{R_\theta + Z_D' + jZ_D''}{(R_\theta + Z_D')^2 + Z_D''^2} + j\omega C_d}$$

$$Z_T = R_u + \frac{1}{\frac{R_\theta + Z_D' + jZ_D'' + j\omega C_d(R_\theta + Z_D')^2 + j\omega C_d Z_D''^2}{(R_\theta + Z_D')^2 + Z_D''^2}}$$

$$= R_u + \{(R_\theta+Z_D')^2+Z_D''^2\}\frac{R_\theta + Z_D' - jZ_D'' - j\omega C_d(R_\theta + Z_D')^2 - j\omega C_d Z_D''^2}{\{(R_\theta+Z_D')^2+Z_D''^2\}+2Z_D''\omega C_d\{(R_\theta+Z_D')^2+Z_D''^2\}+\omega^2 C_d{}^2\{(R_\theta+Z_D')^2+Z_D''^2\}}$$

$$= R_u + \frac{R_\theta + Z_D'}{1+2Z_D''\omega C_d+\omega^2 C_d{}^2\{(R_\theta+Z_D')^2+Z_D''^2\}} + j\frac{-Z_D'' - \omega C_d(R_\theta + Z_D')^2 - \omega C_d Z_D''^2}{1+2Z_D''\omega C_d+\omega^2 C_d{}^2\{(R_\theta+Z_D')^2+Z_D''^2\}}$$

Therefore the real and imaginary components of Z_T are:

$$Z_T' = R_u + \frac{R_\theta + Z_D'}{(1 + \omega C_d Z_D'')^2 + \omega^2 C_d{}^2(R_\theta + Z_D')^2}$$

$$Z_T'' = \frac{\omega C_d(R_\theta + Z_D')^2 + Z_D''(1 + \omega C_d Z_D'')}{(1 + \omega C_d Z_D'')^2 + \omega^2 C_d{}^2(R_\theta + Z_D')^2}$$

For an extended diffusional impedance one substitutes:

$$Z_D' = \sigma\omega^{-\frac{1}{2}} \qquad Z_D'' = -\sigma\omega^{-\frac{1}{2}} \qquad \text{where } \sigma = \frac{RT}{\sqrt{2}n^2F^2}\left(\frac{1}{C_{ox}D_{ox}^{\frac{1}{2}}} + \frac{1}{C_{red}D_{red}^{\frac{1}{2}}}\right)$$

leading to the expressions in Figure C-3. However, the expressions for finite diffusion are:

$$Z'_D = \omega^{-\frac{1}{2}} \sum \sigma_i \frac{\sinh(K_i\omega^{\frac{1}{2}}) + \sin(K_i\omega^{\frac{1}{2}})}{\cosh(K_i\omega^{\frac{1}{2}}) + \cos(K_i\omega^{\frac{1}{2}})}$$

$$Z''_D = \omega^{-\frac{1}{2}} \sum \sigma_i \frac{\sinh(K_i\omega^{\frac{1}{2}}) - \sin(K_i\omega^{\frac{1}{2}})}{\cosh(K_i\omega^{\frac{1}{2}}) + \cos(K_i\omega^{\frac{1}{2}})}$$

Upon substitution of these expressions into the equations for Z'_T and Z''_T, the result is too complex to write, but can easily be solved by computer, as done in this study.

This case leads to the creation of two time constants, and the value of the parameters can be adjusted so that the curves look qualitatively similar to the data. However, as seen in Figure C-4, the right-hand semicircle is constrained to begin on the left side at an angle of no more than 45 degrees. The actual data was found to have an angle much more than 45 degrees. Thus, this case does not appear to be able to adequately fit the observed data.

The second case modelled is a nested set of parallel resistances and capacitances corresponding to polarization resistance, double-layer capacitance, corrosion product pore resistance, and corrosion product capacitance, as shown in Figure C-5. The impedance of this case is shown in the figure and is derived as follows:

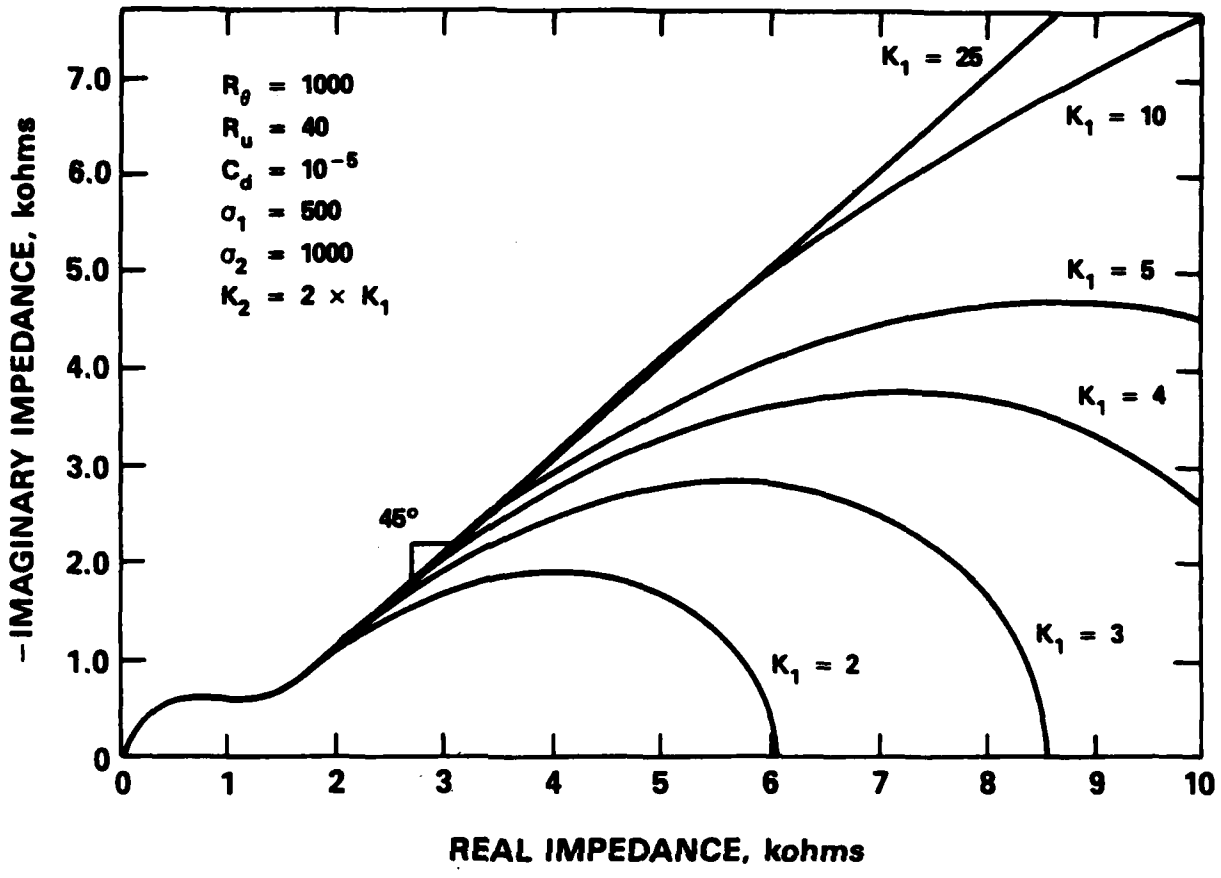

Figure C4.
Results of Extended Diffusion Model

A simple parallel resistor/capacitor circuit can be substituted for the diffusional impedance, yielding a nested circuit with two time constants. The impedance components for a simple parallel circuit are:

$$Z_D' = \frac{R_2}{1 + \omega^2 C_2^2 R_2^2}$$

$$Z_D'' = \frac{\omega C_2 R_2^2}{1 + \omega^2 C_2^2 R_2^2}$$

Substituting into the expressions for the total impedance components yields the equations displayed in Figure C-5.

This case leads to the creation of two overlapping semicircles which look similar to the actual data and, in addition, do not suffer from the 45 degree constraint of the previous case. When detailed fitting of the data was attempted however, the fit could not be made very good for the following reason. The actual semicircles are not perfect but are vertically "squashed" somewhat. This is a common phenomenon referred to as dispersion, because it could be caused by nonuniformity of properties over the specimen surface, or as depression, because the semicircle appears to have its center depressed below the real axis. Besides depressing the semicircle, this phenomenon also causes the Bode phase peaks to be somewhat broadened, as can be seen in the actual data.

The dispersion phenomenon has been handled in a number of ways. An extended diffusion model is obviously not

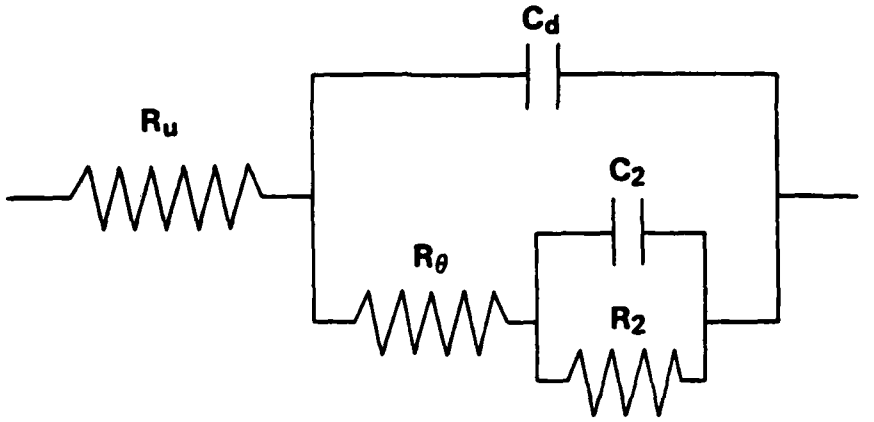

$$Z^{Real}_{Total} = R_u + \frac{R_\theta + \frac{R_2}{1+\omega^2 C_2^2 R_2^2}}{\left[1+\omega\ C_d\left(\frac{\omega\ C_2\ R_2^2}{1+\omega^2 C_2^2\ R_2^2}\right)\right]^2\ {}^2+\omega^2\ C_d{}^2\ \left[R_\theta + \frac{R_2}{1+\omega^2 C_2^2 R_2^2}\right]^2}$$

$$Z^{Imag}_{Total} = \frac{\omega\ C_d\left[R_\theta + \frac{R_2}{1+\omega^2 C_2^2 R_2^2}\right]^2 + \frac{\omega\ C_2\ R_2^2}{1+\omega^2 C_2^2\ R_2^2}\left[1+\omega\ C_d\ \frac{\omega\ C_2\ R_2^2}{1+\omega^2 C_2^2\ R_2^2}\right]}{\left[1+\omega\ C_d\left(\frac{\omega\ C_2\ R_2^2}{1+\omega^2 C_2^2\ R_2^2}\right)\right]^2 + \omega^2\ C_d{}^2\ \left[R_\theta + \frac{R_2}{1+\omega^2 C_2^2 R_2^2}\right]^2}$$

Figure C5.
Two Time Constant Electrical Analogue

applicable in this case. An empirical depression constant has been used[C-6], but its use has no basis in the physics of the problem, but is merely a mathematical construct. The last method is the use of a much more complicated equivalent circuit[C-7], which is beyond the scope of this study to model.

Although the modelling attempts for these data were not successful, some information is still possible to obtain from the effort, notably the absence of a limited diffusion behavior. Thus, it is likely that the observed behavior of 90-10 copper-nickel is not a result of limited diffusion through long, thin pores in the corrosion product film.

REFERENCES

C-1. Gabrielli, C., "Identification of Electrochemical Processes by Frequency Response Analysis", Solartron Instrumentation Group, Monograph SI/Dym/001/Issue 1, October 1980.

C-2. Randles, J. E. B., Discuss. Faraday Soc., 1, P 11, 1947.

C-3. Kendig, M., S. Tsai, and F. Mansfeld, "Influence of Steel Surface Preparation on Coating Performance and Cathodic Delamination", Materials Performance, pp 37-40, June 1984.

C-4. Warburg, E., Ann. Phys., 67, p 493, 1899; 6, p 125, 1901.

C-5. Dawson, J. L., and Johns, D. G., "Diffusion Impedance - An Extended General Analysis", J. Electroanal. Chem., 110, pp 37-47, 1980.

C-6. Cole, K. S., and R. H. Cole, J. Chem. Phys., 9, p 341, 1941.

C-7. Mansfeld, F., "Recording and Analysis of AC Impedance Data for Corrosion Studies - I. Background and Methods of Analysis", Corrosion, 36(5), pp 301-307, May 1981.

INITIAL DISTRIBUTION

Copies

2 ONR
- 1 ONR 431 (Sedriks)
- 1 ONR 0725 (Kelly)

1 NRL 6310 (Crooker)

1 NADC 6062 (Agarwala)

1 NCEL L52 (Drisko)

4 NAVSEA
- 1 SEA 05R25
- 1 SEA 05M1
- 1 SEA 99612

2 DTIC

CENTER DISTRIBUTION

Copies	Code	Name
3	012.3	Moran
1	28	Wacker
1	2801	Crisci
2	2803	Cavallaro
3	281	Gudas
1	2812	Arora
5	2813	Morton
5	2813	Hack
1	2814	Montemarano
1	2815	Holsberg
1	522.2	TIC (A)
2	5231	Office Services

END

DATE

FILMED

MARCH

1988

DTIC